Characterizing a Novel Mutation in MECP2 using an hiPSC Model of Rett Syndrome

by

Leah Christine DeJong

A thesis submitted in conformity with the requirements
for the degree of Master of Science

Department of Molecular Genetics
University of Toronto

Characterizing a Novel Mutation in MECP2 Using an hiPSC Model of Rett Syndrome

Leah DeJong

Master of Science

Department of Molecular Genetics
University of Toronto

2020

Abstract

Rett Syndrome (RTT) is a neurodevelopmental disorder in girls with mutations in the X-linked gene that encodes methyl-CpG-binding protein 2 (MECP2). Using neurons differentiated from patient-derived induced pluripotent stem cells (iPSC), I analyzed the *MECP2* RNA levels, MECP2 protein levels, morphology, and extracellular electrophysiology of a novel L124W *MECP2* mutation. My results show that L124W exhibits no change in RNA, protein, dendrite length, soma size, or electrophysiology but does show a subtle significant change in dendrite order and dendrite complexity. This is the first in vitro iPSC characterization of a mild RTT case. While developing a CRISPR/Cas9 protocol that will eventually genetically rescue the L124W mutation, I also generated the first iPSC knock-out lines for *NEDD4L*, a downstream target of MECP2. Overall, this work can be used to further elucidate MECP2 pathways and eventually identify treatments for RTT.

Acknowledgments

The work in this thesis could not have been completed alone. Firstly, I want to thank my supervisor, Dr. James Ellis, for his support in every phase of this project. Thank you so much for always being available when questions arose, for providing clear guidance with excellent insights, and for being an all-around great mentor. I've learned so much from simply working with you and watching how you run the lab. You've unquestionably re-sparked my love of science time and time again. Thank you for everything. I also have to thank my fellow labmates. The biggest shout-out goes to Rebecca Mok, whose work was foundational for this project and who provided an excellent example as to what good science looks like. Thank you so much for all of your patient explanations and your willingness to teach the skills you've perfected. Thank you to Dr Matthew Hildebrandt, not just for teaching me how to do CRISPR, but also for providing a plethora of nerdy conversations that brought joy to my day. Thank you for every lab trick and tip you taught, they were invaluable, and for always having the time to talk through a difficult problem. Peter Pasceri must be thanked for his amazing, ongoing support, his ability to always know where that thing I needed was, and for all of his really cool ideas. It was a pleasure to sit in the same row as you. I want to thank Dr Maria Sartori for all of her work on the *NEDD4L* KO lines, it was wonderful to work with you. Thank you to Dr Deivid Rodrigues for all of your help with the protein work and your ongoing advice; it absolutely made my project better and helped me think through new ideas. While Loryn Bryes and I worked on very different project, thank you for being a wonderful friend and partner in crime as we worked through the stages of our MScs together. I must thank our technicians Wei Wei, Alina Piekna, and Jiajie Liu for all of the iPSCs and neurons. Thank you so much for all of the advice and your expertise. Without you, none of this work would have been possible. You're amazing. Many thanks go to my committee, Dr. Monica Justice and Dr. Derek van der Kooy. Thank you both for overseeing my project, pushing it to be better, and always asking questions that made me think really hard. It was a delight working with you and I really enjoyed committee meetings. A shoutout to my family for their ongoing support: thanks to my parents for trying their best to understand what in the world I was talking about and yet still being supportive to the end, thanks to my brother for commiserating on the hard days. Finally, thanks to God. You know what you did better than I do.

Thanks to everyone. This was a team effort. I couldn't have done it without you.

Table of Contents

List of Tables

List of Figures

Chapter 1
Introduction

1 Introduction

1.1 Rett Syndrome

Rett Syndrome (RTT) is a neurodevelopmental disorder that affects 1 in every 10,000 girls and is caused by a heterozygous mutation in the gene methyl-CpG-binding protein 2 (*MECP2*) (Chahrour and Zoghbi, 2007; Amir et al., 1999). First described by Andreas Rett in 1966, Rett Syndrome wouldn't officially be recognized by the medical community until 1983 (Balachar et al., 2016) and it would take another 16 years before Amir et al (1999) found that mutations in *MECP2* were the root of RTT. Originally, RTT patients were described to have autism spectrum disorder with additional clinical phenotypes such as severe dementia, loss of purposeful hand movements, jerky trunk ataxia, and acquired microencephaly (Hagberg et al., 1983). However, in 2013 the Diagnostic and Statistical Manual of Mental Disorders, Fifth Edition separated RTT from autism as two separate disorders. Today, RTT is described by clinicians as a neurodevelopmental disorder in girls that features normal developments until 6-18 months of age when the girls begin to undergo a regression and lose acquired purposeful hand movements, motor abilities, gait abilities, speech abilities, and develop stereotypical hand-wringing movements. These features can be accompanied by a number of secondary diagnostic traits such as reduced cognitive ability, repeated rocking, scratching, self- stimulatory behavior, microencephaly, anxiety, breathing abnormalities, and seizures; with overall traits ranging from physiological phenotypes to behavioral and emotional dysregulation (Williamson and Christodoulou, 2006; Chahrour and Zoghbi, 2007; Singh & Santosh, 2018). After this regression period, patients commonly stabilize at a point between 5 – 10 years of age and can live into their late 60s, often developing Parkinsonian features and exhibiting severe debilitation of their physical condition (Hagberg, 2005). There is currently no cure for Rett Syndrome.

1.2 *MECP2* and The Genetics of Rett Syndrome

From a genetic perspective, more than 90-95% of RTT cases are caused by mutations in *MECP2* (Amir et al., 1999) with the few remaining cases related to mutations in the genes *FOXG1* (Ariani et al., 2008) and *CDKL5* (White et al., 2010). With mutations in *MECP2* making up the

majority of RTT cases, it has been the primary focus of study for the field. In fact, eight specific nonsense and missense mutations in *MECP2* make up nearly 60% of all RTT cases (Figure 1) (Percy et al., 2007) with more than 900 RTT related *MECP2* mutations reported in RettBase, a database of patient *MECP2* variants (http://mecp2.chw.edu.au/). The majority of these mutations are missense or nonsense mutations that arise *de novo* from the paternal germline (Trappe et al., 2001). Larger deletions in *MECP2* do occur, although they only have a ~5% prevalence and often result in a more severe form of RTT (Vidal et al., 2019). Mutations most frequently occur in the functional protein domains such as the methyl-CpG-binding domain which binds methylated CpGs (Nan et al., 1993), the transcriptional repression domain which recruits chromatin remodeling proteins (Nan et al., 1997), and the nuclear localization signal (Trappe et al., 2001) with all of these domains located in exons 3 and 4 (Figure 1). *MECP2* has two isoforms, both of which express exons 3 and 4. *MECP2e1* encompasses exons 1, 3, and 4 while *MECP2e2* incorporates exons 2, 3, and 4. Mutations have been found in exon 1 that lead to RTT but no exon 2 mutations are currently known (Mnatzakanian et al., 2004; Itoh et al., 2012; Djuric et al.,2015; Martinez de Paz et al., 2019).

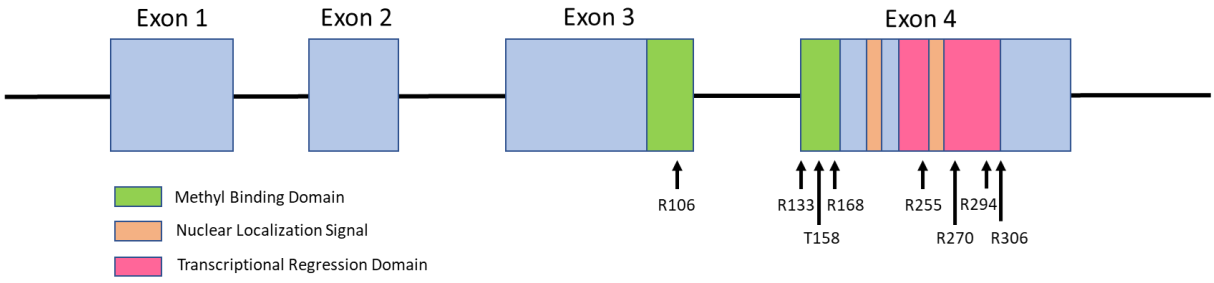

Figure 1. *Mecp2* Schematic with Common Mutation Sites Associated with RTT. The majority of *Mecp2* mutations that lead to RTT cluster in core domains such as the Methyl Binding Domain (MDB in green), the Nuclear Localization Signal (NLS in orange), and the Transcriptional Repression Domain (TRD in pink). Highlighted on the lower side of the schematic are the 8 most prominent amino acids where RTT mutations occur, all of which are located preferentially in the MBD or the TRD. Nonsense and missense mutations at these 8 locations make up 60% of RTT cases.

MECP2 is located on the X chromosome and is therefore an X-linked gene subject to X-Chromosome Inactivation (XCI) wherein one of the two X-chromosomes is randomly inactivated (Escamilla-Del-Arenal et al., 2011). In the case of RTT patients, girls are almost

always mosaic where half their cells express wild type (WT) MECP2 while the other half of their cells express mutant (MT) MECP2. In humans, XCI is typically random however there are cases where it is occasionally nonrandom. This may lead to patients with an increased WT skew being more mildly affected and this idea is currently under debate. Nonrandom skewing is also a common feature of RTT mouse models. Interestingly, in humans roughly 15% of X-linked genes can 'escape' from X-chromosome inactivation and continue to express the inactive allele, possibly creating a link to RTT severity (Zogbhi et al., 1990; Shahbazian and Zoghbi., 2002; Huppke et al., 2006; Knudsen et al., 2006; Peters et al., 2014; Xiol et al., 2019). While RTT is associated with a loss of function of MECP2 and XCI skewing can help increase the amount of functioning MECP2 back up to expected levels, *MECP2* Duplication Disorder is a neurodevelopmental disorder where individuals have additional copies of *MECP2* and produce an excess quantity of MECP2 (Van Esch et al., 2005). These two disorders often cause inverse but complimentary patient phenotypes. The fact that both deficiency and excess of MECP2 can lead to neurodevelopmental disorders highlights both the importance of the gene and the delicate balance held in its required quantities.

1.3 MECP2 Function

As a nuclear protein, MECP2 performs a number of different functions in the cell through the genome-wide tracking of methylated-CpG-density and the eventual binding by MECP2 to single methylated CpGs with adjacent motifs that are rich in A/Ts (Nan et al., 1993; Skene et al., 2010; Tillotson and Bird., 2020). MECP2 was first discovered as a transcriptional repressor through the association of its Transcriptional Repression Domain with co-repressor complexes such as mSin3A and HDACs (Nan et al., 1998; Jones et al., 1998). The mechanistic role of MECP2 as a transcriptional repressor was further elaborated through the determination that MECP2 also interacted with the NCoR/SMRT co-repressor complex and HDAC3 as another means of transcriptional repression. Related microarray experiments showed a subtle overall decrease in gene expression, indicative of overall repression in the absence of *Mecp2* (Tudor et al., 2002; Lyst et al., 2013) More recently, a truncated version of mouse *Mecp2* containing only the methyl-binding-domain and the NCor/SMRT interacting domain was found to leave mice phenotypically near-normal, furthering the idea of MECP2's primary purpose being repression (Tillotson et al., 2019).

However, although the transcriptional repression model is well studied, MECP2 also seems to participate in transcriptional activation through associations with transcriptional activator CREB1 and other promoters (Yasui et al., 2007; Chahrour et al., 2008). In a demonstration of gene expression patterns in a mouse hypothalamus that over or under expressed *Mecp2*, a total 85% of genes were found to be higher when *Mecp2* was activated, making the case for MECP2 as a transcriptional activator (Chahrour et al., 2008). Later research in the cerebellum found abnormal *Mecp2* amounts caused both downregulation and upregulation of various genes (Ben-Shachar et al., 2009) and posited the role of MECP2 not as a specific repressor or activator but rather as an overall transcriptional modulator.

In addition to its role as a transcriptional modulator, MECP2 has also been found to associate with nucleosomes in an N-terminus dependent manner and ultimately influence chromatin compaction (Georgel et al., 2003). Shadowed electron microscopy of nucleosome arrays later showed that this chromatin compaction was further accompanied by higher order structures that lead to inter-chromatin condensation (Adkins and Georgel., 2010). Null mouse models also show a loss of long-range chromatin interactions (Horike et al., 2005). The ability of MECP2 to be involved in chromatin compaction is of particular interest to some RTT point mutations, such as R168X, that lost the ability to form higher order chromatin structures (Georgel et al., 2003).

Overall, MECP2 plays a role in a number of different biological processes ranging from various forms of transcriptional modification to chromatin compaction. This diverse set of roles further highlights the importance of MECP2 function and the potential array of effects that RTT mutations can have on a patient.

1.4 Rett Syndrome in Mouse Models and Post-Mortem Tissue

Mouse models are a well-known tool for studying RTT mutations as the amino acid sequence of MECP2 is highly conserved throughout vertebrate species (Tillotson et al., 2017). After the discovery that RTT is due to mutations in *MECP2*, knock-out mutations were generated in male mouse embryonic stem cells and were found to exhibit developmental defects (Tate et al., 1996). Eventually, two *Mecp2* null mouse models were created. The first, *Mecp2*$^{tm1.1Bird}$, used Cre-*loxP* technology to delete exons 3 and 4 so that the mouse model completely lacked MECP2 protein (Guy et al., 2001). The second mouse null model, *Mecp2*$^{tm1.1Jae}$, used the same technology to delete only exon 3. This model still expressed small Mecp2 protein fragments (Chen et al.,

2001). However, both nulls displayed very similar phenotypes. Together, these papers showed that female mice heterozygous for the null allele started developmentally normal and then developed a stiff gait, breathing difficulties, and hindlimb clasping. Similarly, males showed the same features but developed phenotypes at a more rapid rate with more than 50% of the male mice dying between 8 and 11 weeks of age (Guy et al., 2001; Chen et al., 2001). Since then, a number of other RTT mouse model features have been found including increased sociability (Wu et al., 2016), metabolism changes (Goffin and Zhou, 2012; Justice et al., 2013), abnormal mitochondrial structure (Shulyakova et al., 2017), and microencephaly with mouse neurons exhibiting smaller somas and decreased dendrite complexity phenotypes (Chen et al., 2001; Chapleau et al., 2009; Li et al., 2013). In addition to the well-known null mouse models, 6 of the 8 most common RTT point mutations have been recapitulated in mice through various genetic engineering techniques. Based on this research, there are many similarities between the human and mouse model such as the period of delayed onset and the increased survivability of heterozygous females over hemizygous males (Vashi and Justice, 2019).

Due to the majority of RTT patients being female, the female *Mecp2* mutant mice are often considered the most clinically relevant model. Interestingly, one difference between female mouse models and human RTT cases, as mentioned above, is in XCI skewing where female mice can show non-random XCI skewing that favours the wild type allele. Humans do not usually show this skew. In mice, skewing is determined by alleles at the X chromosome controlling element and is considered a primary activation activity (Amir et al., 2001; Thorvaldsen et al., 2012). This skew towards the WT allele could mean that heterozygous female mice will not experience as severe a phenotype as would be seen in heterozygous humans.

Although there is no current cure for RTT, an ongoing discussion has been the potential reversibility of RTT due to the fact that RTT patients do not exhibit increased neuronal death. With the number of neurons unchanged, only smaller and phenotypically abnormal, it was posited that RTT was reversible. In 2007, this was shown to be true in a mouse model where the endogenous *Mecp2* was silenced by the insertion of a *lox-Stop* cassette that could be conditionally activated with tamoxifen through a Cre-ER transgene (Guy et al., 2007). Upon the injection of tamoxifen, *Mecp2* expression was restored to 80% of normal levels which partially reversed neurological phenotypes and restored lifespan (Guy et al., 2007). It has also been well established that there are potential pharmacological rescues of RTT. For examples, treatment

with BDNF and IGF1 has been shown to partially rescue RTT phenotypes in both male and female mouse models (Chang et al., 2005; Tropea et al., 2009). These, and other studies, have clearly demonstrated that mouse models provide valuable insights into the human RTT condition.

In addition to mouse models, post-mortem brain tissue is another well-known model for studying RTT and has an established neuropathology. Similar to research seen in mouse models, post-mortem brain tissues of RTT patients also shows microencephaly with reduced neuronal size, dendrite branching, complexity, and spine number (Armstrong et al., 1995; Bauman et al., 1995; Chapleau et al., 2009). Other experiments on post-mortem brains have revealed reductions in nerve growth factors and TrkA, both of which are responsible for the later stages of dendritic growth (Lipani et al., 2000) as well as reductions in other neuronal maturation factors such as KCC2 (Hinz et al., 2019). Similar to results seen in mouse and other human studies, post-mortem brain microarrays also show consistent changes in mRNA levels across a variety of transcripts, showing MECP2's role as a transcriptional regulator (Colantuoni et al., 2001). As a result, post-mortem studies align in many ways with the work done on both humans and mice.

Although *Mecp2*-null mice and post-mortem brain tissue have demonstrated utility for studying RTT, they both exhibit benefits and downsides in the study of the disease. As an example, the nature of post-mortem studies means that RTT can only be examined at the end of life and the unique features of the RTT early asymptomatic phase cannot be examined. In addition, RTT post-mortem models are limited by the small number of samples available and are unable to provide any insights on the key behavioral and motor alteration traits of RTT. Mouse models are able to provide insights into these behavioral and motor traits. However, in addition to the skewing mentioned earlier, mouse models may provide an underrepresentation of human disease phenotypes since male mice, who are more severely affected, better recapitulate the symptoms seen in human females while female mice show a less severe phenotype (Guy et al., 2001; Chen et al., 2001). In addition, mouse models display some additional phenotypes that are not seen in human patients (Chen et al., 2001). Therefore, in order to examine RTT from another angle and overcome some of these challenges, human stem cell technology can be used as a complementary model.

1.5 Human Stem Cells in Studying Disease

In addition to using mouse models and post-mortem tissue as a way of studying disease, the use of human stem cells has increasingly become a relevant model system for studying RTT and other diseases. There are currently two prominent pools of human stem cells available to researchers, human embryonic stem cells (hESC) which are isolated from blastocysts (Thomson et al., 1998) or human induced pluripotent stem cells (hiPSC) which are generated from human somatic cells (Takahashi et al., 2007). Both hiPSCs and hESCs are self-renewing pluripotent cells with the ability differentiate into cells from all three embryonic germ layers. These systems both offer similar mechanisms for studying human disease with slight variations.

Human embryonic stem cells were first reported nearly 8 years before the introduction of hiPSCs when researchers isolated the hES cells from the preimplantation epiblast cells of blastocysts (Thomson et al., 1998; Reubinoff et al., 2000). This work built on the methods refined in mouse ES cells derived directly from the mouse blastocyst (Evans and Kaufman, 1981). These original hESCs showed both pluripotency through teratomas that gave rise to all 3 germ layers and the ongoing ability to self-renew, the two key features of human stem cells (Thomson et al., 1998; Reubinoff et al., 2000). This arrival of hESCs represented the first time a potentially indefinite population of human differentiated cells could be available to researchers. For disease modelling, embryos carrying mutations of interest could be detected and then the population of cells in the blastocyst could be isolated in vitro; these cells could then eventually be isolated for further differentiation and modelling as hESCs (Thomson et al., 1998). However, a number of controversies exist around the use of hESCs including the ethical use of human embryos and the possibility of human tissue rejection following patient transplantation.

As such, research increased into the possibility of reprogramming somatic cells into human stem cells. In 1997, reprogramming of mammalian somatic cells first occurred by transferring the somatic cell's nuclear contents into an enucleated unfertilized egg in an experiment now commonly referred to as the 'Dolly the Sheep' experiments (Wilmut et al., 1997). Later experiments would produce a similar effect by fusing somatic cells with ES cells (Cowan et al., 2005) but it wasn't until 2006 that the first true iPSCs would be produced through the reprogramming of adult fibroblasts using four key factors (Takahashi and Yamanaka, 2006). To determine these factors, 24 candidate transcription factors that were known to be associated with

pluripotency were introduced into the mouse fibroblasts and systematically eliminated until it was determined that four 'Yamanaka Factors' were enough to support the generation of stem cells. When these four factors, Oct3/4, Sox2, Klf4, and c-Myc, were retrovirally transduced into the fibroblasts the cells began to express the morphology and cell markers typically found in mESCs. The new cells, called induced pluripotent stem cells, also demonstrated their pluripotency through the generation of teratomas that contained cells from all 3 germ layers (Takahashi and Yamanaka, 2006). A year later, two labs came out with papers detailing the first iPS cell lines from humans. The Yamanaka lab, who pioneered the original 2006 experiment, generated iPSCs from human fibroblasts using the same four 'Yamanaka Factors' and a retroviral system to generate hiPSCs (Takahashi et al., 2007). At the same time, the Thomson Lab used a lentiviral system and the factors Oct4, Sox2, Nanog, and Lin28 to generate human iPSCs (Yu et al., 2007). However, as both retroviruses and lentiviruses are integrating viruses, research began into the generation of clinically safer reprogramming methods that could generate hiPSCs with no noise during integration and no remaining factors inside the target cell. Later systems would therefore seek to use non-integrated viruses, such as Sendai viruses which replicate only as RNA in the cytoplasm, to reprogram human fibroblast or peripheral blood cells into human iPSCs using similar factors (Ban et al., 2011; Hildebrandt et al., 2019) (Figure 2).

As human stem cells, both iPSCs and ESCs exhibit pluripotency and self-renewal. However, there is a constant ongoing discussion about how similar the two human stem cell types truly are. Some reports have demonstrated that there are little to no significant differences in gene expression (Park et al., 2008) while other studies looking at gene expression found that there was a recurrent pattern in iPSCs of all origins that were not in ESCs (Chin et al., 2009; Parotta et al., 2017). The underlying rationale for this potential difference has not been determined although some theorize that iPSCs might retain traits from their original cell line (Kim and Webster, 2010; Parotta et al., 2017). For example, Polo and colleagues (2010) found that iPSCs generated from three different types of starting cells all exhibited differences in iPSC transcriptional and epigenetic patterns. They suggested that early-passage iPSCs retain the transient epigenetic memory of their cell of origin, potentially accounting for the differences between iPSCs. More recent mass spectrometry and gene expression profiling for proteogenomic analysis has revealed that a number of distinct pathways are differentially enriched in iPSCs when compared to ESCs (Parrota et al., 2019). Overall, the studies generally agree that there are remarkable similarities

between iPSCs and ESCs however the number of subtle changes between the two types of human stem cells requires further study to determine possible biological relevance (Phanstiel et al., 2011; Parrota et al., 2019).

Shortly after the discovery of iPSCs, various research groups began generating iPSCs from various disease models (Park et al., 2008; Dimos et al., 2008; Ebert et al., 2009). For example, in 2008 Dimos and colleagues generated iPSCs from a woman with amyotrophic lateral sclerosis (ALS) and subsequently differentiated the ALS iPSCs into motor neurons, allowing them to demonstrate the disease in an iPSC model for the first time. At the same time, another paper (Park et al., 2008) showed iPSCs generated from 10 different individuals with diseases ranging from pancreatic to immunological. One year later, studies began comparing patient-derived iPSCs to wild type iPSCs from an unaffected family member. For example, a study comparing spinal muscular atrophy (SMA) iPSCs to a wild type control found deficits in soma size and SMA aggregates (Ebert et al., 2009). This was the first demonstration that disease-specific phenotypes could be found in iPSC cells generated *in vitro* and strengthened the use of iPSCs as a valuable model for disease.

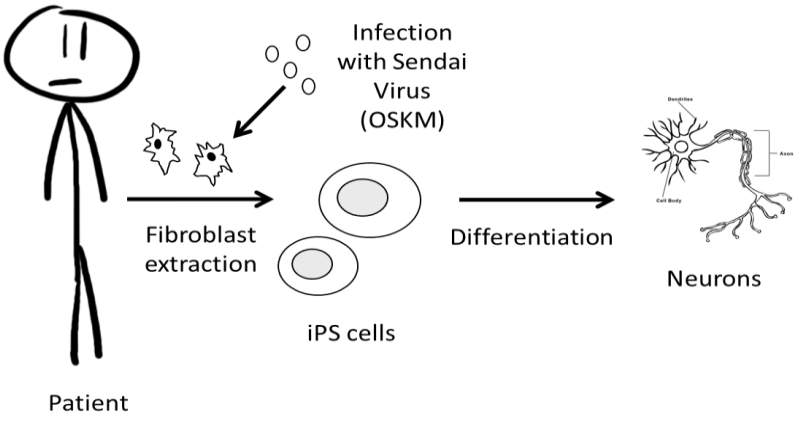

Figure 2. Model of Generating hIPS cells and Neurons from Patients. Patient fibroblasts can be extracted and then infected with 4 transcription factors (Oct4, Sox2, klf-4, c-MYC). The resulting iPS cells can be differentiated *in vitro* to generate neurons or other cell types for further study.

Overall, this early work provided a solid foundation of evidence that hiPSCs had valuable use as a disease model, exhibiting a wide range of disease types and providing quantifiable differences from wild type controls. Today, hiPSCs have been generated for hundreds of different diseases

and are being investigated for further use in translational medicine such as increased disease modeling, drug screening, and cellular therapy (Moradi et al., 2019; Braganca et al., 2019).

1.6 Rett Syndrome in hiPS Cells and Neurons

While hiPSCs were becoming an established disease model, work turned to developing an hiPSC RTT disease model. This required two key innovations in the field: the generation of the first human iPSC lines and, as RTT is primarily a neurodevelopmental disorder, the ability to differentiate those iPSC lines into neurons. In 2009, we generated the first RTT-hiPSC lines using the EOS (Early Transposon promoter and Oct-4 (Pou5f1) and Sox2 enhancers) system to make reprogrammed iPSC colonies derived from RTT patient fibroblasts (Hotta et al., 2009). At this time, there was significant interest in differentiating the iPSC RTT lines into neurons as RTT is neurodevelopmental disorder and as MECP2, although ubiquitously expressed, is found to be most abundant in neurons (Shahbazian et al., 2002).

There are a number of different methods for differentiating iPSCs into neurons. One early method is a rosette-based method that generates a mix of excitatory and inhibitory cortical neurons (Marchetto et al., 2010; Brennand et al., 2011). In this process, embryoid bodies are generated from iPSC lines and maintained in media until visible structural rosettes form. The rosettes are then manually dissected and the neural precursor cells (NPCs) are maintained to a high density. These NPCs are then differentiated in neurons. Overall, this process takes ~13 weeks and is described in more detail in section 2.2.2. Although this is the type of protocol used for the first generation of RTT neurons from hiPSCs (Marchetto et al., 2010), since then, other differentiation methods have become common in the field. For example, this report primarily uses a transcription factor-based differentiation method as it has a number of benefits relative to the rosette-method such as a purer population of excitatory cortical neurons, reporting 100% purity compared to the ~70% of other protocols, and a shortened total differentiation time, making larger scale studies more feasible (Zhang et al., 2013). In this process, iPSCs are taken directly to neurons without a rosette or NPC stage through the lentiviral infection and overexpression of *Neurogenin-2* (*Ngn2*) under the control of doxycycline in a tetracycline-inducible system (Zhang et al., 2013) (Figure 3).

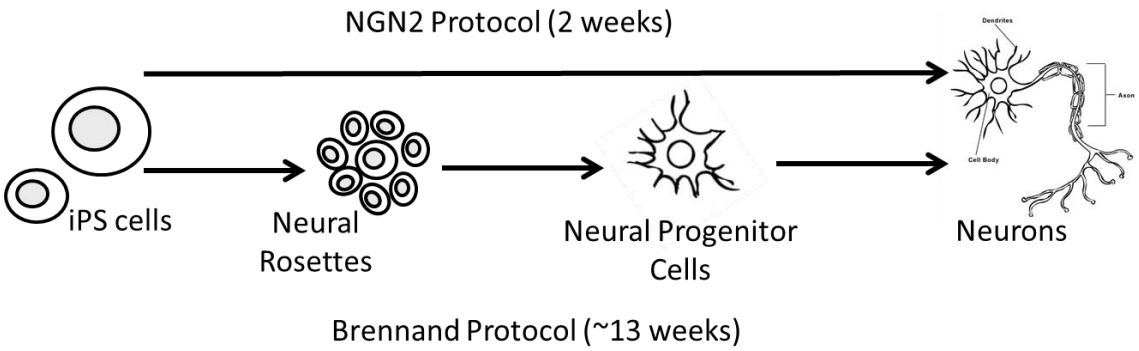

Figure 3. Differentiation Method Comparison. The NGN2 protocol takes only 2 weeks to move from iPSCs to neurons with no intermediary steps. The Brennand Protocol (a type of rosette-based method) takes 13 weeks to differentiate iPSCs into neurons and relies on two intermediary steps.

Using the rosette-based method, in 2010 Marchetto and colleagues differentiated RTT hiPSCs from 4 distinct patients into neurons for the first time. The patients had a range of RTT mutations including deletion, nonsense, and missense mutations in *Mecp2* and these mutations were compared to 5 hiPSC unrelated controls. The final hiPSC derived neurons were found to exhibit a reduced soma size, a reduction in dendritic spines, and a reduction in glutamatergic synapses (Marchetto et al., 2010). This paper also demonstrated that the RTT neurons had reductions in the frequency and amplitude of spontaneous excitatory and inhibitory currents, reductions in calcium oscillations, and the ability to be partially rescued by an increase in IGF1 (Marchetto et al., 2010). Of note, these phenotypes match the phenotypes previously established by mouse and post mortem models.

This original study was quickly followed up by other hiPSC RTT models which further confirmed the similarity between *Mecp2* mouse models and hiPSC RTT models including reduced soma size, reduced dendrite length, reduced dendrite spine density, lower expression of neuronal markers, and a decrease in spontaneous currents. (Cheung et al., 2011; Ananiev et al., 2011; Farra et al., 2012; Li et al., 2013). For example, a paper by Cheung and colleagues (2011) compared an isogenic pair of WT and RTT null neurons missing almost the entire *MECP2* gene and confirmed that the RTT lines saw a reduction in soma size. Anaviev and colleagues (2011) looked at the R294X mutation and found a reduction in nuclear size, often correlated with soma size. This work by Anaviev (2011) directly compared its results to the work by Cheung (2011)

and began to discuss the idea that their R294X mutation, which retained some of its function while lacking others, might produce a different phenotype relative to the complete deletion seen in the Cheung nulls. Although the R194X was not found to be this 'intermediary' mutation, it did build on the idea generated in clinical studies which suggested correlations between *MECP2* genotype and RTT phenotype (Huppke et al., 2000; Bebbington et al., 2007; Neul et al., 2008). Two seminal studies of clinical data in the late 2000s both demonstrated a key link between phenotype and genotype to the degree that they even agreed on which mutations could be categories as severe, such as R270X, R255X, and R168X, and as less severe, such as R133C, R294X, and c-terminal deletions (Bebbington et al., 2007; Neul et al., 2008). They both also demonstrated that individuals with more severe mutations were less likely to retain their hand usage, walking ability, or speech ability (Bebbington et al., 2007; Neul et al., 2008). A follow-up paper which examined the 'less severe' mutation group of c-terminal mutations found that these patients typically had a later onset of regression and stereotypes (Bebbington et al., 2010). While these milder mutations like R133C, R294X, and R306C are known in the literature, with R133C being one of the 8 most common RTT mutations, (Dajani et al., 2013), iPSC work has focused on mutations in the 'severe' category. To date, the R133C mutation has been gene edited into LUHMES cells, a diploid human female mesencephalic cell line, using CRISPR (Shah et al., 2016) however no phenotypic analysis of the resulting neurons has been done and the mutation does not yet exist in a stem cell context.

Moving forward from the initial creation of RTT iPSCs, more and more types of RTT stem cells were being examined. Li and colleagues (2013) used TALENs to generate an *MECP2* loss-of-function line in ES cells. They were the first to examine the RTT iPSC-derived transcriptome and found an overall transcriptional down-regulation of RTT neurons. They also found a soma size reduction, a decrease in dendrite arborization through Sholl analysis, and a reduction in action potentials in RTT neurons as seen in the first multi-electrode array RTT results. Many of these phenotypes could be rescued with IGF1 (Li et al., 2013). These lines, called WIBR3 in the original paper, are of particular interest as they are used as a control in this paper alongside the null lines reported in 2011 (Cheung et al., 2011). Looking forward, in 2015 our lab provided the first isoform specific patient-iPSC line and found that three e1 lines had decreased soma size, reduced dendrite complexity, and impairment in patch clamp electrophysiology such as reduced cell capacitance, action potentials, and miniature excitatory synaptic current (Djuric et al., 2015).

At the same time, studies began to show that RTT iPSC-derived neurons showed alterations in neuronal differentiation, migration and branching (Williams et al., 2014; Fernandes et al., 2015). Work on astrocytes at this time began to show that RTT also affected other types of brain cells and that RTT astrocytes could create RTT phenotypes in WT neurons (Williams et al., 2014). Building on iPSC work, Mellios and colleagues (2018) generated cerebral organoids from an RTT isogenic line and found that RTT organoids had increased ventricular area but decreased thickness relative to the WT control. They also found a reduction in neurogenesis due to reductions in neuronal markers MAP2 and DCX (Mellios et al., 2018). These organoid models represent a new complimentary model to existing mouse, post-mortem, and 2D neuronal cultures. Work also continued on RTT iPSC lines where, for example, RTT iPS derived neurons were found to have increased signs of stress, leading to an induction of P53 and senescence. This induction of P53 was linked to the previously seen reduction in dendritic complexity for RTT neurons and an inhibition of P53 was found to restore complexity phenotypes (Ohashi et al., 2018). Recent work in iPSCs has also found differences in the cargo of exosomes and that treating RTT cells with WT exosomes can rescue neurodevelopmental defeats such as neurogenesis (Sharma et al., 2019). Most recently, our lab used iPSC-derived neurons in RNA sequencing approaches to find that RTT neurons have reductions in global translation, with strong reductions in ubiquitinated protein levels (Rodrigues et al., 2020). Overall, the use of iPSCs and iPSC-derived neurons have provided a number of advances for the field and continue to be a well-used RTT model.

One unique reason for the use of iPSCs as an RTT model compared to other disease models is the previously discussed location of *Mecp2* on the X-Chromosome and the effect of XCI skewing. Unlike non-X-linked diseases which typically use a related wild type control, RTT girls have cells that express either the wild-type *Mecp2* or the mutant *Mecp2*. As such, hiPSC wild type and mutant lines can be derived from the same patient, creating isogenic pairs that differ only in their expression of *Mecp2* (Cheung et al., 2011). One way of examining X inactivation is through an androgen receptor assay (AR assay) where the *AR* gene, an X-linked gene, is analyzed to determine which X is active (Shabazian et al., 2010). This is possible because a feature of the *AR* gene is that it contains a region where the triplicate CAG is repeated multiple times. As the two X-chromosomes have different numbers of CAG repeats, usually between 10 and 36, the two X-chromosomes can be differentiated (Plath et al., 2010). By using this method,

cells can be identified to have either the WT or RTT X-chromosome and by acquiring one of each from the same patient, researchers have access to isogenic pairs that are identical other than their X-chromosome (Figure 4). Typically, cells retain their X-inactivation state through their life however in some rare cases the iPSCs will experience XCI erosion due to a loss of *XIST* and H3-K27 trimethylation, resulting in two active X-chromosomes (Mekboubad et al., 2013).

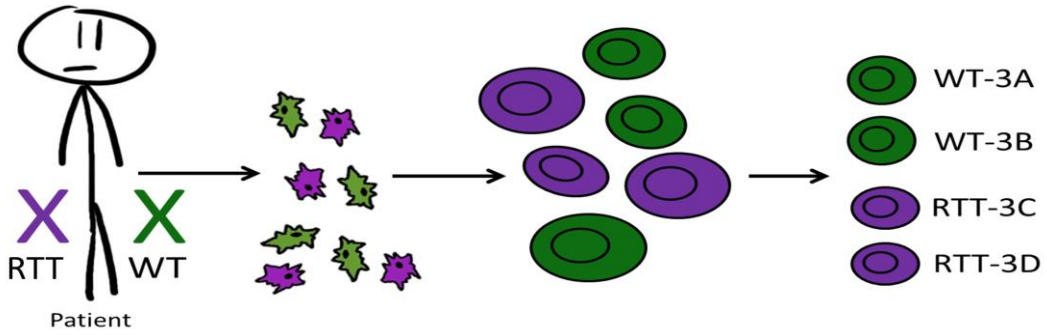

Figure 4. X-Chromosome Skewing in RTT Girls. Girls who are heterozygous in *MECP2* will have one X that is wild-type (green) and one X that is mutant (purple). The X-linked nature of *MECP2* means that in each of their cells one of these X's will be randomly shut down, leaving individual cells to present all wild-type *MECP2* (green) or all mutant *MECP2* (purple). This skewing allows us to create cell lines that are either wild-type or mutant from the same patient.

Today, a wide variety of RTT and control iPSC and hESC lines exist, allowing the examination of many different *MECP2* mutations. While some of these cell lines come directly from patients, others are generated from control lines using gene editing methods. Many of the initial RTT gene editing experiments used TALEN editing (Boch et al., 2009; Li et al., 2013), but the field has moved towards the use of CRISPR for RTT gene editing techniques (Ran et al., 2013; Shah et al., 2016; Le et al., 2019; Croci et al., 2020). For example, Shah and colleagues (2016) used CRISPR to re-create 4 different RTT missense mutations. Our lab has also used CRISPR to genetically edit RTT lines; we took healthy control lines from the Personal Genome Project Canada (PGPC) (Hildebrandt et al, 2019) and used a CRISPR plasmid based method to create both a 1bp insertion in *MECP2* leading to an early stop and a 51bp in-frame deletion in the methyl binding domain of *MECP2* (Mok et al., in prep). Both of these edits result in cell lines null for *MECP2*.

Whether looking at newly generated RTT lines, such as the PGPC NULL/Del lines, or patient derived iPSC lines, the use of well-established RTT phenotyping techniques is vital in understanding the effects of the genotype on the cells. The mutations themselves can be determined by using gDNA and cDNA sequencing, however more complicated techniques must be used to understand the effect on phenotype. To examine the effect of an RTT mutation on MECP2 levels, there are a number of different assays that can be used. The most common is to use a western blot analysis to label the protein of interest with primary and secondary fluorescent antibodies on a membrane (Djuric et al., 2015) and examine the blot for protein quantity differences between WT and RTT. Another way to examine for protein is to use the relatively newer In Cell Western (ICW) analysis which fixes cells of interest to a plate and stains the protein of interest with primary antibodies and secondary fluorescent antibodies. The level of fluorescence is then normalized to the number of cells in the well of the plate, allowing a comparison between WT and RTT (Egorina et al., 2005; Nageshappa et al., 2016). The benefit of an In-Cell Western is the ability to examine large batches of cells at one time by using 96 well plates, making it a viable protein assays for large scale drug scenes or related assays.

In addition to the effect that genotype has on protein levels, RTT literature has a number of key phenotypes that can be searched for when dealing with RTT iPSC-derived neurons. Morphology is often a key aspect of RTT phenotype. These assays are performed by labelling the neurons of interest with a green fluorescent protein (GFP) (Moriyoshi et al., 1996; Knott et al., 2009; Djuric et al., 2015) and images are taken of each neuron. These images can then be traced manually or automatically and relevant morphometric analyses are taken. For example, soma size is determined by tracing the area of the soma and dendrite length is determined by summing the length of all dendrites in a single neuron together (Marchetto et al., 2010; Li et al., 2013; Djuric et al., 2015). There are two assays used to measure dendrite complexity. For a Sholl analysis, one starts at the soma and then draws concentric, evenly spaced circles outward and counts the number of times each circle is ‘cut through’ by a dendrite (Sholl, 1953; Li et al., 2013; Bird & Cuntz, 2019). For a dendrite order analysis, the primary dendrite is traced until a branch point is reached. Both the branches off the primary are labelled secondary and followed until another branch point, these branches are labelled tertiary. This process continues until the end of the dendrite (Abdel-Maguid & Bowsher, 1984; Costa et al., 2010; Reitveld et al., 2015.) Finally, an examination of electrophysiology is common phenotype of RTT lines with patch-clamp analysis

finding deficits in RTT. However, the appearance of the new multi-electrode array (MEA) provides a less individualized way of examining electrophysiology. iPSCs of interest are plated and differentiated in wells with microelectrodes on the bottom and their extracellular electrophysiological signal is tracked over the duration of the experiment. Research has found that RTT lines typically display less activity, less action potentials, and less network bursting in both duration and frequency (Li et al., 2013; Nageshappa et al., 2016; Mok et al., in prep).

With these types of phenotyping assays, the link between genotype and phenotype can be further examined. For example, in our PGPC CRISPR edited lines our results indicate that both of these null lines show the expected reduction in soma size, dendrite length, dendrite complexity, and electrophysiology (Mok et al., in prep), indicating that these lines match the phenotypic severity of other established null lines (Marchetto et al., 2010; Cheung et al., 2011; Li et al., 2013). Overall, the combination of these phenotyping tools with the ability to generate patient-derived iPSC lines and CRISPR iPSC lines allows researchers to continually uncover new characteristics of RTT mutations and how various mutations alter the severity of RTT.

1.7 Thesis Rationale

We continue to discover new *MECP2* mutations that lead to RTT in patients however it is not yet clear if they all share the same core alterations in gene expression and neuronal function. For this project, our lab obtained iPSC lines from an RTT patient with a novel L124W *MECP2* (c.317T>G) mutation in the crucial methyl binding domain (Figure 5) and with unknown neuronal consequences. Recent research has shown that the methyl binding domain is one of two key domains required for *MECP2* to function (Tillotson et al., 2017). While patient information is limited, the patient does have a milder RTT phenotype and was diagnosed at a relatively later age. Interestingly, results from John Vincent's group on the ability of L124W MECP2 to bind heterochromatin through the over-expression of point mutant-GFP fusions in mouse cells (Sheikh et al., 2017), shows that the L124W mutation has an intermediate phenotype that minimally disrupts heterochromatin foci and has only transitory heterochromatin binding (Mok et al., in prep). WT-MECP2 fusion protein was shown to bind tightly to DAPI rich chromocenters while more severe L124F or R106C fusion proteins showed diffuse localization throughout the cell. The L124W MECP2 fusion showed an intermediate phenotype where GFP bound chromocenters showed hazy, less distinct boundaries (Mok et al., in prep). The Vincent

lab also used Fluorescence Recovery After Photobleaching on the L124W MECP2 GFP bound chromatin and found that the L124W mutation was more mobile and recovered after ten seconds while the WT was still bleached by 100 seconds. This implies that the L124W MECP2 is only transiently bound to the heterochromatin and is easily replaced with non-bleached MECP2 nearby. As such, these experiments indicate that the L124W mutation may have a less severe phenotype relative to other mutations and that the L124W mutation may create a binding change in MECP2 (Mok et al., in prep).

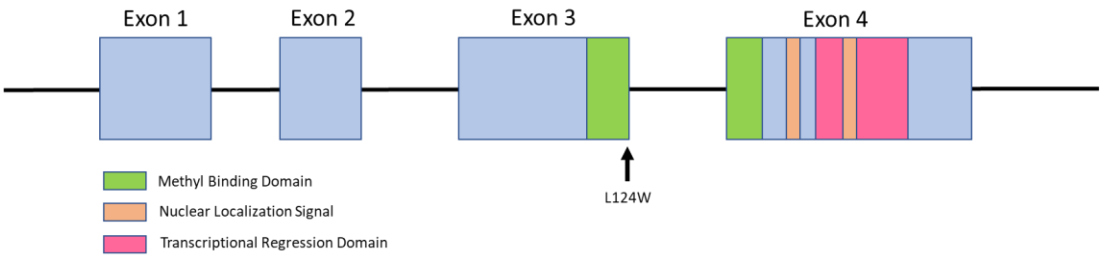

Figure 5. Location of the L124W Mutation. The L124W (c.317T>G) mutation is located at the very end of exon 3 in the middle of the methyl binding domain (green).

The goal of this project was to better understand the novel L124W mutation. Based on the results from the Vincent lab (Mok et al, in prep) and our knowledge that the L124W mutation is not a null, we posited that perhaps the L124W mutation would have a less severe or intermediary phenotype. As such, the first aim was to investigate a number of core RTT phenotypes including protein level, soma size, dendrite length, dendrite complexity, dendrite order, and extracellular electrophysiology. To follow-up on this goal, the second aim of this project was to rescue the L124W mutation through CRISPR/Cas9 gene editing. By achieving a successful L124W rescue line, we would be able to determine if a genetic rescue is enough to eliminate any phenotypes found in Aim 1. This would ultimately provide confirmation that the L124W mutation is causative while providing a high-quality control for future experiments. In addition, the CRISPR/Cas9 protocol developed in this aim could be used in other gene editing experiments, such as targeting other prominent proteins regulated directly or indirectly by MECP2.

Chapter 2
Materials and Methods

2 Materials and Methods

2.1 Cell Culture

hiPSC and hESC were cultured on plates coated with Matrigel (Corning) and maintained in StemMACS iPS-Brew (Miltenyi) or Complete mTeSR (STEMCELL Technologies) with 100X penicillin and streptomycin (Gibco). Pluripotent cells (hiPSC and hESC) were detached with ReLeSR (STEMCELL Technologies) and passaged once per week. All human patient derived iPSC and hESC were cultured under the approval of the SickKids Research Ethics Board and Canadian Institute of Health Research Stem Cell Oversight Committee.

2.2 Neuronal Differentiation

This project used three distinct neuronal differentiation methods. The primary method, a transcription factor-based differentiation using *neurogenin-2*, was based on Zhang et al., (2013). The secondary method, a rosette-based differentiation, was based on Brennand et al., (2011). Finally, I briefly experimented with a new protocol using dual SMAD inhibition that we refer to as the 6F protocol (Ross et al., 2020).

2.2.1 Transcription Factor Differentiation

To establish cell lines with inducible *Ngn2*, two lentiviral vectors, rtTA and TetO-*Ngn2*, were packaged and transduced into target lines as per Hotta et al., (2009). Briefly, flasks were seeded with $7.5x10^6$ 293T cells each in 10% FBS (10X; Gibco) with 1% 100X Penicillin/Streptomycin (100X; Gibco) in DMEM (Gibco). The following day, the 293T cells were transfected using Lipofectamine 2000 (Thermo Fisher) with 10µg Gag-pol, 10 µg Tat, 10 µg Rev, 5 µg VSV-G and 15 µg of either rtTA or TetO-*Ngn2*. The media was changed and the virus-containing media was harvested. The virus was concentrated by ultracentrifugation at 90,000G for 2 hours, divided into 10 µl aliquots, and stored at -80C.

Target iPSCs were washed with PBS (1X, Wisent), aspirated, and then detached with accutase (Innovative Cell Technologies) and incubated for 10 minutes at 37C. Cells were transferred to a

15mL falcon tube along with 5mL of mTeSR (STEMCELL Technologies) and ROCK inhibitor (1000X; STEMCELL Technologies) before being centrifuged at 123 RCF for 2 minutes. Cells were then aspirated and resuspended in mTeSR (STEMCELL Technologies) and ROCK inhibitor (1000X; STEMCELL Technologies). Cells were counted and seeded on Matrigel (Corning) at $3.0x10^5$ cells per 6-well plate. The following day, iPS cells were infected with 5µL of concentrated virus and subsequent daily media changes were used to wash away virus.

To induce neuronal differentiation, previously infected cells were seeded in 6-well plates on Matrigel (Corning) at a concentration of $5.0x10^5$ cells per well. Cells were then cultured in CM1 Complete base media [DMEM-F12 (Gibco), N2 (100X; Gibco), NEAA (100X; Gibco), Penicillin/Streptomycin (100X; Gibco), Laminin (1000X; Sigma-Aldrich)] with BDNF (10000X; Peprotech), GDNF (10000X; Peprotech), Doxycycline (1000X; Sigma-Aldrich), and ROCK Inhibitor (1000X; STEMCELL Technologies). On day 3, the cells were switched to CM2 Complete base media [Neurobasal (Gibco), B27 (50X; Gibco), Glutamax (100X; Gibco), and Penicillin/Streptomycin (100X; Gibco) with BDNF (10000X; Peprotech), GDNF (10000X; Peprotech), Doxycycline (1000X; Sigma-Aldrich), laminin (1000X; Sigma-Aldrich) and ROCK Inhibitor (1000X; STEMCELL Technologies). This was repeated for three days with the addition of 2µg/mL of puromycin (500X; Sigma-Aldrich) from days 2 to 4. On day 5 puromycin was removed and AraC (50X; Sigma-Aldrich) was added. On day 7 cells were reseeded as to the specific conditions of their chosen assay.

2.2.2 Rosette-Based Differentiation

Pluripotent stem cell colonies were detached from Matrigel (Corning) coated plates using warmed collagenase IV (Invitrogen) and harvested colonies were transferred to 1x100mm low cluster dishes at a density of 1:1. Cells were then cultured in EB media [DMEM/F12 (Gibco), N-2 (100X; Gibco), NEAA (100X; Gibco), Penicillin/Streptomycin (100X, Gibco) Heparin (2µg/mL; Sigma-Aldrich), FGF2 (10ng/mL; R&D Systems), Dorsomorphin (2µM; Sigma-Aldrich), and SB431542 (10µM; Stemgent)] for 7 days before they were transferred to plates coated in Poly-L-Ornithine (0.1mg/mL; Sigma-Aldrich) and Laminin (20 µg/mL; Sigma-Aldrich). To promote the formation of primary neural rosettes, cells were cultures in adherent conditions and maintained in Neural Rosette media (DMEM/F12 (Gibco), N-2 (100X; Gibco), NEAA (100X; Gibco), Penicillin/Streptomycin (100X; Gibco), Heparin (2µg/mL; Sigma-

Aldrich), FGF2 (10ng/mL; R&D Systems), and Laminin (1µg/mL; Sigma-Aldrich) for another 7 days. The primary neural rosettes were then manually resected with a p20 micropipette tip and needle before they were transferred to poly-L-ornithine/laminin coated plates and cultured in NPC media [DMEM/F12 (Gibco), N-2 (100X;Gibco), NEAA (100X; Gibco), Penicillin/Streptomycin (100X;Gibco), Heparin (2µg/mL; Sigma-Aldrich), FGF2 (10ng/mL; R&D Systems), Laminin (1µg/mL; Sigma-Aldrich) and B27 without Vitamin A (50X; Gibco).

To transition NPCs towards a neuronal fate, cells were seeded at $5x10^4$ cells per well in a 24 well plate coated in poly-L-ornithine/laminin and switched to cND media [Neurobasal (Gibco), N-2 (100X;Gibco), NEAA (100X;Gibco), Penicillin/Streptomycin (100X;Gibco), Laminin (1µg/mL; Sigma-Aldrich), B27 without Vitamin A (50X; Gibco), BDNF (10ng/mL; Peprotech), GDNF(10ng/mL; Peprotech), IGF-1 (10ng/mL; Peprotech), ascorbic acid (200ng/mL; Sigma-Aldrich), and cAMP (1µM; Sigma-Aldrich). cND media was subsequently changed every other day.

2.2.3 6F – Dual SMAD inhibition

For neural induction, the pluripotent stem cells were cultured in mTESR1 (Stem Cell Technologies) and the media was refreshed exactly 15 minutes before starting the protocol. The cells were then detached using accutase (Innovative Cell Technologies) at 37°C and gently tapped until the majority of the cells were floating. Cells were centrifuged at 300G for 2 minutes, aspirated, and resuspended to a 10X volume in mTESR1 (Stem Cell Technologies). The cells were then counted with a Countess (Invitrogen). 100,000 cells were then plated in N2B27 SB/LDN Media [DMEM-F12 (1X; Gibco), Neurobasal (1X;Gibco), N2 (0.5X;Gibco), B27 Supplement with Vitamin A (0.5X; Gibco), Glutamax (2mM;Gibco), Beta-mercaptoethanol (0.1mM; Sigma-Aldrich), SB431542 (10µM; Stem Cell Technologies), LDN193189 (100nM; Sigma-Aldrich)] with an addition of ROCK Inhibitor (10µM; STEMCELL Technologies) for the first night. Media was then changed every second day.

Once neuroepithelial-like stem cells (NES) were apparent, they were detached with EDTA (500µM; Invitrogen) in PBS (1X; Wisent). The EDTA solution was then aspirated and the cells were washed with DMEM-F12 (Gibco) containing 0.1% BSA (Gibco). The cells were diluted to 5mL, centrifuged at 150G for 2 minutes, aspirated, and resuspended as ‘cell clumps’ in 6F media [DMEM-F12 (1X; Gibco), Neurobasal (1X;Gibco), N2 (0.5X;Gibco), B27 Supplement with

Vitamin A (0.5X; Gibco), Glutamax (2mM;Gibco), Beta-mercaptoethanol (0.1mM; Sigma-Aldrich), K02288 (100nM;Sigma-Aldrich), AKTiVIII (100nM; Millipore), MK2006 (AKT1/2/3i) (75nM; Sigma-Aldrich), XAV939 (1µM; Sigma-Aldrich)] with an addition of ROCK Inhibitor (10µM; STEMCELL Technologies) for the first three passages. These cells were plated at 300x103 cells per cm2 in the 6F media with both CHIR99021 (2µM; Sigma-Aldrich) and XAV939 (1µM; Sigma-Aldrich) added.

For neural differentiation, the NES cells were plated at $5x10^4$ cells per cm^2 on laminin (Sigma-Aldrich) coated plates in Neural Differentiation I Media [DMEM-F12 (1X; Gibco), Neurobasal (1X;Gibco), N2 (0.5X;Gibco), B27 Supplement with Vitamin A (0.5X; Gibco), Glutamax (2mM;Gibco), Beta-mercaptoethanol (0.1mM; Sigma-Aldrich)]. The media was changed every other day and on day 14 the cells were dissociated with accutase (Innovative Cells Technologies) and re-plated onto a coating of laminin (Sigma-Aldrich) and poly-ornithine (1µg/cm2; EMD-Millipore) at a concentration of $1\text{-}5x10^4$ cells per cm^2 in Neural Differentiation II Media [DMEM-F12 (1X; Gibco), Neurobasal (1X;Gibco), N2 (0.5X;Gibco), B27 Supplement with Vitamin A (1X; Gibco), Glutamax (2mM;Gibco), Beta-mercaptoethanol (0.1mM; Sigma-Aldrich), BDNF (10ng/mL; Peprotech), Forskolin (10µM; Simga-Aldrich]. Half of the media was replaced every 2 days as neurons formed.

2.3 RNA Analysis

RNA was extracted from iPSCs or 4-week-old neurons by washing them in 1X PBS (Wisent) and then adding TRIzol Reagent (Ambion by Life Technologies) to the aspirated pellet. Chloroform (Anachemia) was added according to Invitrogen's TRIzol Reagent Protocol and the mixture was centrifuged in a fume hood for 15 minutes. The colourless upper aqueous layer was taken and the RNA precipitated into a white gel pellet. The pellet was cleaned with 75% ethanol and then air dried for 10 minutes. Finally, the pellet was resuspended in 35µL of sterile water (Multicell).

To reverse transcribe the RNA into cDNA, the RNA concentration was first determined by a NanoDrop Microvolume Spectrophotometer. The Deoxyribonuclease I Kit (Invitrogen) was used to prepare the RNA for reverse transcription. Briefly, the RNA was mixed with DNase I (Invitrogen) for 15 minutes at room temperature before DNase inactivation by 25mM EDTA (Invitrogen). First-Strand synthesis was then performed using random hexamers (Invitrogen)

followed by reverse transcription with SuperScript III Reverse Transcriptase (Invitrogen) to generate cDNA.

For RNA analysis by qRT-PCR, cDNA was serially diluted into 10X, 100X, and 1000X dilutions in sterile water (Multicell) and placed into a SYBR Select PCR Master Mix (Applied Biosystems). Fold changes were calculated by the ΔΔCt method using 18S rRNA as a house-keeping gene and results were averaged between technical and biological replicates.

2.4 Protein Analysis

To extract protein, cells on ice were washed with ice cold PBS (1X; Wisent) and aspirated. Total protein was extracted in radioimmune precipitation assay (RIPA) buffer [25mM Tris-HCL, 150mM NaCl, 1% Nonidet P-40, 1% Sodium deoxycholate, 0.1% SDS] with Halt Protease Inhibitor Cocktail (100X; Thermo Fisher) and Phosphatase Inhibitor Cocktail (100X; Thermo Fisher). Pellets were then sonicated at level 3 for 10 seconds and stored at -80C.

Protein levels were quantified by the BioRad DC Protein Assay (BioRad). Standard curves were set up with BSA and desired proteins in duplicate using a starting concentration of 2mg/mL. All antibody information is listed in Table 1.

Antibody	Company	Species	Use
anti-puromycin	Kerafast	Mouse	ICW
anti-ß-Actin	Sigma	Mouse	WB/Wes
DAPI	Sigma		ICC
MAP2	Synaptic Systems	Guinea Pig	ICC
MECP2	Cell Signaling	Rabbit	ICC/ICW/WB
NEDD4-2	Abcam	Rabbit	WB/Wes
PSD95 (SAP-90)	Neuromab	Mouse	ICW

Table 1. Antibodies Used In Protein Assays. This table lists all of the antibodies used in this report. The ‘Use’ column indicates the type of assay that the antibody has been used in ICW stands for In Cell Western, WB stands for Western Blot, ICC stands for Immunocytochemistry, and Wes stands for the Wes Analysis.

2.4.1 Western Blot

For western blot analysis, proteins were prepared to a concentration of 30µg per lane and mixed with Bolt 10X Sample Reducing Agent (Thermo Fisher) and Protein Loading Buffer 4X (LI-COR). Samples were boiled at 75C and then loaded in equivalent protein mass into a Bolt 4-12% Bis-TRIS Plus 12 Lane gel (Invitrogen). The gel was run for ~1 hour at 180V. The protein was then transferred to a Hybond ECL (GE Healthcare) nitrocellulose membrane through overnight transfer at 60V. The membrane was then trimmed and washed in REVERT 700 Total Protein Stain (LI-COR) for scanning in the 700 channel of the Li-Cor Odyssey CLx. The stain was removed with Revert Destaining Solution (LI-COR). The membrane was allowed to incubate in either 5% Skim Milk or 5% BSA (Sigma Aldrich) in PBS (1X; Wisent) for the duration of the day. The membrane was then packaged with primary antibodies and either 5% Skim Milk or 5% BSA (Sigma Aldrich) in PBS-T [PSB (1X; Wisent), Tween-20 (1%; Sigma Aldrich)]. The following morning, the membrane was washed three times with PBS-T [PSB (1X; Wisent), Tween-20 (1%; Sigma Aldrich)] and packaged for 1 hour with near-infra red-conjugated secondary antibodies in either 5% Skim Milk or 5% BSA (Sigma Aldrich) in PBS-T [PSB (1X; Wisent), Tween-20 (1%; Sigma Aldrich)]. The membrane was then imaged in the Li-Cor Odyssey CLx in both the 700 and 800 channels and analyzed using ImageStudio.

2.4.2 WES

The WES (ProteinSimple) is a capillary based western blot and all assays were carried out according to the ProteinSimple protocol. The samples were diluted in 0.1X Sample Buffer (ProteinSimple) and combined with the Fluorescent Master Mix (ProteinSimple) for a final concentration of 0.4mg/mL. The proteins were denatured with heat and the Jess/Wes 12-230 kDa Pre-filled Plates with Split Buffer (ProteinSimple) were set up with the biotinylated ladder, antibody diluent, primary antibody, Streptavidin-HRP, secondary conjugate, and the luminol-peroxide mix (all from ProteinSimple). The protein mix was added to the plate and the plate was run in the Wes for 3 hours.

2.4.3 In Cell Western

Cells were left in 12 well plates and washed with PBS (1X; Wisent) before they were left for 15 minutes in 4% paraformaldehyde (PFA) [dd$H_2$0, PBS (1X; Wisent), PFA (4%; Sigma Aldrich) for fixation. Once cells were fixed, the PFA was removed and the wells were washed 3 times for

5 minutes each with 1X PBS (Wisent) with 0.1% Triton X-100 (Sigma Aldrich). Wells were aspirated manually and Odyssey Blocking Buffer PBS (LI-COR) was added for 1.5 hours at room temperature. The primary antibody dilution was made in Odyssey Blocking Buffer PBS (LI-COR) and pipetted into all experimental wells while the blocking buffer without antibody was added to control wells. Plates were then incubated at 4°C overnight. In the morning, the wells were washed 3 times with 1X PBS (Wisent) with 0.1% Tween-20 (Sigma Aldrich). The fluorescent secondary antibodies (LI-COR) were diluted in Odyssey Blocking Buffer PBS (LI-COR) alongside CellTag 700 Stain (LI-COR). The secondary with CellTag 700 Stain (LI-COR) was added to experimental wells while secondary only was added to the control wells. Plates were wrapped in aluminum foil and incubated at room temperature for 1 hour. Wells were washed 3 times with 1X PBS (Wisent) with 0.1% Tween-20 (Sigma Aldrich) and then imaged in both the 700 and 800 channels on the LiCor Odyssey CLx with ImageStudio.

For the puromycin incorporation assay, cells received 1µg/µL of puromycin for 1 hour. The ICW protocol was then started as normal.

2.4.4 Immunocytochemical Staining

Immunocytochemical Staining (ICC) was performed in µ-Plate 24 well black plates (Ibidi). Cells were fixed for 15 minutes in 4% paraformaldehyde (PFA) [dd$H_2$0, PBS (1X; Wisent), PFA (4%; Sigma Aldrich) and then washed 3 times for 5 minutes each in PBS (1X; Wisent). A permeabilization solution was prepared [0.1% Triton X-100 (Sigma Aldrich), PBS(1X; Wisent)] and placed on the cells for 8 minutes at room temperature. Wells were aspirated and blocking solution was added [PBS (1X;Wisent), 0.1% Triton X-100 (Sigma Aldrich), 10% Goat serum (Sigma Aldrich)] for 1 hour. Primary antibodies were then diluted in PBS (1X;Wisent), 0.1% Triton X-100 (Sigma Aldrich), and 5% Goat serum (Sigma Aldrich)], placed in the wells, and left at 4°C overnight. In the morning, wells were washed 2 times with PBS (1X;Wisent) containing 0.1% Triton X-100 (Sigma Aldrich). Secondary antibodies were diluted in PBS (1X;Wisent) containing 0.1% Triton X-100 (Sigma Aldrich) and placed in the wells for 1 hour at room temperature. Plates were protected from light from this moment forward. The secondary solution was removed and wells were washed with PBS (1X;Wisent) containing 0.1% Triton X-100 (Sigma Aldrich). DAPI (2mg/mL;Thermo Fisher) was diluted in PBS (1X;Wisent) containing 0.1% Triton X-100 (Sigma Aldrich) and placed in the wells for 5 minutes. Wells were

then washed with PBS (1X;Wisent) containing 0.1% Triton X-100 (Sigma Aldrich) and stored in a final solution of only PBS (1X, Wisent). Images were acquired on the Leica DM14000B epifluorescence microscope using a DFC7000T camera and LAS X software (Leica).

2.5 Neuronal Morphometric Analysis

Neuronal morphology assays were performed on neurons differentiated for 6 weeks *in vitro* according to the transcription factor differentiation (Zhang et al., 2013). Prior to fixation, neurons were transfected with the EF1αEGFP plasmid through Lipofectamine 2000 (Invitrogen). Cultures were exposed to the transfection mixture over night (~16hrs) before the mixture was replaced with fresh media. Neurons were fixed in PKS [4% PFA in Krebs-Sucrose buffer, 50 mM KCl, 1.2 mM CaCl2, 1.3 mM MgCl2, 20 mm HEPES pH 7.4, 12 mM NaH2PO4, 400 mM sucrose, 145 mM NaCl, 10 mM glucose in water] and imaged in 10 micron stacks with an Olympus 1X81 spinning disk confocal microscope using a Hamamatsu C9100-13 EM-CDD camera and Volocity software (Perkin Elmer). All images were then blinded by an outside source and analyzed in Imaris (Bitplane).

In Imaris (Bitplane), the images were projected to 2D and flattened. Then the soma of each neuron was manually traced using the surface tool. For dendrite tracing, I used semi-automated reconstruction on sparsely labelled GFP neurons that were co-stained with MAP2. Using this tracing, sholl results were exported through the auto-generated filament statistics. A series of concentric circles were drawn starting with the soma outward, at a distance of 10µm increments. The number of intersections between the traced dendrites and the circles was then counted by Imaris (Bitplane). Dendrite order was manually counted and assessed.

2.6 Multi-Electrode Array

For plating on the cytoview MEA 12 well plates (Axion Biosystems), I followed the transcription factor differentiation method described in 2.2.1 until day 7 when the CM2 base media was switched to BrainPhys Neuronal Media (Stem Cell Technologies) instead of the Neurobasal (Gibco) described above. Cells were reseeded at a density of $1x10^5$ cells per 100µL droplet. Droplets were placed directly on top of the electrodes in each well and incubated for 1 hour at 37°C before additional CM2 BrainPhys media with extra lamin (10µg/mL; Sigma Aldrich) was slowly added. Plates had been previously coated in 0.1% poly(ethylenimine)

solution (Sigma Aldrich) in borate buffer pH 8.4 for 1 hour at room temperature. Plates were then washed 4 times in water and left to drive overnight.

One day after reseeding, $2x10^4$ mouse astrocytes were seeded on top of the neurons located in each well. Cells were fed twice a week, directly 24 hours prior to recordings on the Maestro MEA platform (Axion Biosystems). For recordings, plates were removed from their 37°C incubators and plates in the machine for 5 minutes to acclimatize on a 37°C heated pad. Each plate was then recorded using AxIS 2.0 software (Axion Biosystems) under the same conditions over a 5-minute period. Spikes were detected based on a calculation of 6x the standard deviation of the noise inherent in the spontaneous activity. Plates were then returned to their 37°C incubator until the next recording. Plates were tested two times a week over a period of 6 to 8 weeks. Data analysis used the Neural Metric Tool (Axion Biosystems). Electrodes were considered active if more than 5 spikes/minutes were detected under the conditions of a poisson surprise burst. Further analysis was performed in R Studio.

2.7 Sequencing

2.7.1 gDNA

DNA was extracted from cells by washing them in 1X PBS (Wisent) and leaving them in accutase (Innovative Cell Technologies) for 7 minutes. The accutase was deactivated with a small amount of media [StemMACS iPS-Brew (Miltenyi)] and cells were scraped from the bottom of the well as necessary. The cell solution was extracted with a pipette and spun down at 123RCF in the Beckman Coulter Allegra X-22R Centrifuge for 4 minutes. The pellet was aspirated and frozen at -20°C. Samples were then prepared according to the Quick-DNA Miniprep Kit (Zymo).

Samples then proceeded directly to PCR (polymerase chain reaction) using either the platinum taq kit (Invitrogen) or the hifi taq kit (Invitrogen) and final results were run on a 1% agarose gel with ethidium bromide. The resulting PCR product was then sent to the TCAG facility for sequencing.

2.7.2 cDNA

To sequence cDNA, RNA was first extracted as descripted in section 2.3 RNA analysis. 1µg of RNA was taken and was digested with Deoxyribonuclease I (1U/µl;Invitrogen) for 15 minutes

before the mixture was inactivated with EDTA solution (25mM; Invitrogen). The solution was heated to 65°C for 10 minutes and then put through the SuperScript III First Strand Synthesis System (Invitrogen). In brief, 5.5µL of the solution was mixed with random hexamers (50ng/µL; Invitrogen) and a dNTP mix (10mM; Invitrogen) for 5 minutes at 65°C and then put on ice. 5X First Strand Buffer (Invitrogen), DTT (0.1M; Invitrogen), and SuperScript II RT (200U/µL; Invitrogen) were added to the solution. The solution was then heated to 25°C for 5 minutes, 50°C for 1 hour, and 70°C for 15 minutes before the final cDNA was used or stored at -20°C.

Samples then proceeded directly to PCR (polymerase chain reaction) using either the platinum taq kit (Invitrogen) or the hifi taq kit (Invitrogen) and final results were run on a 1% agarose gel with ethidium bromide. The resulting PCR product was then sent to the TCAG facility for sequencing.

2.8 X Chromosome Inactivation Status

To determine X chromosome inactivation status, the androgen receptor assay was used (Cheung et al., 2011; Shabazian et al., 2010). As all cell lines of interest were female, a male PGPC control line was also used. All gDNA was diluted to 100ng/µL and a total of 500ng of gDNA was used. To digest the gDNA a mixture of CutSmart Buffer (New England Bio Labs), with methylation sensitive enzymes Hpall and Hhal was used. An undigested control without Hpall and Hhal was also prepared. To ensure complete digestion, the mixtures were incubated for 6 hours and then heated to 65°C for 20 minutes in the morning. The samples were then processed through PCR using the HiFi Taq Kit (Invitrogen) with the fluorescently labelled ARF primer and the ARR primer. The PCR products were visualized on a 2.5% agarose gel with ethidium bromide. Samples were sent to TCAG for Genetic Analysis electrophoresis. Results were analyzed with Peak Scanner software (Thermo Fisher).

2.9 CRISPR Protocols

The CRISPR protocols used in this project are based on the protocol described in Hildebrandt et al., 2019 with some modifications. For all experiments, CRISPR guide choices were determined used the tools and algorithms provided by the online Benchling software. All oligos were ordered from IDT Industries.

2.9.1 sgRNA and ssODN Based

This process was primarily used to attempt CRISPR corrections or single base changes.

On the day of nucleofection, all the ordered components were prepared. The synthetic crRNA (IDT) was resuspended at 1.4µg/µL in nuclease-free duplex buffer at 4°C and the tracrRNA (IDT) was resuspended in the same way at 2.6µg/µL. Then 4µL of each RNA was taken and combined to form the sgRNA through heating the RNAs to 60°C for 15min, 37°C for 30 minutes, and then cooling to RT. The single-stranded guide oligo (ssODN) (IDT) was resuspended at 200pmol/µL. Once the sgRNA cooled to RT, 4µL was removed and combined with 0.4µL of NaCl and 2µL (20µg) of alt-R S.p. HiFi Cas9 Nuclease V3 (IDT). This Cas9 RNP complex was left for 30-45 minutes while the rest of the nucleofection was set up.

For nucleofection, a six well plate was coated with Matrigel (Corning) and 100 CloneR Media which was made of 19.8mL of complete iPS Brew MACs media [iPS Brew MACs (Miltenyi), penicillin (100X;Gibco), streptomycin (100X;Gibco)] with an additional 2.2mL of CloneR (2.2mL; Miltenyi)]. The cells of interest were washed with PBS (Wisent) and then lifted with an accutase (Innovative Cell Technologies) incubation of 7 minutes at 37°C. Cells were shaken to ensure lift and then inactivated with complete iPS Brew MACs media [iPS Brew MACs (Miltenyi), penicillin (100X;Gibco), streptomycin (100X;Gibco)] in a falcon tube. The tubes were centrifuged at 123RCF for 4 minutes and the resulting pellet aspirated, resuspended in 1mL of media and then counted in the Countess. 800,000 cells were taken for each nucleofection and moved into microcentrifuge tubes where they were pelleted at 0.3G for 3 minutes.

The Neon Transfection System (Invitrogen) was then turned on and prepped. As per the directions of the 100µL kit, 3mL of E2 (Invitrogen) was pipetted into the Neon 100µL Tube (Invitrogen) and clicked into the Neon Transfection System (Invitrogen). One tube was used for each transfection unless there was a duplicate transfection wherein the same tube was used a maximum of twice. The cell pellets were aspirated. The Cas9 RNP which had been incubating during the above process had 105µL of R Mixture (Invitrogen) added. In addition, 1µL of the ssODN was added to this tube. Then the whole solution was taken up using the Neon Pipette (Invitrogen) and the Neon 100µL pipette tips (Invitrogen) and used to resuspend the cell pellet. Using the Neon pipette and tips, the cell mixture was slowly mixed. Then, careful as to ensure no bubbles entered the tube, the full amount of mixture was taken into the pipette tip. The pipette

was clicked into the Neon Transfection System (Invitrogen) and the nucleofection run with 1 pulse of 1300V for 30ms. If a flash was seen, the cells were discarded and the protocol was repeated with fresh cells. The nucleofected cells were then transferred into two wells of a six well plate filled with 100 CLoneR Media.

On the day following nucleofection, the cells were left untouched in the incubator. On day 2, the cells received fresh 100 CLoneR Media. On days 3 and 4, the cells received fresh 25 CloneR media [75% iPS Brew MACs (Miltenyi), penicillin (100X;Gibco), streptomycin (100X;Gibco), 25% 100 CLone R media]. On all subsequent days, the cells received iPS Brew Macs media as per their usual schedule. The cells were allowed to grow, passaged, and eventually had their genomic DNA extracted for sequencing and further analysis.

2.9.2 Plasmid Based

This plasmid based CRISPR method was used for Knock-Down and Knock-Out experiments such as the *NEDD4L* KO.

This project used the pSpCas9(BB)-2A-Puro (Ran et al., 2013) cloning backbone for sgRNA that is available from AddGene. The vector was digested using *Bbs*I and the guide (a pair of annealed oligos) were cloned scarlessly into the vector (Ran et al., 2013). The preparation of the plasmid was done by Dr. Maria Satori and a stock was frozen down.

Then, I began the process of nucleofection. A six well plate was coated with Matrigel (Corning) and ‘100 CloneR Media’ which was made of 19.8mL of complete mTesR [mTesR (STEM CELL Technologies), penicillin (100X;Gibco), streptomycin (100X;Gibco)] with an additional 2.2mL of CloneR (2.2mL; STEMCELL Technologies)]. The cells of interest were washed with PBS (Wisent) and then lifted with an accutase (Innovative Cell Technologies) incubation of 7 minutes at 37°C. Cells were shaken to ensure lift and then inactivated with complete MTesR [mTesR (STEM CELL Technologies), penicillin (100X;Gibco), streptomycin (100X;Gibco)] in a falcon tube. The tubes were centrifuged at 123RCF for 4 minutes and the resulting pellet aspirated, resuspended in 1mL of media and then counted in the Countess. 800,000 cells were taken for each nucleofection and moved into microcentrifuge tubes where they were pelleted at 0.3G for 3 minutes.

The Neon Transfection System (Invitrogen) was then turned on and prepped in the same way as listed in the 2.9.1 sgRNA and ssODN Based protocol. The cell pellets were aspirated and then resuspended with 105µL of R Mixture (Invitrogen). Once the cells were resuspended, 1.5µg of plasmid was added to the mixture. The solution was gently mixed used the Neon Pipette (Invitrogen) and the Neon 100µL pipette tips (Invitrogen). Then, ensuring no bubbles entered the tube, the full amount of mixture was taken into the pipette tip. The pipette was clicked into the Neon Transfection System (Invitrogen) and the nucleofection run at 1500V for 20ms. If a flash was seen, the cells were discarded and the protocol was repeated with fresh cells. The nucleofected cells were then transferred into two wells of a six well plate filled with 100 CloneR Media.

Cells were allowed to rest in the incubator undisturbed for one day. On the second day, the 100 CloneR media was replaced with 25 CLoneR media [75% mTesR (STEM CELL Technologies), penicillin (100X;Gibco), streptomycin (100X;Gibco), 25% 100 CLone R]. Puromycin selection was also started on this day. Amounts of puromycin varied by cell line and were chosen based on an independent puromycin curve done before each nucleofection. On days 3 and 4 the cells continued to receive fresh 25 CLoneR media with puromycin. On day 5, the puromycin was removed and the cells received only fresh 25 CLoneR media. From day 6 onward, the cells received regular complete mTesR as according to their usual schedule. These cells were then grown and clonally picked to allow future analysis.

2.10 Analysis of the *NEDD4L* KO Lines

After the generation of two new *NEDD4L* KO lines from the PGPC-3 control line, karyotyping and off-target analysis were performed to ensure that no unexpected changes were made during the edit. Karyotype analysis was performed by TCAG. Each cell line was prepared in two 6cm dishes and fed at exactly 10am each morning for three days. On the third day, when the cells were at 50% confluence, they were deposited at the facility for analysis. For off-target analysis the guide portion of the sgRNA was inputted in Benchling software and the software's off-target tool was used to assess for most likely potential off-target locations. Benchling was used as it was the software in which the guide was originally designed. From the list of most likely targets, the two most likely off-target locations were tested by cDNA sequencing (Section 2.7.2).

2.11 Statistics & R Code

2.11.1 Statistical Analysis

All datasets were managed in Microsoft Excel 2019 Home and Student and, unless otherwise noted, all statistical tests were performed in R Studio. All datasets were first tested for normality using the Shapiro Wilks Test. In instances of normality, where only two samples were being compared a student's t-test was used and where three or more samples were compared an ANOVA test was used. However, in most cases, datasets were revealed to be non-normal. As such, nonparametric tests were primarily used. In all such cases, the data was first tested with a Kruskal Wallace test to determine if there was any difference between any of the samples. If more than two samples were being compared and the Kruskal Wallace test showed a significant difference, the data was run through a Dunn Test (Scholl, Dendrite Order, Soma Area, Dendrite Length). In all cases, the significance cut-off was determined to be a p of 0.05.

For the Multi-Electrode Array, bursts were determined by the Axion Software. To find single bursts, a Poisson Surprise algorithm set to a minimum surprise of 3 was used and to determine network bursts and envelope algorithm was used with a minimum electrode percentage of 25. The results outputted by this software were then further analyzed in Excel and R. This analysis included a one sample t-test or two way ANOVA with Bonferroni multiple comparisons.

2.11.2 R Code for Testing Significance

This and the following code are modified from work by Rebecca Mok.

```
head(den_data)
names(den_data)
Summarize(Primary~name, data=den_data)
shapiro.test(den_data$Primary)
kruskal.test(Primary~name, data = den_data)
dunn_list <-
  dunnTest(Primary ~ name,
           data = den_data)
# Extract the dataframe generated  from dunnTest and asign to new dataframe
dunn_df <- dunn_list$res
# Add Sig column if < 0.05. TRUE = reject null hyp
d_list <- mutate(dunn_df, Sig = P.unadj < 0.05)
print(d_list,dunn.test.results=TRUE)
write.csv(
  d_list,
  row.names = FALSE,
```

```
  file = paste(path_data, "TITLE.csv", sep = "/")
)
```

2.11.3 R Code for Graph Creation

```
give.n = function(x) {return(c(y = 20, label = length(x)))}
colour_soma = c("cyan3", "deeppink3", "chartreuse", "chartreuse","darkorchid", "darkorchid")
shape_pro = c("circle","square","triangle")
#circle is bren, square is ngn, 6f triangle

###plot data###

ggplot(data=data_1, aes(x= Line, y= mecp2_quant))+
  geom_boxplot(outlier.shape=NA,
               fatten = 4) +
  geom_jitter(width = 0.2,
              alpha = 0.5,
              size = 4,
              aes(x=Line,
                  y = mecp2_quant,
                  shape = method,
                  colour = Line)) +
  ggtitle("MECP2 Western Blot Protein Results") +
  ylab(expression(paste("Fold Change Relative to WT-1"))) +
  scale_y_continuous(expand = c(0,0),
                     limits = c(0,3)) +
  scale_color_manual(values = colour_soma) +
  scale_shape_manual(values = shape_pro) +
  theme_classic() +
  theme(title = element_text(face = "bold", size = 20),
        plot.subtitle = element_text(face = "plain", size = 20),
        axis.title.x = element_blank(),
        axis.title.y = element_text(size = 24, margin = margin(r = 20)),
        axis.text.x = element_text(size = 24, angle = 45, hjust = 1.05, colour = "black"),
        axis.text.y = element_text(size = 24, hjust = -0.1, colour = "black"),
        axis.ticks.length = unit(0.2, "cm"),
        legend.position = "none")

ggsave(paste(path_base_all, "TITLE.pdf", sep = "/"),
       width = 8,
       height = 6)
```

Chapter 3
Results

3 Results

3.1 Cell Lines Used In This Project

The goal of this project is to understand the phenotype of the L124W mutation, referred to as RTT-3, in comparison to its wild-type control WT-3. To perform this work, two WT-3 lines (WT-3A, WT-3B) and two RTT-3 lines (RTT-3C, RTT-3D) were derived from the L124W patient by Alysson Muotri's group and characterized by Rebecca Mok. All four of these lines were used in the reported assays. These novel lines were then compared to established and new null lines. Control lines include the RTT-1/WT-1 iPSC pair (Cheung et al., 2011), the ESC RTT-2/WT-2 pair (Li et al., 2013), and the newly CRISPR created iPSC PGPC-14 Null and Del lines (Mok et al., in prep) with their PGPC-14 Parental Control (Hildebrandt et al., 2019). The *NEDD4L* CRISPR experiments used the PGPC-3 control line as the base line for gene editing (Hildebrandt et al., 2019) (Table 2).

Line Name	Cell Type	Mutation	Citation
RTT-1/WT-1	iPSC	Null – deletions removing exons 3 &4	Cheung et al, 2011
RTT-2/WT-2	ESC	Null – TALEN edit targeting exon 3	Li et al, 2013
RTT-3/WT-3	iPSC	Missense, point mutation L124W	Mok et al, in prep
PGPC-14 Parental	iPSC	Control Line	Hildebrandt et al, 2019
PGPC-14 Indel Null	iPSC	1bp insertion, premature stop	Mok et al, in prep
PGPC-14 Indel Del	iPSC	51bp in-frame deletion	Mok et al, in prep
PGPC-3 Control	iPSC	Control Line	Hildebrandt et al, 2019

Table 2. Description of Cell Lines Used. Listing line name, type, mutation, and origin of all cell lines used in this project. The RTT-3/WT-3 lines (L124W) are the novel lines of interest.

3.2 X Inactivation Status of WT-3 & RTT-3 Lines

When starting the project, I wanted to determine the current X-inactivation (XCI) status of the WT-3 and RTT-3 lines to ensure that the lines had not been subject to erosion over time. XCI is a

strategy used in mammalian cells to transcriptionally silence one of the X chromosomes in XX creatures to equalize the gene dosage when compared to XY creatures (Escamilla-Del-Arenal et al., 2011). At the onset of XCI, either the maternal or paternal X is randomly silenced through methylation and this X should remain inactivated through all subsequent cell divisions (Escamilla-Del-Arenal et al., 2011). The *MECP2* gene is located on the X-chromosome and is subject to X-inactivation (Zoghbi et al., 1990). While it is worth noting that ~15% of X chromosome genes escape X-inactivation, the majority of escapees are located on the p arm (Carrel & Willard, 2005). As *MECP2* is located on the q arm, the potential effect of gene escape is limited. In Rett syndrome patients, the majority of which are female, this means that one X-chromosome will be wild type while the other will be mutated in the *MECP2* gene. For patient derived iPSCs, all cell lines will randomly have either an active wild type *MECP2* gene or a mutant *MECP2* gene from the patient (Cheung et al., 2011). Each cell line will reflect the status of the original fibroblast from which they were derived (Tchieu et al., 2010), however, it has been shown that over time this XCI can erode in hIPSCs leading to cells that express both mutant and wild type *MECP2* genes (Mekhoubad et al., 2012; Vallot et al., 2015).

Therefore, I used the androgen receptor (AR) endonuclease digestion assay (Cheung et al., 2011) as described in section 2.8 to examine the XCI status of my lines of interest. Briefly, methylation sensitive enzymes were used to digest the active X as the inactive X was protected by its hyper-methylated state. The remaining X was examined through PCR with a fluorescent primer set to amplify the androgen receptor gene. These samples were then genetically analyzed by TCAG using electrophoresis. The androgen receptor is used because it is located on the X chromosome and is made up of polymorphic CAG-tandem repeats that vary between X chromosomes, making the two peaks distinguishable from each other.

The XCI status of the WT-3 and RTT-3 lines was preserved (**Figure 6**). In the undigested control samples that did not receive the methylation sensitive digestion enzymes, two peaks can be seen, indicating that both X chromosomes were still present. In the digested sample, only one peak can be seen in each cell line. This indicates that only 1 X is active in each sample and highlights that the cell lines are not expressing both wild type and mutant MECP2. This assay also shows that the WT-3A and WT-3B skew one way while RTT-3C and RTT-3D skew the other way, indicating that there was no switching of the active X. The wild types remain wild type and the

mutants remain mutant. Finally, the male PGPC3 control line shows complete digestion of the sole X and indicates that the assay is working as expected.

Based on these results, I concluded that the XCI status was not eroded and that the WT-3 and RTT-3 lines were good subjects for further study.

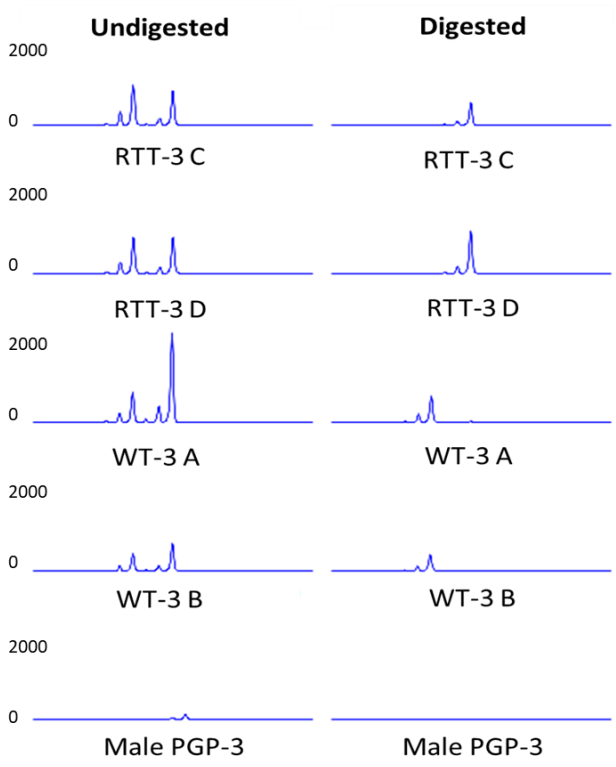

Figure 6. X-Inactivation Status of WT-3 and RTT-3 hiPSCs. Human iPS cells were found to have no changes from the expected XCI status with RTT-3 lines expressing only the mutated *MECP2* X-chromosome and WT-3 lines expressing only the wild type *MECP2* X-chromosome.

3.3 *MECP2* mRNA Levels

As the WT-3 and RTT-3 lines were newly isolated cell lines, my first goal was to establish the phenotypic characteristics of the RTT lines in comparison to their wild type isogenic controls. To do this, I started by examining *MECP2* mRNA levels in iPSCs through quantitative real-time PCR (q-RT-PCR) analysis as listed in section 2.3. Briefly, RNA was processed using TRIzol Reagent (Ambion by Life Technologies) and SuperScript III Reverse Transcriptase (Invitrogen) with random hexamer primers. Then to prep the samples for q-RT-PCR, I used SYBR Select

PCR Master Mix (Applied Biosystems). I analyzed the results with the ΔΔCt method using 18S mRNA as a house-keeping gene.

I found that there was no significant difference between WT-3 and RTT-3 in *MECP2* mRNA levels **(Figure 7)**. This implies that the L124W mutation does not create a change in the level of *MECP2* mRNA in the cells.

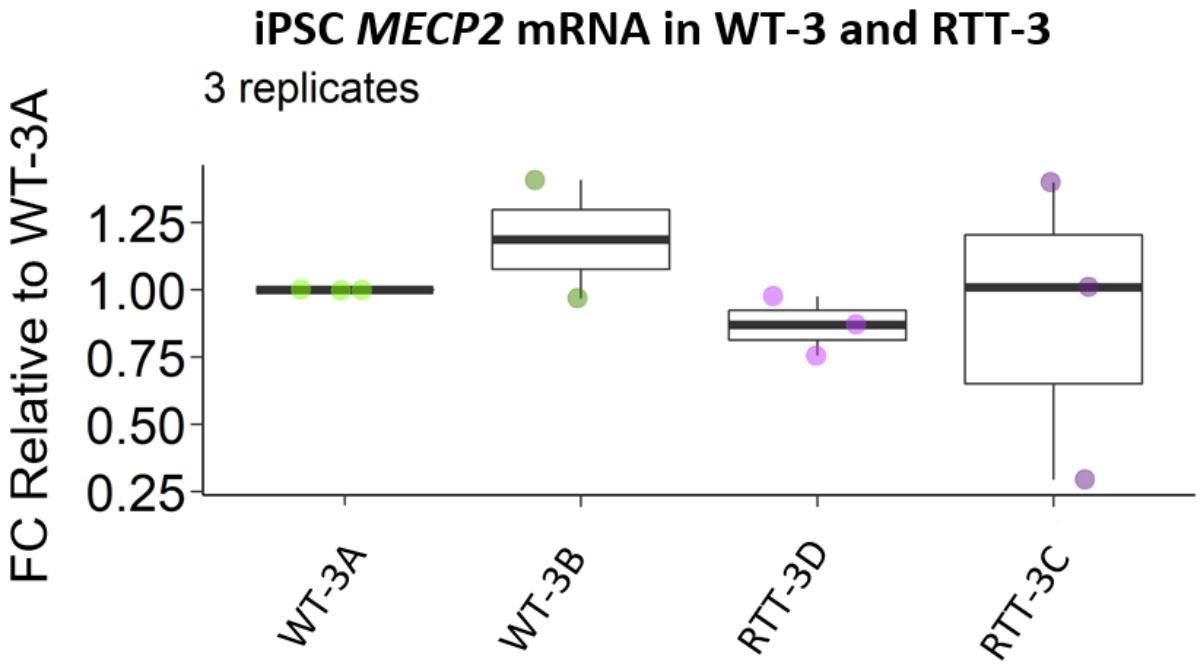

Figure 7. iPSC *MECP2* mRNA in WT-3 and RTT-3. There is no significant difference between WT-3A, WT-3B, RTT-3C, or RTT-3C demonstrating that there is no change in the mRNA of *MECP2* in iPSCs.

3.4 MECP2 Protein Levels

To identify an MECP2 antibody that could be used in both traditional western blot analysis and in In-Cell Western assays, I evaluated the Cell Systems antibody using immunocytochemical staining (ICC). Four-week-old NGN2 WT-1 neurons were fixed and co-stained with DAPI, MAP-2, and the MECP2 antibody (Figure 8) revealing that DAPI and MECP2 colocalize in the nucleus as expected (Koch & Strätling, 2004). The MAP-2 detected dendrites and confirmed that the cells were neurons.

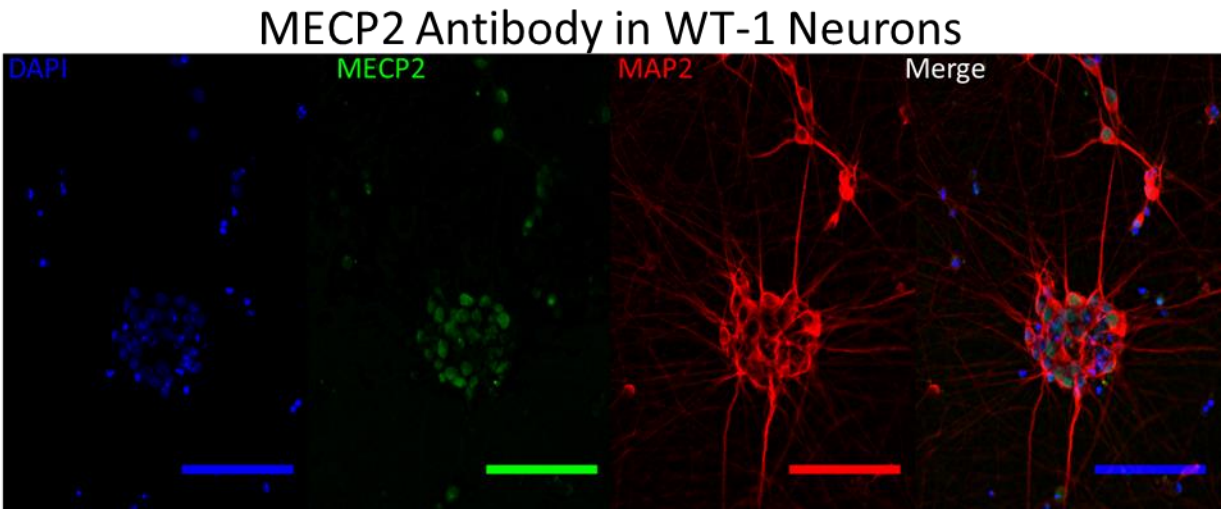

Figure 8. ICC of the new MECP2 Antibody. MECP2 and DAPI colocalize in the soma of the neuron revealing that the new antibody does appear to detect MECP2 protein.

To further validate the antibody, I proceeded to conduct two different protein assays in control and null cells, while attempting to determine if there was any difference in MECP2 protein levels when between WT-3 and RTT-3. With the help of our technicians, I differentiated WT-3 and RTT-3 neurons using three neuron differentiation protocols described in Section 2.2 (NGN2, Brennand, 6F) to isolate protein for western blots. Briefly, total protein was extracted with RIPA buffer and equivalent protein mass was loaded into a Bolt 4-12% Bis-TRIS Plus 12 Lane gel before transfer to a nitrocellulose membrane. The membrane was incubated with primary antibodies overnight and then Near-Infra Red conjugated secondary antibodies; then membrane was then scanned using the LI-COR Odyssey CLx scanner.

A significant difference can be seen in the null RTT-1 and its WT-1 isogenic pair **(Figure 9 A,B,C)** validating the specificity of the antibody. There is no significant difference between WT-3A, WT-3B, RTT-3C, and RTT-3D MECP2, suggesting that the L124W MECP2 protein level is equivalent to WT MECP2 in neurons derived from isogenic iPSC lines.

9A

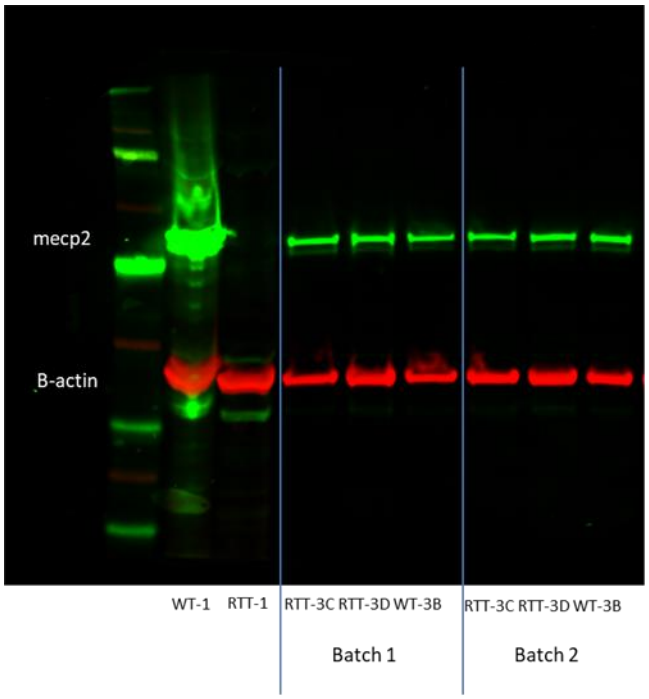

9B

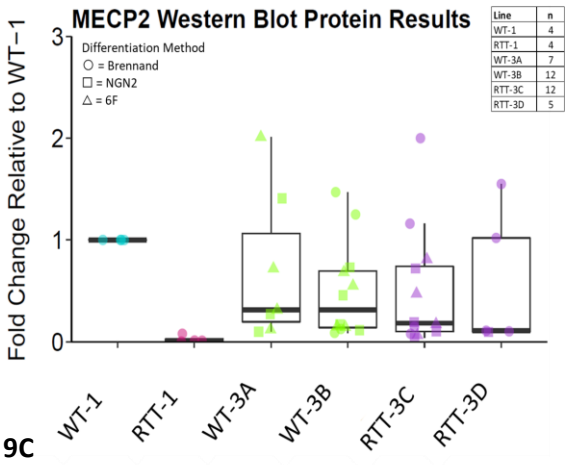

9C

Comparison	Z	P.unadj	P.adj	Significant Difference?
WT-1 v RTT-1	3.4693	0.00052	0.008	TRUE
WT-3A v WT-3B	0.4386	0.66095	1	FALSE
WT-3A v RTT-3C	0.807	0.41964	1	FALSE
WT-3B v RTT-3C	0.4292	0.66777	1	FALSE
WT-3A v RTT-3D	0.5358	0.59209	1	FALSE
WT-3B v RTT-3D	0.1975	0.84343	1	FALSE
RTT-3C v RTT-3D	-0.132	0.89524	0.895	FALSE

Figure 9. Examination of MECP2 Protein by Western Blot Analysis. (A) An example western blot of 4-week neurons differentiated according to the Brennand method showing MECP2 in green and the b-actin control in red. Two replicate batches of the WT-3/RTT-3 lines can be seen. (**B)** A plot of all WT-3/RTT-3 western blots done to examine MECP2 in comparison to WT-1. Results from different differentiation methods are signified by variable shapes. No significant difference between any WT-3 line to any RTT-3 line was found. A significant difference was seen between WT-1 and RTT-1. (**C)** A more detailed layout of the statistics for the WT-3 and RTT-3 comparisons. Statistics were performed using the Kruskal Wallace and Dunn Tests.

Seeing no significant difference in the western blot results, I confirmed this result with the In-Cell Western (ICW) assay. This assay is of interest for the purposes of potential high throughput screens and testing MECP2, our key protein of interest, represents the first step of this process. Briefly, the ICW is a quantitative fluorescence-based assay where cells are fixed to the wells and then labelled with the primary protein of interest and a Near-Infra Red conjugated secondary antibody. The wells were scanned with on LI-COR Odyssey CLx and the degree of fluorescence

in MECP2 was compared to the fluorescent levels of LiCor's Cell Tag 700 stain, a non-specific cell stain that allows normalization to cell number. The protein of interest is labeled in green while the cell count tag is labelled in red. Where red overlaps green, a yellow colour can be seen.

I found that the ICW protein assay was able to replicate the results of the western blot. There was no significant difference in MECP2 between the WT-3 and RTT-3 lines **(Figure 10A,B,C)**. In addition, this assay also replicated previous western blot work (Li et al., 2013) showing that there was a significant difference between the control null WT-2 and RTT-2 lines (**Figure 10 B).** These results further indicate that the L124W mutation does not affect protein level. It also demonstrates that ICW is an effective protein assay.

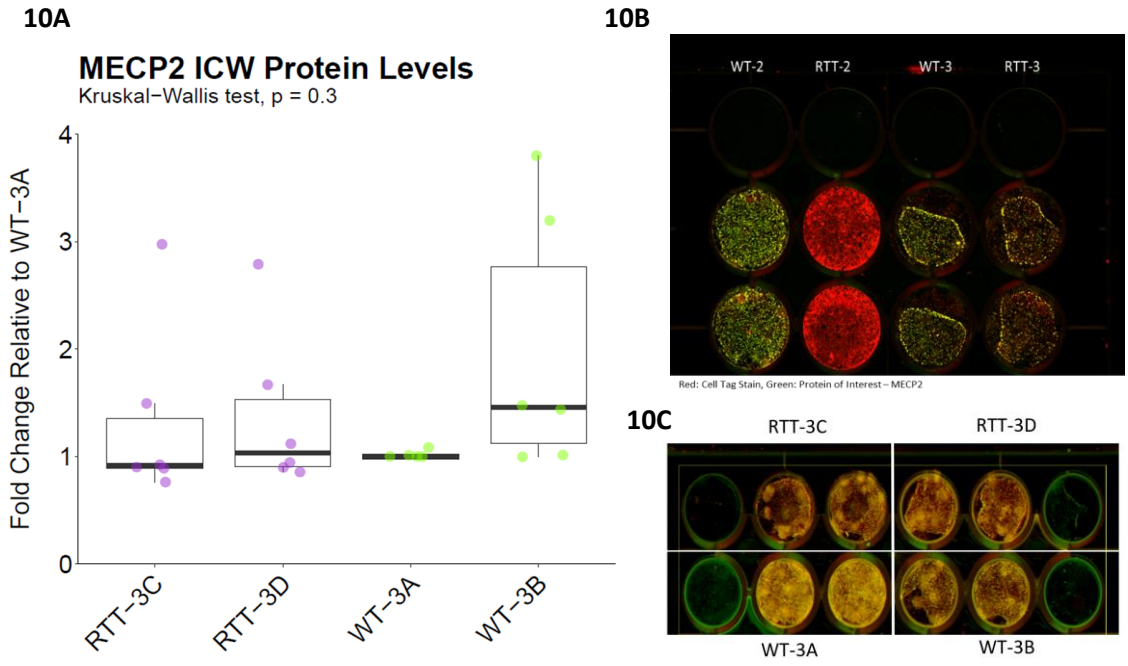

Figure 10. Examination of MECP2 Protein by In Cell Western. (A) A plot of all ICW MECP2 results show that there is not significant difference between WT-3 (n = 12 wells) and RTT-3 (n = 11 wells). **(B)** An example ICW where MECP2 is present in the WT-2 but not the null RTT-2 line. In comparison, the WT-3 and RTT-3 lines clearly show protein. **(C)** An example ICW of all 4 WT-3/RTT-3 lines.

3.4.1 ICW Tests for Screening

To explore the potential of using ICW to screen other proteins or activities related to RTT, I tested antibodies for SAP-90 (previously known as PSD95) and puromycin. SAP-90 is known to

be reduced in RTT (Tropea et al., 2009) and was recently used in an ICW drug screen for MECP2 Duplication Syndrome (Nageshappa et al., 2016). The puromycin antibody is used to examine the results of the puromycin incorporation assay, sometimes called a SUnSET assay (Schmidt et al., 2009), which measures protein synthesis through the incorporation of puromycin into the amino acid chain. Preliminary results (n=1) of these antibodies in the ICW reveal that WT-2 cells have a higher amount of SAP-90 relative to RTT-2 **(Figure 11 A, B)** and that WT-2 cells have a higher degree of puromycin incorporation than RTT-2, **(Figure 11 C, D)** implying that they have a higher rate of protein synthesis.

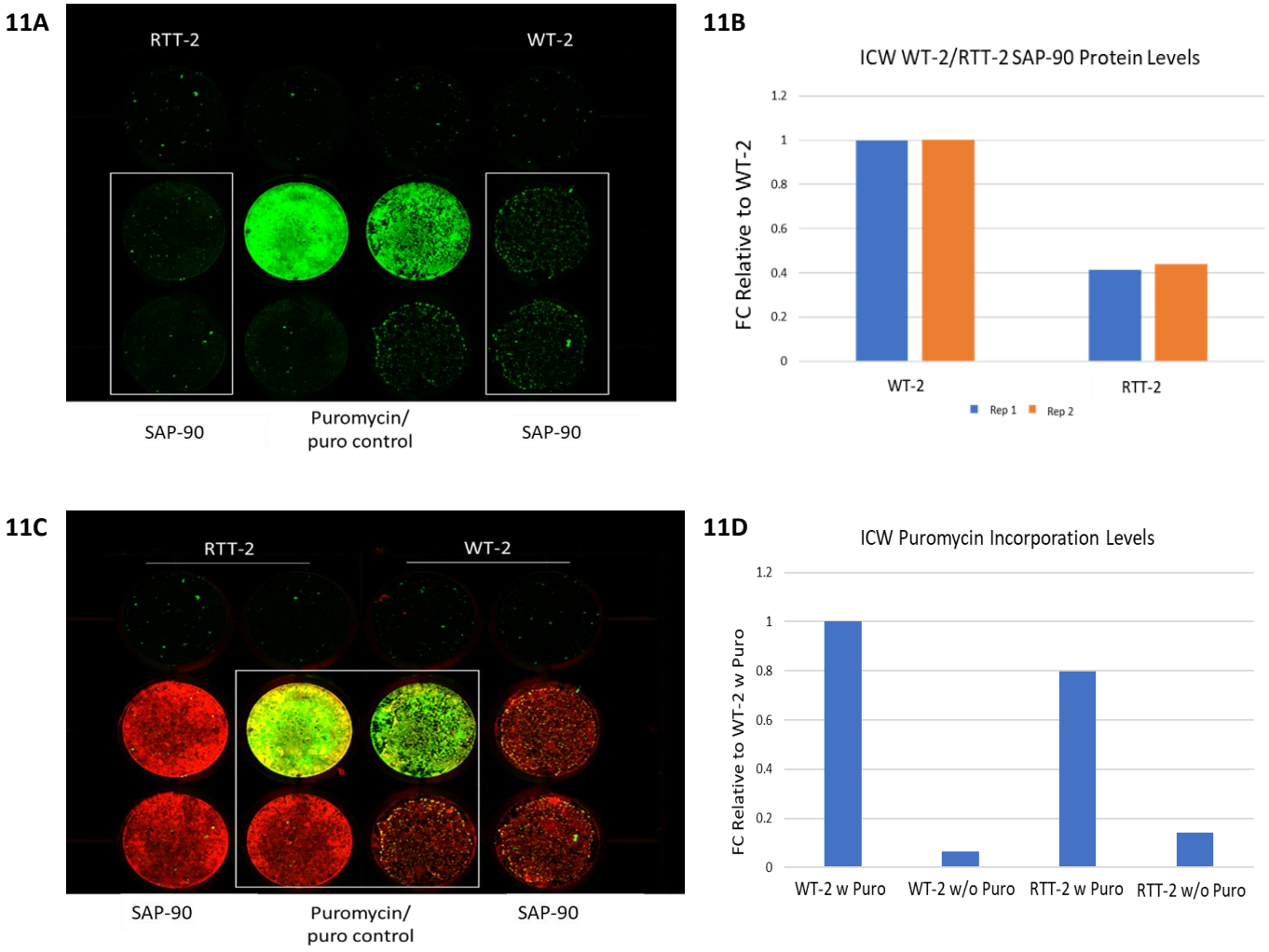

Figure 11. ICW Tests of SAP-90 and Puromycin. (A) The white boxes show ICW results of SAP-90 in RTT-2 and WT-2 4 week old neurons. The red channel cell tag stain 700 has been removed for better viewing of SAP-90 green fluorescence. **(B)** Quantification of a the preliminary experiment

suggests that SAP-90 is higher in WT-2 than in RTT-2. The blue and orange represent individual wells on the plate. **(C)** The white box shows ICW results of the puromycin incoporation assay where the green fluorescence is puromycin and the red fluorescence is the cell tag stain. The top row shows the fluorescence with puromycin. The bottom row shows the puromycin control that received no puromycin. **(D)** Quantification of a preliminary experiment suggests that WT-2 has a higher amount of puromycin incorporation than RTT-2.

Although these ICW tests are preliminary, it does appear that the ICW is capable of picking up differences using these antibodies. As such, the ICW could potentially be used in a larger scale screen where SAP-90 or puromycin incorporation levels are tested.

3.5 Neuronal Morphometric Analysis

Having seen that there was no change in L124W mRNA level or protein level, my next step was to examine if there were any changes in the morphology of the RTT-3 neurons. We and others have shown that RTT neurons have smaller somas and shorter dendrites than their wild type controls (Chen et al., 2001; Cheung et al., 2011; Li et al., 2013). To examine this, I used images generated by PhD candidate, Rebecca Mok. Briefly, 6-week-old NGN2 neurons were transfected with an EF1αEGFP plasmid through Lipofectamine 2000 before the cells were fixed and imaged in stacks with the Olympus 1X81 spinning disk confocal microscope. All images were then blinded, shifted to 2D, and analyzed.

3.5.1 Soma Area and Dendrite Length

I measured between 31 and 35 replicates from each line of neurons (WT-3A, WT-3B, RTT-3C, RTT-3D) and determined that there was no significant difference in either soma size or dendrite length between WT and RTT **(Figure 12A, B)**. This demonstrates that, although the patient presents with Rett Syndrome, the L124W mutation does not induce the ‘classic’ morphology changes seen in literature and in previous work done on the null RTT lines (Cheung et al., 2011; Li et al., 2013).

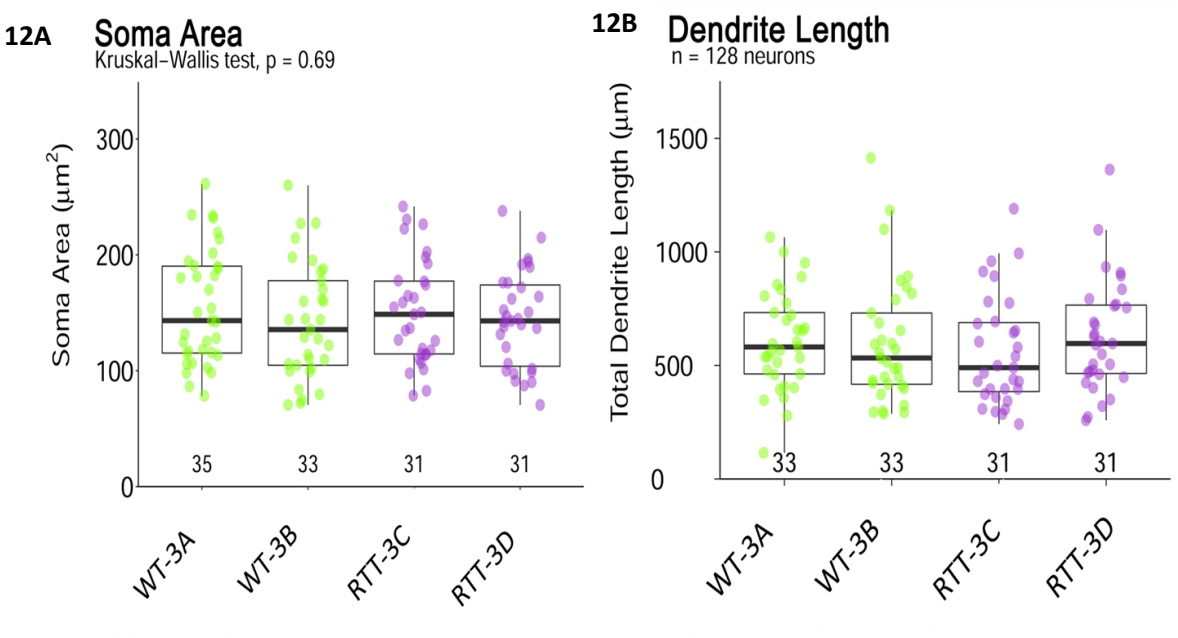

Figure 12. L124W Soma & Dendrite Analysis. (A) A test of soma area reveals that there are no significant differences in soma area between WT and RTT in the L124W mutation (n= 128 neurons over 3 replicates). **(B)** A test of dendrite length reveals that there is no significant difference in total dendrite length between WT and RTT in the L124W mutation(n= 128 neurons over 3 replicates).

3.5.2 Sholl Analysis

Sholl Analysis (Sholl., 1953; Chapleau et al., 2009) is a measure of dendrite complexity where concentric circles are made outwards from the soma and a measure is taken of how many times each circle intersects with a dendrite **(Figure 13A)**. For my experiment, the distance of the circles was set to 10µm and intersections were determined by Imaris (Bitplane) based on the trace I created when analyzing dendrite length. Using Sholl analysis, there was a subtle but significant difference between WT-3 and RTT-3 at the beginning of the analysis, closest to the soma (**Figure 13B)**. There was a significant overall difference in WT-3 vs RTT-3 lines **(Figure 13C)**, narrowing in, this significant difference was in the number of intersections only at the 10 – 80µm distance as seen by pairwise comparison (**Figure 13D)**. As only a few neurons had dendrites extending to the farthest circles, near 400 µm, the power of statistical tests was too low to determine significance. However this early Sholl difference, found only at the beginning levels of concentric circles, represents the first phenotype found in this novel L124W mutation.

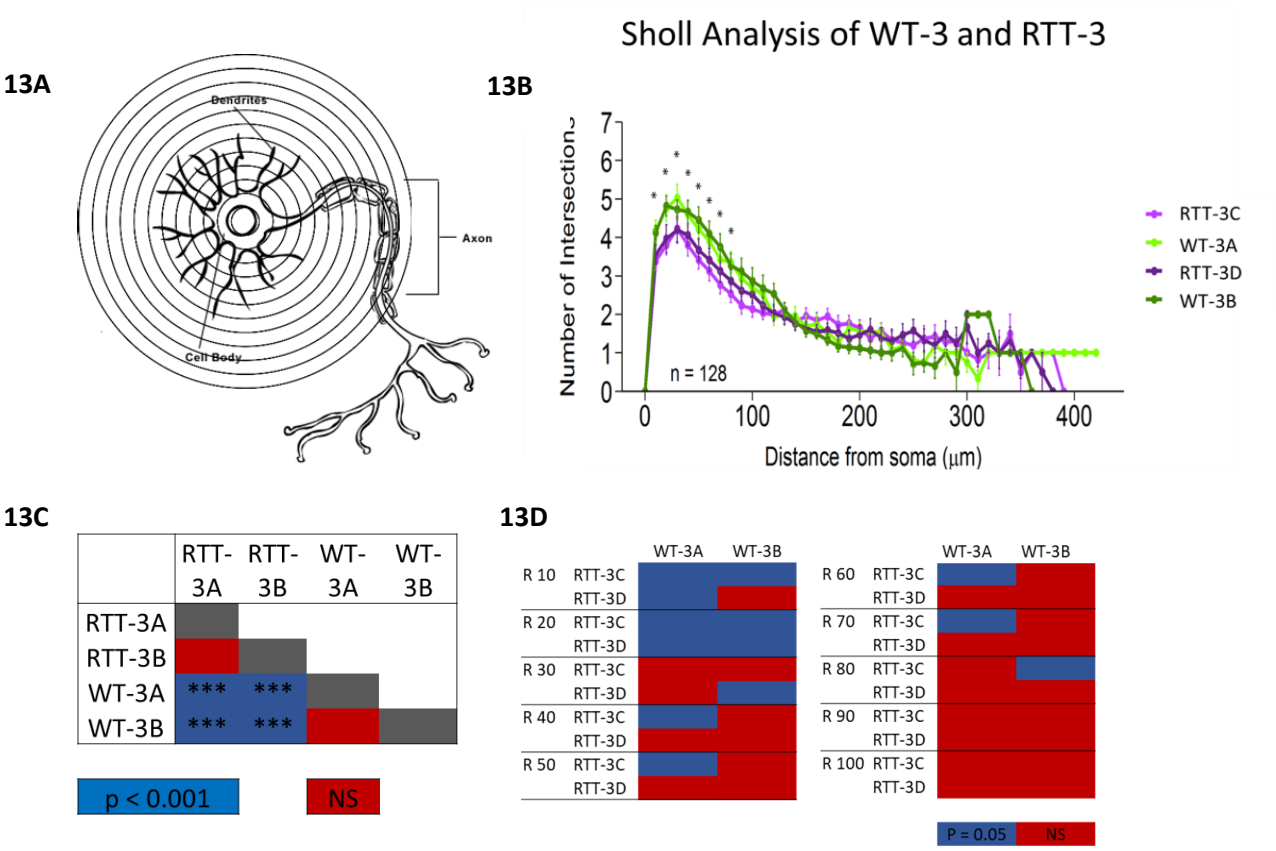

Figure 13. Sholl Analysis of WT-3 and RTT-3 6-week-old Neurons. (A) A demonstration of Sholl analysis where concentric circles are created a 10µm intervals outwards from the soma and then the number of times a dendrite intersects each ring is counted. **(B)** Sholl analysis reveals a significant difference between WT-3 and RTT-3 lines. The circles at a distance of 10 – 80µm from the soma specifically show this difference occurring at least once when comparing WT and RTT, as shown in Figure 13D. (n= 128 neurons over 3 replicates). **(C)** Statistical tests (Tukey ANOVA, p = <0.001) reveal a significant difference between all WT-3 lines with all RTT-3 lines no difference between internal WT-3 and RTT-3 lines. **(D)** Statistical analysis (Pair-wise comparison, Dunn Test, p<0.05) showed that the lines had at least one statistical difference at distance of 10 – 80µm from the soma

3.5.3 Dendrite Order Analysis

I wanted to look further into the unique subtle phenotype in the L124W mutation found at the 10 – 80µm distance of the Sholl analysis. As such, I then performed a Dendrite Order assay on the

same images. This assay uses the existing traces of the dendrites to manually count the number dendrites at each level of the order **(Figure 14A)**. Starting at the soma, each dendrite coming directly off the soma was labelled as 'Primary' and then each primary dendrite was traced until there was a branch point. Both of the branches were labelled as secondary. These secondary dendrites were followed until a subsequent branch point lead to tertiary dendrites. This continued until the end of all dendrites was found.

I found that in the WT-3 and RTT-3 neurons, there is only a difference in dendrite order at the level of the primary dendrites **(Figure 14B)** where there is an average of 4.28 primary dendrites on WT-3 neurons and only an average of 3.53 primary dendrites on RTT-3 neurons.

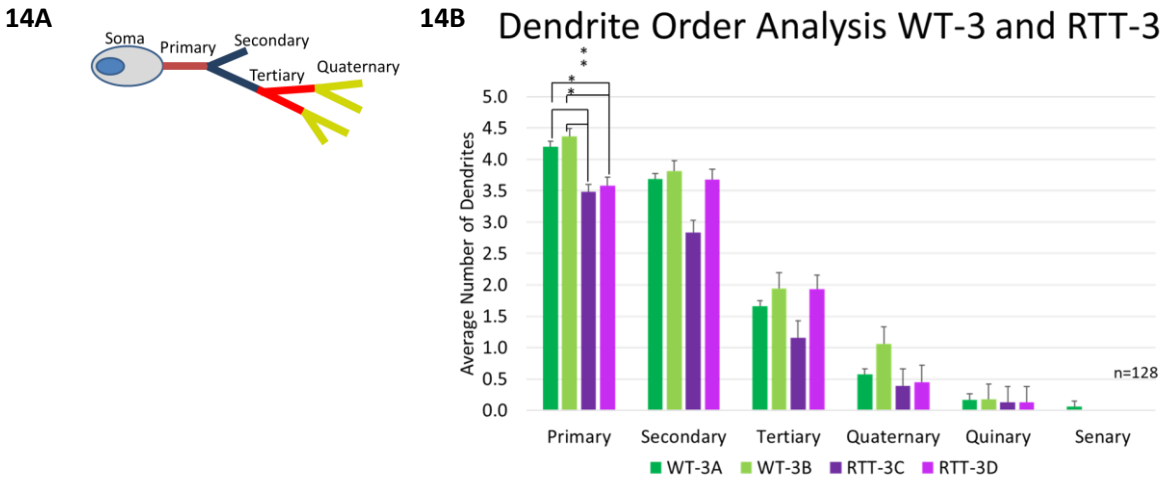

Figure 14. Dendrite Order Analysis of WT-3 and RTT-3. (A) A demonstration of the definitions for each dendrite order level. Primary dendrites come directly off the soma. Secondary dendrites branch directly off the primary. (n= 128 neurons over 3 replicates). **(B)** Dendrite order analysis that there is a significant difference between WT-3 and RTT-3 only at the level of the primary dendrites as per Kruskal Wallace and Dunn tests.

Having found this increasingly subtle phenotype where dendrite complexity seems affected only at the level of primary dendrites, I examined the null RTT lines for a similar phenotype. Existing images, from PhD candidate Rebecca Mok, of these neurons at 6 weeks were used. First examined were the WT-1 and RTT-1 lines which have a deletion removing exons 3 and 4 (Cheung et al., 2011). I found that there was a significant difference between WT-1 and RTT-1

at the level of the primary dendrites with additional differences at the secondary and quaternary levels **(Figure 15A)**. I then performed the dendrite order analysis on our WT-2 and RTT-2 lines which are ES cells with a TALEN edit to remove exon 3 (Li et al., 2013) and found that there was no significant difference between WT-2 and RTT-2 at any of the order levels **(Figure 15B)**. Finally, I performed another dendrite order analysis on the new CRISPR created PGPC14 NULL and PGPC14 DEL lines against their pre-existing PGPC14 Parental control (Hildebrandt et al., 2019). I found that both PGPC14 Indels, the NULL and the DEL, showed a significant difference at the level of primary dendrites from their Parental control **(Figure 15C)**. The PGPC14 NULL, which is a 1bp insertion in exon 3 leading to an early stop, also showed significant differences at the secondary and tertiary levels. I also analyzed new images of the WT-1/RTT-1 lines as a control and again found the primary dendrite phenotype.

15A

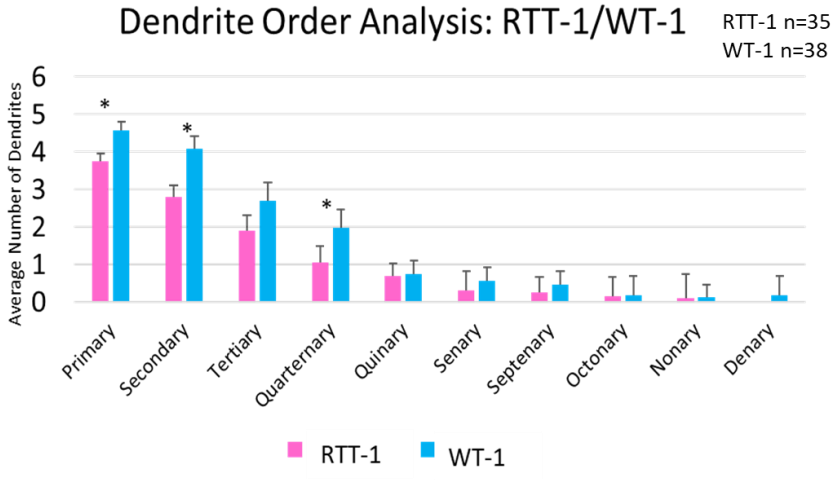

15B

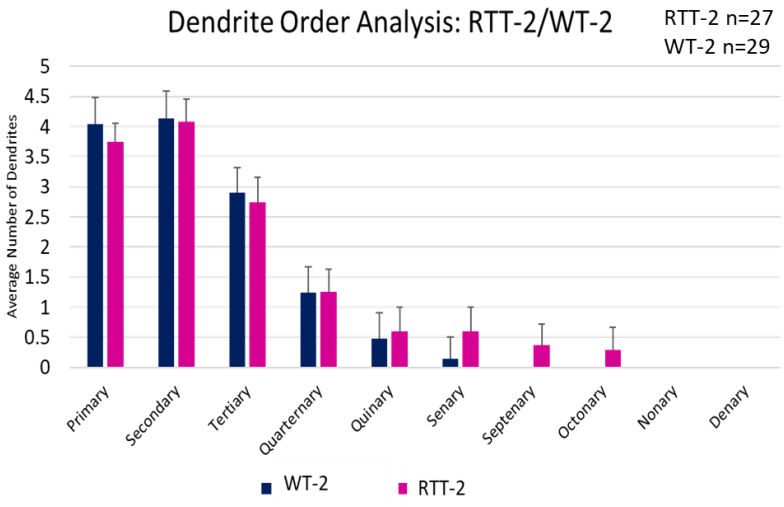

15C

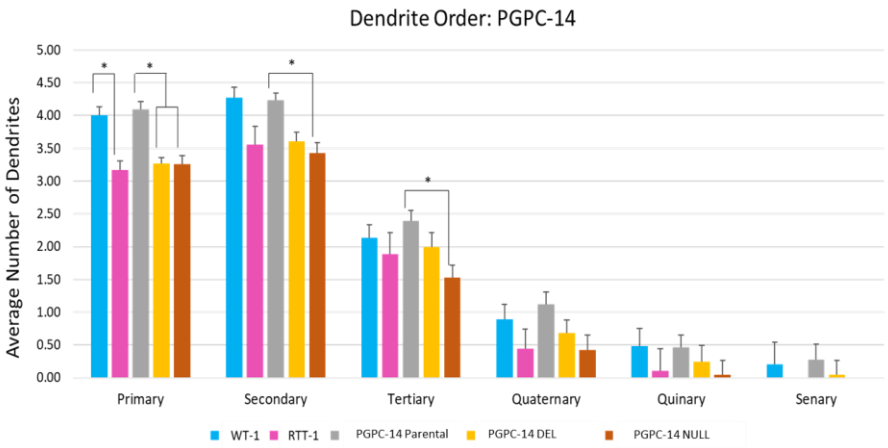

Line	n
WT-1	29
RTT_1	18
PGPC14 Parental	43
PGP14 DEL	41
PGPC14 NULL	42

Figure 15. Dendrite Order Analysis of RTT Null Lines. (A) Dendrite order analysis of WT-1/RTT-1 reveals a significant difference between WT and RT at the level of the primary dendrites as well as the secondary and quaternary levels. **(B)** Dendrite order analysis of the WT-2/RTT-2 lines reveal no significant difference at any of the levels. **(C)** Dendrite order analysis of the PGPC-14 lines show that both the PGPC-14 DEL and PGPC-14 NULL have a significant difference relative to the PGPC-14 Parental line. The PGPC-14 NULL also shows significant differences at the secondary and tertiary levels. New images of the WT-1/RTT-1 continue to show the primary dendrite difference.

Overall, I have found a subtle morphology phenotype in dendrite complexity in the WT-3/RTT-3 neurons with the unique primary level dendrite order phenotype being replicated in all of the hiPSC isogenic pairs but not the hESC null isogenic lines.

3.6 Electrophysiology on the Multi-Electrode Array

To determine whether the L124W mutation affected neural connectivity, I next decided to examine extracellular electrophysiology on our Multi-Electrode Array (MEA). The MEA is a device that allows us to capture ongoing extracellular electrophysiological phenotypes in neurons as they grow and develop over a grid of 64 electrodes. iPS cells that are one week into the NGN2 differentiation process are re-seeded into the MEA plates with mouse astrocytes. The differentiation is continued and the plates are recorded twice a week, every week, for up to 8 weeks. This allows us to track the progress of the same neurons over time. Rebecca Mok, a PhD candidate in our lab, has used this method to test WT-1/RTT-1, WT-2/RTT-2, and PGPC

Parental/NULL/DEL lines for extracellular electrophysiological and has found alterations in network burst length and duration (the frequency and length of time that electrodes fire together as a single 'burst'). I tested the WT-3/RTT-3 lines in this same assay **(Figure 16A)** and found there was no significant difference in either network burst frequency **(Figure 16B)** or network burst duration **(Figure 16C)**.

16A

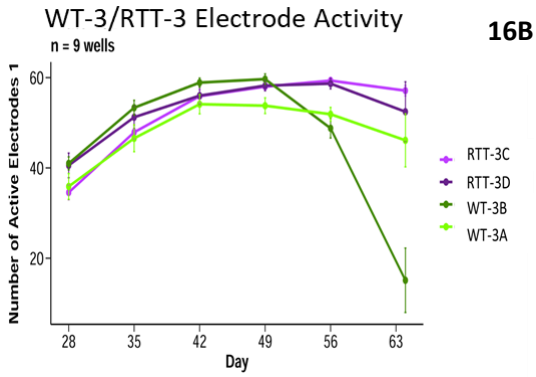

16B

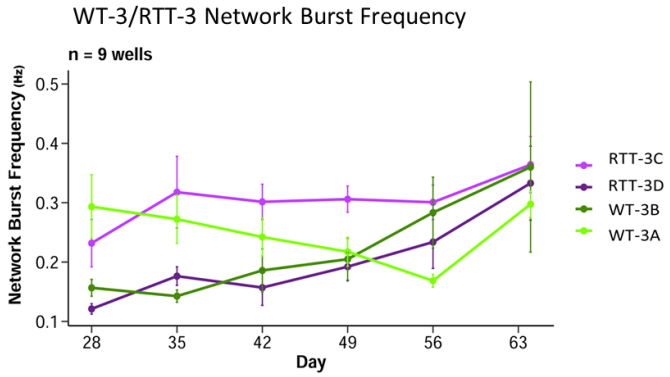

16C

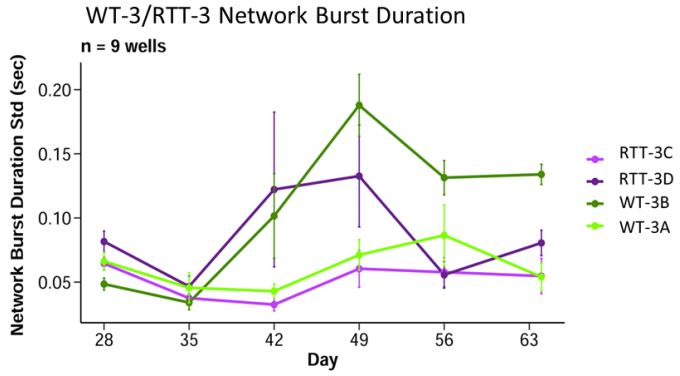

Figure 16. WT-3/RTT-3 Electrophysiology on the Multi-Electrode Array. (A) Results from the multi-electrode array (MEA) showing that all wells have a high level of activity with all wells reaching a total active number of 60 out of 64 electrodes. This reflects a high plate quality. N for all MEA is 9 wells over 3 plates. **(B)** MEA results examining network burst frequency over a period of 63 days shows no significant difference between WT-3 and RTT-3 **(C)** MEA results examining network burst duration over a period of 63 days shows no significant difference between WT-3 and RTT-3.

3.7 CRISPR Correction of the L3124W Mutation

To confirm that the L124W mutation is causative and to demonstrate that it can be rescued, I attempted to correct the L124W mutation in iPSCs by editing the altered ‘T’ back to a ‘G’ using a Cas9 ribonucleoprotein complex (Cas9 RNP) and a de-salted single-strand oligo repair temple (ssODN) CRISPR protocol. To do so, I first tested my protocol using KOLF2-C1 iPS cells where a BFP gene was inserted into the AAVS1 locus (Skarnes et al., 2019). Applying a protocol developed in conjunction with our previous postdoc (Hildebrandt et al., 2019), I successfully made the one base pair edit that transformed BFP to GFP. The edited cells were examined using fluorescent -activated cell sorting and I found that 6.94% of the cells were successfully edited from BFP to GFP, showing that the protocol worked (**Figure 17A)**. From there, I designed the ssODN to have two edits. One was the expected L124W edit and the other was an edit of the targeted protospacer adjacent motif (PAM) site to ensure that the sgRNA could not bind the same location twice. I then designed the probes for digital droplet PCR (ddPCR) to target the PAM, allowing me to examine for positive edits **(Figure 17B)**. The PAM site was chosen due to relative ease of ddPCR at the PAM site when compared to the L124W and because the large distance between the PAM and the L124W point mutation made edits at the L124W increasingly difficult.

With everything ready, I performed the CRISPR process on the RTT-3C iPSCs. Due to ongoing delays in ddPCR results increasing passage number, for the final CRISPR I performed a single ddPCR analysis and confirmed that there were successful PAM edits in the population **(Figure 17C)**. With the help of our technicians, I then picked 136 clones from the population. These clones were expanded and, during passage, I removed a portion of the cells from each clone for gDNA analysis.

Sequencing results for the gDNA revealed that none of the 136 clones were successfully corrected; this was likely due to the long 35bp distance between the cut site and the desired edit. However, I did successfully generate edits of the PAM site **(Figure 17D)** and generated indels in the non-coding region where the closest PAM was located **(Figure 17E)**.

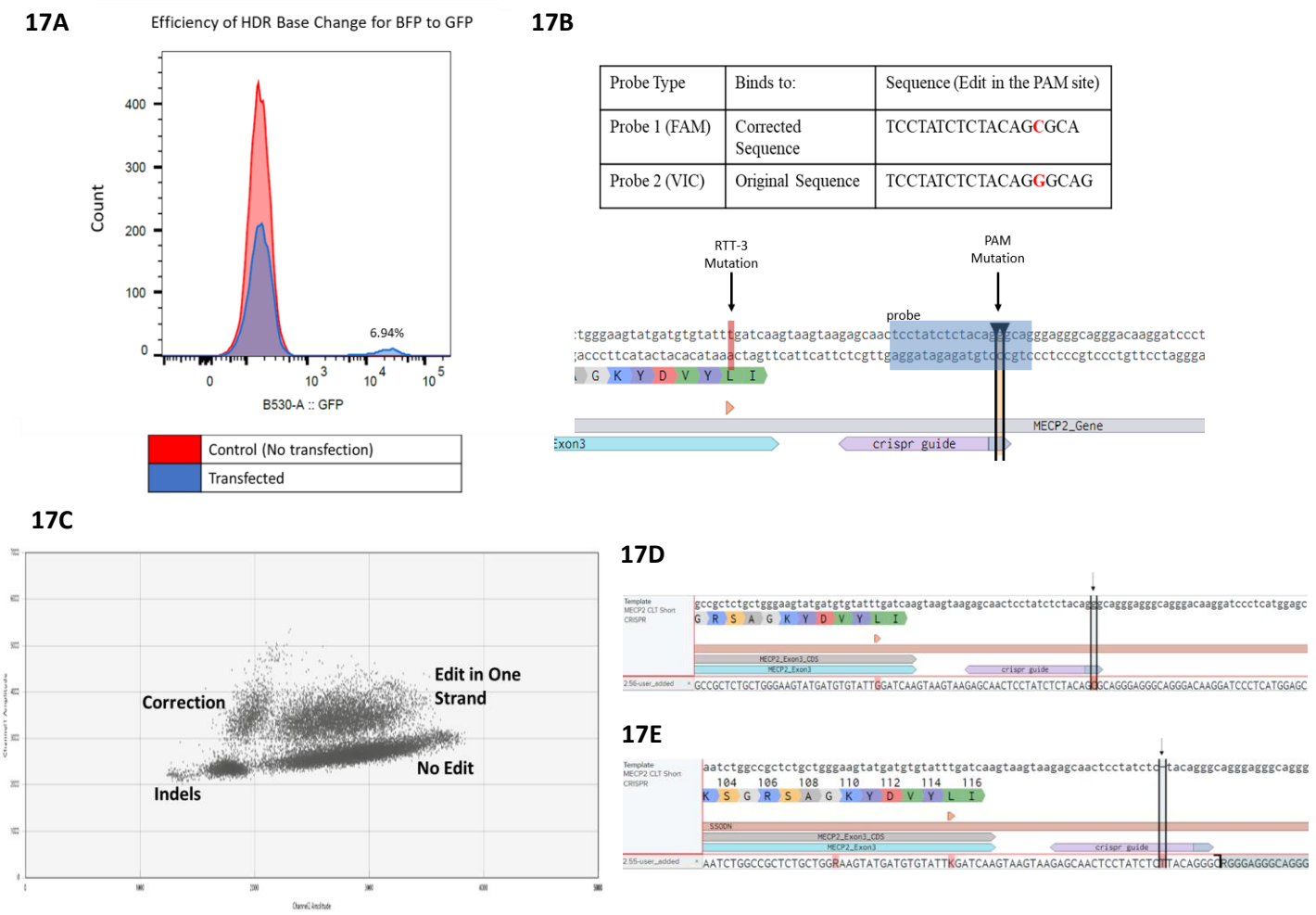

Figure 17. L124W CRISPR Correction in iPSCs. (A) A demonstration that the protocol can be used successfully by transforming the consistently expressed BFP in KOLF2-C1 iPS cells into a GFP in 6.94% of cells. **(B)** Description of probes used in ddPCR and proposed PAM edit. Below is a layout of the targeted CRISPR with the L124W RTT-3 edit 34 base pairs away from the closest PAM site. The blue box denotes where the ddPCR probes will bind. **(C)** ddPCR results from the final CRISPR reveal 4 distinct populations. The 'correction' population represents where only Probe 1 the corrected sequence bound. The 'edit in one strand' represents where Probe 1 and Probe 2 bound. The 'no edit' population has only probe 2 bound. The indel population is where no probe has bound. The size of the correction population represents the successful PAM edits. **(D)** This is an example clone showing a successful edit of the PAM site from the ssODN. It can be seen that the original

GGG of the PAM has been edited to a GCG. **E)** This is an example clone showing a successful indel generation, in this case, a one base pair insertion. It is in the noncoding region.

Overall, although I was not able to generate a successful L124W correction, I did successfully generate both a PAM edit and indels. The PAM edit indicates that the ssODN was successfully used as a template however the lack of L124W edit indicates that the distance between the PAM site and the L124W mutation was a negative factor in success. The generation of indels demonstrates that this protocol could be used on PAM sites within the coding sequence to create indels in lines of interest.

3.8 Impact of Differentiation Method on Detection of NEDD4L

For the majority of this project, I used the NGN2 differentiation methods for my cells allowing me to generate functional neurons in 14 days (Zhang et al., 2013). However, the lab does use other differentiation protocols such as the rosette-based 'Brennand' differentiation method (Brennand et al., 2011) and the 6F protocol (Ross et al., 2020). While using Brennand derived WT-/RTT-1 protein extracts as a control in western blots, we noticed that the Brennand differentiated lines seemed to express higher amounts of MECP2 than lines differentiated according to the 6F protocol or my preferred NGN2 protocol **(Figure 18A,B)**. Our technicians then successfully differentiated 3 of the 4 WT-3/RTT-3 lines according to the Brennand differentiation method. I ran a western blot comparing WT-3/RTT-3 lines differentiated according to the NGN2 or Brennand methods and found that the Brennand WT-3/RTT-3 lines were expressing higher amounts of protein **(Figure 18C,D)**.

One interesting component of generating the WT-3/RTT-3 lines with the higher level of MECP2 protein that seems to be found in the Brennand differentiated cells is that I was able to look at NEDD4L levels in WT-3/RTT-3 lines for the first time. NEDD4L is an E4 ubiquitin protein ligase that our lab has found to be significantly reduced in RTT cell lines (Rodrigues et al., 2020). Using the new Brennand differentiated WT-3/RTT-3 cell lines, I used a western blot to search for NEDD4L and found it visible for the first time **(Figure 18E, F)**. Although the blot could not be repeated and refined due to COVID-19 shutdown, this represents our first experience of NEDD4L in these lines.

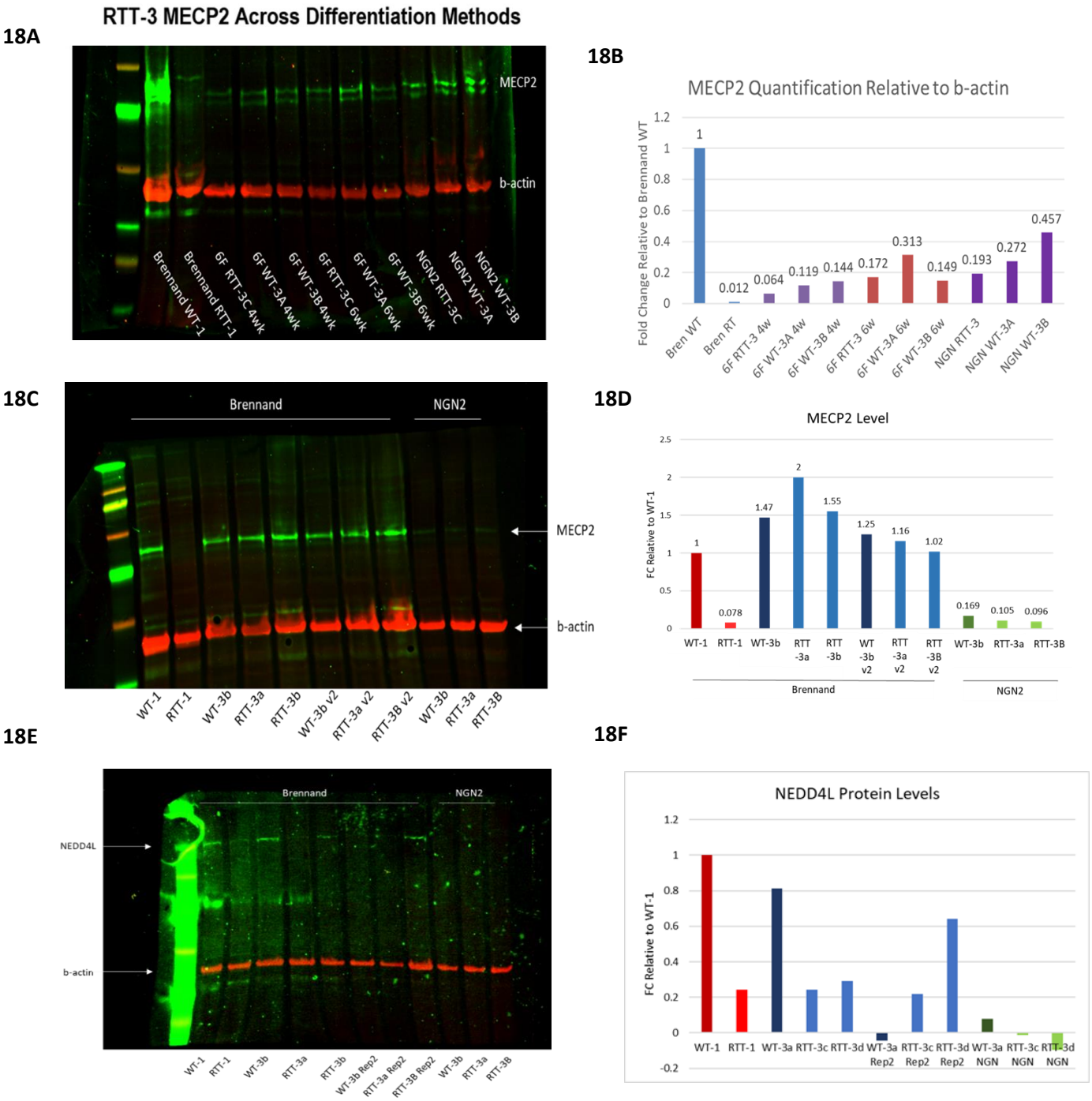

Figure 18. Western Blot Analysis of Various Differentiation Methods. (A) A western blot (n=2) comparing the amount of MECP2 in Brennand differentiated neurons, NGN2 differentiated neurons, and 6F neurons shows a higher amount of MECP2 in Brennand WT-1/RTT-1 over WT-3/RTT-3 lines

in the other two methods. ‘v2’ represents an additional replicate. **(B)** A quantification of Figure 12A. **(C)** A western blot comparison of MECP2 in Brennand differentiated WT-1/RTT-1 and WT-3/RTT-3 compared to WT-3/RTT-3 NGN2 differentiated neurons shows higher protein in all the Brennand lines compared to the NGN2 lines. ‘v2’ represents an additional replicate. **(D)** A quantification of Figure 12C. **(E)** A preliminary western blot showing for the first time that NEDD4L is visible in WT-3/RTT-3 lines when they are differentiated according to the Brennand method but not according the NGN2 method. **(F)** A quantification of Figure 12E reveals discrepancies between replicates.

3.9 Generating *NEDD4L* KO Lines with CRISPR/Cas9

To follow-up on our recently published paper which described a reduction in NEDD4L in RTT lines (Rodrigues et al., 2020), I created two *NEDD4L* Knock-Out (KO) lines using CRISPR/Cas9. This was done in conjunction with Dr Maria Sartori and accomplished using a plasmid-based CRISPR method where the sgRNA was cloned into the pSpCas9(BB)-2A-Puro plasmid backbone (Ran et al., 2013) for transfection into the male PGPC-3 and the female PGPC-14 iPSCs. (Hildebrandt et al., 2019). Two separate guide plasmids were generated to respectively target both exon 7 and exon 10 of *NEDD4L*. To increase the likelihood of a complete knockout, I performed eight transfections simultaneously with the two plasmids being transfected either individually or in tandem. With the puromycin-resistance offered by the backbone, we used a 3-day puromycin selection to select for transfected cells. From the surviving cells, we picked ~100 clones which were then grown to confluency. Half of the cells from each clone were then harvested for protein analysis.

To test large numbers of protein extracts, we used the WES, a capillary based western blot. This revealed a number of clones that appear to be full NEDD4L KOs (**Figure 19A)**. We then tested the most likely candidates with a traditional western blot, which uses a higher quantity of protein extract, and found two true NEDD4L KOs: Indel E10 #17B and Indel E7 +E10 #7B **(Figure 19B)**. Both of these KOs were in the male PGPC-3 line with only knock-downs in the female PGPC-14 line. Once the protein KOs were found, we performed both gDNA and cDNA sequencing to understand where the genome had been edited to generate the KOs. We found that

both clones had a single base pair insertion in exon 10 leading to an early stop **(Figure 19C)**. The cDNA also revealed that Indel E10 #17B had a mixed population of the 1bp insertion and a 149 base pair deletion in exon 10 **(Figure 19D)**. Both populations appear to achieve a full KO of NEDD4L. To confirm that the CRISPR process had not altered the cell lines in some unexpected way, I inputted the sgRNA into Benchling software which performed an off-target analysis to determine the most likely regions of off-target edits. I then selected the two most likely off-target locations and sequenced their cDNA. I found that there was no difference between the PGPC-3 control and the two Indels in either off target location **(Figure 19E)**. Finally, I sent the cell lines for karyotyping and found that both cell lines maintained a normal karyotype **(Figure 19F)**.

19A

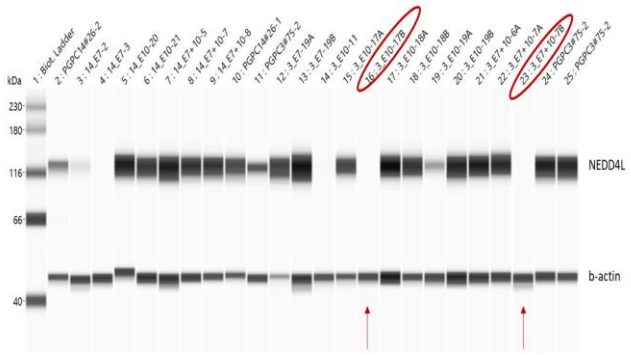

19B

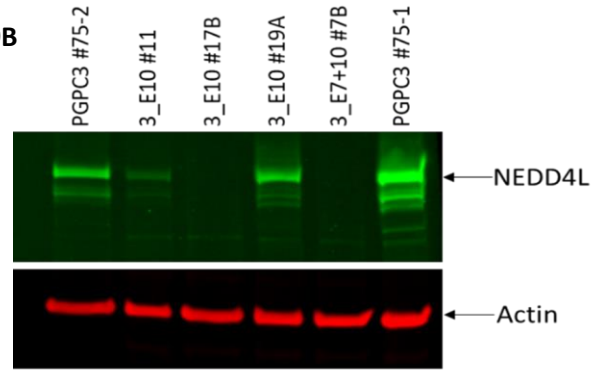

19C

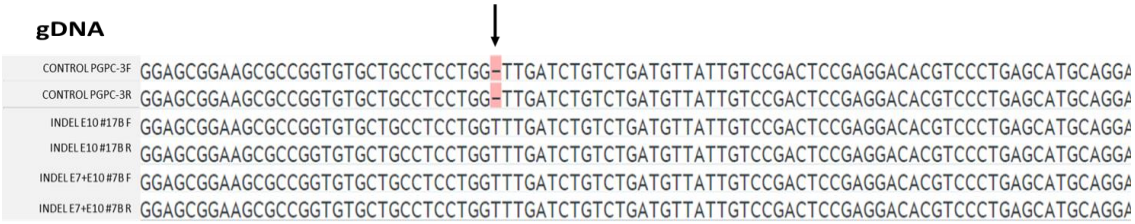

19D

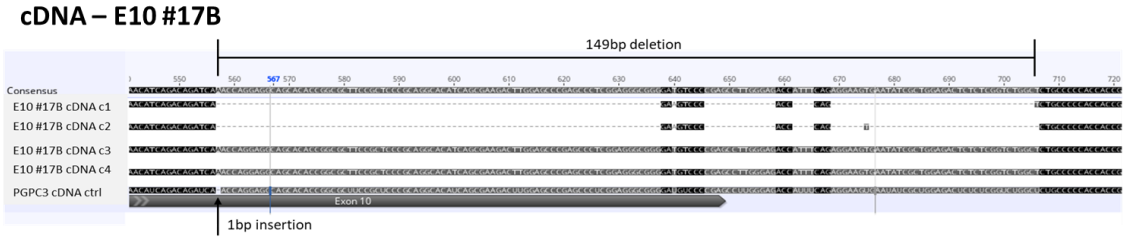

19E

19F

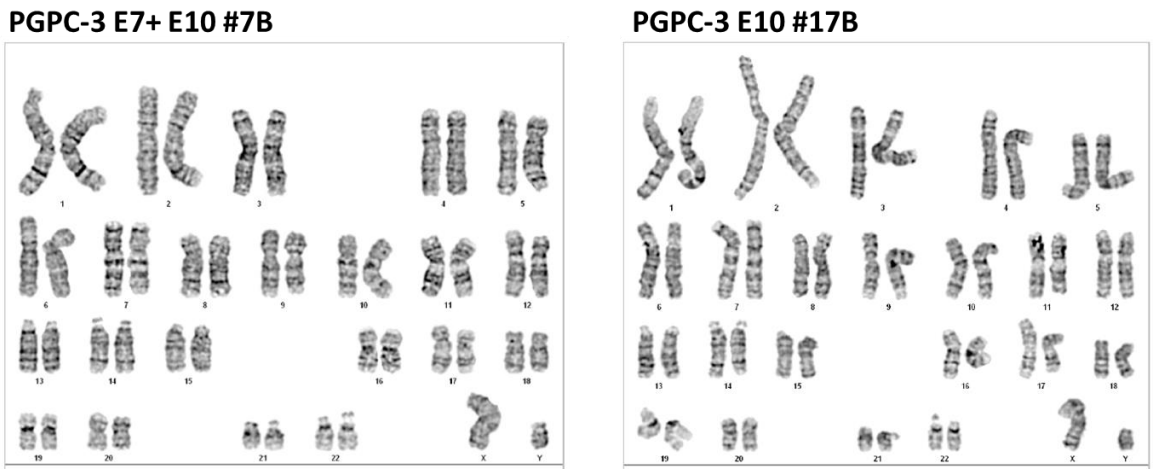

Figure 19. NEDD4L CRISPR Knock-Out. (A) Protein analysis done on the WES, a capillary based western blot, shows a number of potential KOs in NEDD4L. Two cell lines are highlighted in red as these lines will be revealed in 13B to be true KOs. **(B)** Protein analysis done by traditional western blot show two complete KOs, PGPC3 E10 #17B and PGPC3 E7 +E10 #7B. One line that appeared to be a KO on the WES, E10 #11, has revealed to be a knockdown and not a KO. **(C)** gDNA sequencing shows that both KO lines have a 1bp insertion in exon 10. **D)** cDNA sequencing of E10 #17B reveals a mixed KO population with a 1bp insertion and a 149 base pair deletion. **E)** Off target sequencing of two potential off target sites reveals that no changes were made to the cDNA sequence. **F)** Karyotyping results of both KOs show that the CRISPR process did not make any karyotype changes and cell lines remain normal.

These *NEDD4L* KO lines will be used by the lab to determine NEDD4L targets and as a control for future experiments.

Chapter 4
Discussion

4 Discussion

4.1 RTT-3 Lines Show A Less Severe Phenotype

One of the core goals of the work detailed in this thesis was to understand the novel L124W mutation and to find, for the first time, what phenotypes it displays. The results detailed above show that the RTT-3 L124W mutation produces a limited phenotype. An investigation into *MECP2* RNA levels by qRT-PCR showed that there was no significant difference between WT-3 and RTT-3. Performing protein analysis by traditional Western blot and the new In Cell Western showed that there was no significant change in MECP2 levels. I also looked at electrophysiology levels as determined on the Multi-electrode array and found again that there was no significant difference between WT-3 and RTT-3. When examining morphology there was no significant change in either soma area or dendrite length however there was a significant difference in dendrite complexity as determined by Sholl analysis and dendrite order analysis.

4.1.1 Dendrite Complexity Reduction in WT vs RTT

In the literature and in our own lab, a frequent hallmark of RTT neurons is a reduction in both soma area and dendrite length (Bauman et al., 1995; Chen et al., 2001; Li et al., 2013; Djuric et al., 2015), however I do not see this reduction phenotype in the RTT-3 lines. Instead, I found only the more subtle dendrite branching phenotype. Previous research in mice, iPSC-derived neurons, and post-mortem brains have only found the dendrite complexity phenotype in conjunction with the more frequently examined soma area and dendrite length (Armstrong et al., 1995; Kishi et al., 2004; Stuss et al., 2012; Nguyen et al., 2012).

Using 6-week-old NGN2 neurons transfected with the EF1αEGFP plasmid, I employed methods to trace and reconstruct individual neurons for morphometric analysis across a number of different assays. This was performed in triplicate across several different RTT lines and their controls including RTT-1-/WT-1, RTT-2/WT-2, RTT-3/WT-3, and PGPC14 Null/DEL/Parental lines (Table 3). The RTT-1 line showed a reduction in all four of the morphometric analyses including soma size, dendrite length, Sholl analysis, and dendrite order. The RTT-2 line showed a reduction in soma size, dendrite length, and Sholl analysis but did not show a difference in

dendrite order. The RTT-3 line showed a reduction in Sholl analysis and dendrite order with no changes in soma size or dendrite length. For the PGPC Null/DEL lines, PhD candidate Rebecca Mok has found that they show reductions in soma area, dendrite length, and Sholl analysis (Mok et al., in prep) while this thesis shows that both lines also exhibit reduced dendrite order. In summary, the RTT-1 and the PGPC Null/DEL lines show reductions in all four assays, the RTT-2 line shows reductions in all assays except the dendrite order analysis, and the RTT-3 lines show reductions only in the Sholl and dendrite order assays.

	Soma Area	Dendrite Length	Sholl Analysis	Dendrite Order
RTT-1	Differ	Differ	Differ	Differ
RTT-2	Differ	Differ	Differ	
RTT-3			Differ	Differ
PGPC3 DEL	Differ	Differ	Differ	Differ
PGPC3 Null	Differ	Differ	Differ	Differ

Table 3. Summary of Morphology Assays in RTT Lines. A table examining all 5 RTT lines in each of the morphology assays. Red boxes indicate that the RTT lines significantly differed from the WT in this assay. Green boxes indicate that there was no difference.

Interestingly, although all of the RTT lines showed a morphometric reduction in at least one of the assays, there were differences between the individual lines. Three of our null lines, the RTT-1 line, PGPC DEL, and PGPC Null, showed reductions in dendrite length, soma area, and both dendrite complexity assays. Contrastingly, my core line of interest, the RTT-3 L124W mutation does not see significant reductions in dendrite length or soma area however it does see a subtle reduction in dendrite complexity as shown by Sholl analysis and dendrite order. This once again appears to be an intermediary phenotype where the RTT-3 line does not have as severe a phenotype as the null lines but instead has a more subtle phenotypic response.

Of note in this is the null RTT-2 line, which showed reductions in dendrite length and soma area but only showed dendrite complexity changes in the Sholl analysis and not in the dendrite order assay. While it follows our previous trend of the null having a more severe phenotype relative to the RTT-3 L124W, the lack of dendrite order difference makes it an outlier from our other nulls. One potential explanation for this difference is that the RTT-2/WT-2 lines are the only

embryonic stem (ES) cell lines used in this report. All of the other lines reported here are iPS cell lines. Previous research has shown that there are a number of small gene expression signature differences between ES and iPS cells, possibly due to transient epigenetic memory, (Chin et al., 2009; Polo et al., 2010), and it is possible that these changes contribute to the already subtle dendrite order assay. Overall, RTT-2 maintains a more severe morphology phenotype relative to RTT-3 as it does have the sholl dendrite complexity phenotype in conjunction with reduced soma area and dendrite, further cementing the hypothesis that RTT-3 is an example of a less severe RTT mutation.

Although we know that this dendrite complexity phenotype exists in all of our RTT lines, we are still uncertain as to the underlying cause. One strong possibility is that the RTT neurons are less mature than their WT pairs which results in less complex dendrite growth. It has been previously shown that RTT-iPSCs display defects in neuronal maturation (Chen et al., 2001; Kishi et al., 2004) where, for example, the mature neuronal marker TuJ has been found to be reduced in RTT lines (Kim et al., 2011). This reduction in maturity could lead to delayed growth or an overall slower rate of dendritic growth, possibly leading to stunted neurons. An alternative hypothesis is that RTT neurons experience increased dendritic atrophy (Nerlie et al., 2020).

4.1.2 Multi-Electrode Array Results Link to Dendrite Length

Whatever the reason for the dendrite complexity phenotype, it is possible that the reported changes in morphology directly link into the electrophysiology results shown in this report. I performed electrophysiology assays on the multi-electrode array (MEA) which measure extracellular firing and found no changes in network burst frequency or duration between WT-3 and RTT-3. In comparison, work done in parallel to this thesis by PhD candidate Rebecca Mok has found MEA changes in both network burst frequency and duration in our RTT null lines (Mok et al., in prep). As these lines also show RTT reductions in dendrite length and soma area, it is possible that the reduced dendrite length found in the null lines means that the dendrites of an individual neuron are not able to reach as many nearby dendrites. This creates less opportunities to pass the signal, resulting in a less defined network and therefore a change in network burst frequency and duration. As such, because the RTT-3 lines do not have reduced dendrite length and therefore would have the same dendritic reach as the WT-3 lines, I

hypothesize that this is why I do not see changes in the MEA electrophysiology results for the L124W mutation.

4.2 Impact of Rosette vs Transcription Factor Differentiation

In this project, I primarily used a transcription factor differentiation where neurogenin-2 (NGN2) was lenti-virally infected into the target iPSCs and controlled using doxycycline. However, during the course of my protein assays, I often used protein extracts from our rosette-based protocol (referred to as 'Brennand') as a control. It was during analysis of these blots that the research associate in our lab, Dr Rodrigues, pointed out that it seemed the rosette protein extracts had significantly more MECP2 relative to the NGN2 lines. At the time, we had only differentiated the WT-3/RTT-3 lines according to the NGN2 method and the control line, WT-1/RTT-1, according to the rosette-based method. This observation started a small side project to examine if the two differentiation methods did result in different final amounts of MECP2. I also compared these two methods to a third differentiation method, called '6F', which used dual-SMAD inhibition during differentiation. It was recently reported that between 2004 and 2017 more than 74 modified or novel protocols for deriving neurons were published and that while they were all able to recapitulate key characteristics, there were a number of small differences in the final neurons (Marton & Ioannidis, 2018). As such, it is vital for each lab to examine their preferred differentiation methods and examine the differences between them.

I found that the NGN2 and 6F protocols both result in lower amounts of MECP2 relative to the much higher amount of MECP2 protein generated by the Brennand protocol. In fact, when we differentiate three of our WT-3/RTT-3 lines according to the Brennand protocol, these lines produced much higher amounts of MECP2 than they had during the NGN2 protocol, pointing to the change resulting from the protocol itself and not the specific line. We know that modulation of the quantity of MECP2 is important as patients with reduced MECP2 have Rett Syndrome and patients with too much MECP2 have MECP2 Duplication Disorder, a disorder where patients are neurodevelopmentally delayed and have speech abnormalities, seizures, and progressive spasticity (Ramocki et al., 2010). Small changes in MECP2 dosage affecting severity can also be seen in the effects of XCI skewing (Zogbhi et al., 1990; Shahbazian and Zoghbi., 2002). Neurons differentiated according to the NGN2 protocol seem to have less MECP2. Therefore, it seems likely that if the same cell lines were differentiated according to the Brennand protocol, which

produces more MECP2 and therefore has a larger difference in MECP2 quantities between WT and RTT, the differences presented in this thesis would be even more significant. In addition, knowing that different protocols produce different amounts of MECP2, this might allow us new opportunities to examine RTT. For example, I used this difference to examine new characteristics of the L124W mutation. NEDD4L, a ubiquitin protein ligase, is of great interest in to the lab due to its reduction in RTT MECP2 null lines (Rodrigues et al., 2020). However, this protein could not be detected in the NGN2 derived neurons due to low abundance. By using the L124W lines that had been Brennand differentiated, I was able to see NEDD4L in the L124W lines for the first time. Overall, these experiments demonstrate the importance of understanding the limitations and advantages of different differentiation methods and using the appropriate one.

4.3 Experimental Limitations

4.3.1 Rationale for Lack of RTT-3 CRISPR Correction

In addition to the work already discussed, my results also detailed work to use CRISPR to correct the L124W mutant line with the idea of using this line to both provide evidence that the mutation was responsible for the dendrite complexity phenotype and to control for the different X chromosome between WT-3 and RTT-3. Through this work, I did successfully optimize an ssODN CRISPR protocol and generated both indels and corrections of the PAM site. However, I was unable to obtain the actual L124W correction itself. Based on the successful generation of indels at the cut site location, it appears that the CRISPR and the guide both worked as anticipated. In addition, the successful PAM site edit indicates that the ssODN template worked as expected. Therefore, it seems there are two likely candidates as to why no correction was generated: distance from the PAM site and number of clones picked.

Despite PAM sites occurring frequently throughout the genome with an average of every 8-12bp (Ran et al., 2013), the L124W mutation is 34 base pairs away from the closest PAM site. Recently, a number of different papers have shown that the distance between the cut site (4bp upstream of PAM) and the desired mutation is a key factor to editing efficiency (Yang et al., 2013; Bialk et al., 2015; Kwart et al., 2017). These studies found that while a correction at 34bp is possible, it suffers from a low editing efficiency as the repair mechanisms reading the ssODN will often fall off before reaching the desired mutation resulting in bases more distant to the cut site being incorporated less frequently. In addition, when the edit is more than 16bp from the cut

site, the amount of accurate HDR drops from 80% to less than 20% with continued drops in efficiency the farther the desired edit was from the cut site (Kwart et al., 2017). With HDR itself only occurring in stem cells at a 2.1-6.7% rate under ideal distances (Paquet et al., 2016), this additional distance reduction resulted in an extremely low efficiency rate for the L124W mutation of roughly 1.5%.

When starting these experiments, I had hoped to overcome the low efficiency by screening a higher number of cells through the use of 96 well plates and ddPCR. Unfortunately, the L124W cells experienced high rates of cell death when plated in 96 well plates. This could be due to altered cell densities, increased handling, increased passage, or low adhesion to the alternative plate type. Although some cells from a 6 well plate were sent for ddPCR, the length of time between results meant that the iPSCs reached high passage numbers and were not viable for picking. As such, I was not able to use the ddPCR 96 plate method to overcome the low editing efficiency. I ended up performing a single ddPCR to ensure that the edit existed within the population and then manually picked and cultured 136 clones to search for the correction. Unfortunately, the combination of low efficiency and relatively low number of clones picked meant that I did not successfully pick one of the few cells from the original 800,000 that was successfully edited. As such, I believe that the issue was not in the generation of the clone but in its isolation. Looking forward, I believe that if a better screening method was used to isolate the desired clone, the same protocol could be used to successfully generate the L124W correction.

4.3.2 Differences in Phenotypic Trends Within RTT-3 and WT-3 Lines

The WT-3 and RTT-3 lines were originally generated from fibroblasts derived from the L124W patient. In the iPSC generation process, each line was derived from a distinct fibroblast and a number of different pluripotency metrics were assessed to define the best iPSC lines to phenotype. At the end of this process, we retained 2 WT-3 (A & B) lines and 2 RTT-3 (C & D) lines where the two WT-3 lines should have been identical and the two RTT-3 lines should have been identical. Having two lines for each isogenotype allowed me to determine a significant change only if both WT-3 lines significantly differed from both RTT-3 lines. It was under these conditions that the dendrite complexity phenotype was found. However, for unknown reasons, experiments sometimes showed a difference between the two WT-3 lines with one trending more like a ‘wild-type’ (differed from the RTT lines) and one trending more in the direction of the

RTT lines. Similarly, sometimes one of the RTT lines would trend in the direction of the WT and appear to give more WT-like results. My original hypothesis was erosion of the X-inactivation skew, a known phenomenon in iPSCs (Mekhoubad et al., 2012; Ohhata & Wutz, 2013), however when I repeated the androgen receptor assay it showed that there had been no erosion of the inactive X-chromosome. One additional possibility for the variability is in the chosen NGN2 differentiation method (Zhang et al., 2013); as the iPSCs are lenti-virally infected with NGN2, each cell line will carry a different number of NGN2 copies. This could potentially create differences in the differentiation process, affecting the phenotype of the final neurons. To control for this, future work could place a single copy of NGN2 within the AAV1S safe harbour site, thereby ensuring that all lines receive the same amount of NGN2. In addition, as the WT-3/RTT-3 is the only RTT line in which we have patient duplicates we do not currently know if this level of variability within isogenic lines is normal. One alternative would be to take some of the other WT-3/RTT-3 lines that were cryopreserved and repeat the same assays to see which way these lines trend.

4.4 Tying Results to L124W Mutation Work by Collaborators

In conjunction to the work done in this report, we also had a number of collaborators working on projects related to the L124W mutation. Their work provides additional information on the mutation and provides insights back to my own work.

4.4.1 L124W Mutation Creates a Binding Defect

My thesis showed that there was no change in RTT-3 *Mecp2* RNA or MECP2 protein levels. This lack of change in RTT-3 MECP2 at the RNA or protein levels suggests that the L124W mutation does not interfere with the production or final quantity of the protein itself. As such, we hypothesized that perhaps the L124W mutation, which is located in the key methyl binding domain at the end of exon 3, interferes with the binding of MECP2 to DNA. Although the L124W mutation has not been previously reported, an L124F mutation had been found to have severely impaired chromatin binding (Kudo et al., 2003). Furthermore, the crystallized structure of the WT MECP2 methyl binding domain bound to the BDNF promoter (Ho et al., 2008) showed that the R106 mutation, one of the 8 most common mutation points, is located very close to the L124 mutations. As such, we thought that the L124W mutation might have the same chromatin binding problems seen in these other two mutations. Through a collaboration with the

John Vincent lab where they expressed the L124W, L124F, and R106 mutations in mouse cells and looked at chromocenter disruption, we have found that the novel L124W mutation has reduced chromocenter binding and showed an intermediate phenotype between the WT and the complete disruption of binding seen in the L124F and the R106. In addition, a fluorescence recovery after photobleaching (FRAP) assay showed that the L124W MECP2-GFP fusion protein was highly mobile, binding and releasing chromocenters very quickly (Mok et al., in prep). Based on these results, it appears that the L124W mutation does not cause a disruption in MECP2 quantity but rather impedes the ability of MECP2 bind DNA, causing only a transient binding before quickly falling off. As such, L124W MECP2 does not show a severe impairment like L124F or R106 which were not able to bind at all but does show more impairment than the WT control. Together, this seems to contribute to the L124W having an intermediary or less severe phenotype when compared to null RTT lines.

4.4.2 L124W Mutation & Single Neuron Electrophysiology

I examined the extracellular phenotypes of the L124W mutation on the multi-electrode array and demonstrate that there was no significant change between WT-3 and RTT-3. Interestingly, work done by Dr Wenbo Zhang in Michael Salter's lab with whole-cell patch clamp electrophysiology showed that the 6-week NGN2 RTT-3 lines do show some intracellular electrophysiology alterations compared to WT-3. While the MEA looks at network connections, patch clamp analysis is performed on a single neuron at a time allowing an examination of intracellular electrophysiology. Parallel work on our null lines found that the RTT null lines exhibited higher resting membrane potential, increased input resistance, decreased cell capacitance, fewer invoked action potentials, reduced AMPAR-nESPC amplitude and frequency, and diminished Na^+ and K^+ currents (Mok et al., in prep). In contrast, the RTT-3 lines displayed only a subset of these phenotypes, with increased input resistance, impaired invoked N^+ and K^+ currents, and a trend towards reduced AMPAR mEPSC amplitude and frequency (Mok et al., in prep). This supports the idea that the RTT-3 lines have a less severe phenotype relative to our null lines.

4.5 Novelty of L124W Mild Genotype/Phenotype Correlation

Overall, this report highlights potential phenotypic differences in our RTT lines and reinforces the idea that different RTT mutations confer different levels of severity in patients. The field has examined the idea of *MECP2* mutation and phenotype-genotype correlations since its early days

when patient mutations were compared to clinical traits and other factors such as electrophysiological data, and cerebrospinal fluid neurochemistry (Amir & Zoghbi, 2000; Cheadle et al., 2000; Huppke et al., 2000). These first investigations found variable results with some papers claiming no correlation between mutation and severity (Amir & Zoghbi, 2000) and others finding that patients with missense mutations had a less severe version of RTT relative to truncation mutations (Huppke et al., 2000). However, all of the papers agreed that X-chromosome inactivation was an important modulator of phenotype, demonstrating that severity of RTT could be affected (Amir et al., 2000). As the field progressed, clinical studies continued to investigate this question and the field began to move towards the idea that severity and mutation type were linked, albeit with nuance beyond the missense vs truncation idea that the early studies had examined. For example, a clinical cross-sectional study found that particular mutations were less severe relative to other mutations and began to create what was essentially a 'severity scale' for each of the mutations where the R133C mutation was less severe than the R168X or where large DNA deletions were considered more severe than late carboxy truncating mutations (Neul et al., 2008). Since then, several papers have shown a link between clinical severity and MECP2 mutation (Neul et al., 2010; Cuddapah et al., 2014). More recently, another clinical study found that particular MECP2 mutations were linked to the severity of patient phenotypes such as bone density (Caffarelli et al., 2020). To date, all of these studies have been performed *in vivo*. My research represents the first description of an *in vitro* less severe phenotype.

In summary, I found the first phenotype for the RTT-3 L124W mutation, a subtle dendrite complexity phenotype. This is novel in that it is the first of our lines to show a dendrite complexity phenotype without the more severe dendrite length and soma area phenotypes typically found in RTT patients. It is also novel in that it is the first *in vitro* example of a mild RTT case.

4.6 Future Directions

The results presented in this report provides a number of first steps that could be followed up with additional work and experiments. I would propose that there are two key areas of investigation available. Firstly, there is the continued investigation into the L124W mutation and its nature as an intermediary or subtle RTT mutation and secondly, I would propose using the

NEDD4L KO line I created to better understand the roll of NEDD4L in RTT. In addition, there are a number of secondary areas that could be pursued including the use of the In Cell Western protocol that I tested in drug screening trials or looking into the difference in MECP2 protein levels seen between differentiation methods.

4.6.1 The L124W Mutation Follow-Up

The L124W mutation has been shown to demonstrate a subtle or intermediary phenotype across a number of key assays however further assays could be used to continue to understand the affected pathways of this particular mutation. Here, I described a morphology phenotype in dendrite complexity, however another well-known morphology alteration in RTT patients is synapse development (Johnston et al., 2001). It has been demonstrated in patients and mice that RTT consistently features a reduction in synapse number and an overall reduced excitatory synaptic response while microarray analysis shows reductions in gene products related to synapses such as NMDA receptor subunits and synaptic vesicle proteins (Johnston et al., 2001; Chao et al., 2007). In addition, both RTT human ES cells and iPS cells have been previously reported to show defects in synapse formation and function (Marchetto et al., 2010; Li et al., 2013) and our lab has performed synapse counting assays in our autism cell lines (Zaslavsky et al., 2019). As we know that the L124W mutation does confer some morphology phenotypes and as we also know that the L124W lines exhibit electrophysiology reductions in patch clamp, it is possible that they also possess a subtle reduction in synapse number or response. To pursue this, WT and L124W neurons have been sparsely transfected with GFP for immunostaining and counted for puncta containing both SYN1 and HOMER1, markers of mammalian cortical synapses.

In addition to the synapse count, future examination of the L124W mutation should include a comparison of the WT-3 and RTT-3 lines to each other and our null lines through RNA sequencing (RNA-Seq) analysis. RNASeq is currently underway on the L124W lines, and the RTT null lines will be evaluated over the summer. This would allow an examination of the overall changes in the presence and amount of RNA in each of these lines. It is known that RTT lines typically display a wide range of subtle RNA changes across models with dysregulation in gene transcription and global translation (Li et al., 2013; Lyst et al., 2013; Renthal et al., 2018). However, we hypothesize that the unique nature of the L124W phenotypes may provide

additional insights. The lab is considering the idea that as an intermediary mutation, it seems likely that the L124W lines will have reduced RNA changes relative to the null lines and perhaps only express a subset of the null's differences. By examining what changes lies in common and different between the L124W and the nulls, we can begin to better understand the pathways and mechanisms that underlie these varying phenotypes. Ultimately, this would allow additional insights into potential therapies and provide better points for patient-specific drug targets. Another related area of personal interest is the link between RTT phenotypes and diagnostics. One possibility would be using the L124W lines to search for the 'core features' of RTT diagnostics. As the L124W patient has been diagnosed with RTT but does not show the traditional neuronal phenotypes (dendrite length, soma size, electrophysiology), it is possible that these phenotypes do not contribute to the physical and behavioral traits that clinicians look for. As such, with a better understanding of the patient's diagnostic record, the L124W lines could be used to better narrow in on and elucidate the pathways behind these traits.

Looking farther ahead, I would also propose additional work into L124W rescue experiments with both gene editing and treatment with compounds that affect dendrite arborization pathways. For gene editing, the work presented in this paper demonstrates that the CRISPR-Correction protocol I used could successfully work if a better screening method was found. Some possibilities could include cloning the guide into a plasmid with puromycin resistance, as done in the *NEDD4L* KO experiment, to allow screening by resistance. Another option would be to boost the survivability of the cells in 96 well plates through the addition and optimization of cell supporting compounds such as CloneR or ROCK inhibitor. If the distance from the PAM site continues to be an issue, the traditional Cas9 could be switched for a Prime editor (Anzalone et al., 2019). This new gene editing technique, often called CRISPR Prime, increases the efficiency of the edit and works at distance of more than 100bp from the PAM site by fusing the reverse transcriptase to an RNA-programmable nickase and the prime editing extended guide RNA (pegRNA), ultimately directly copying the new genetic information off the pegRNA (Anzalone et al., 2019). The generation of an L124W correction by one of these means could then be put back through the dendrite complexity assays, hopefully showing a complete elimination of the phenotype and demonstrating that is truly is the L124W mutation leading to these changes. This correction will also create a more accurate control, as the RTT and rescue lines will no longer differ in their active X-chromosome, that could be used in future experiments. Alongside

performing an L124W rescue, it would also be interesting to use CRISPR/Cas9 to generate another mutation in the RTT-3. In the event that a genetic CRISPR rescue does not rescue the L124W phenotypes, I would propose either targeted sequencing of genes *FOXG1* and *CDKL5,* which have mutations implicated in atypical RTT and make up just under 10% of RTT cases, or full genome sequencing to determine other mutations that may be generating the phenotypes.

In addition to a CRISPR rescue, it would be interesting to see the effect of various compounds on the L124W lines. Most notably, BDNF and its downstream hormone IGF-1 have both been well established to be regulated by MECP2 (Chang et al., 2006; Abuhatzia et al., 2007; Chahrour et al., 2008) and has been found to affect dendritic growth and arborization (Larimore et al., 2009) and rescue synaptic function (Kline et al., 2010). More recently, BDNF overexpression has also been found to partially-rescue dendrite atrophy (Nerli et al., 2020). Although BDNF has a well-established history of rescuing RTT dendrite morphology phenotypes, it has never been tested for its effectiveness on dendrite complexity phenotypes like seen in the L124W. In addition, it is possible that the addition of BDNF will result in the neurons growing too large which could have negative impacts on the cells such as are seen in MECP2 Duplication Syndrome.

Finally, my worked showed a preliminary examination of NEDD4L for the first time in the L124W lines. Our lab has shown that NEDD4L is reduced in null RTT lines (Rodrigues et al., 2020). Further work could optimize the protocol and determine if NEDD4L is significantly changed in the intermediary L124W lines.

4.6.2 Using the NEDD4L CRISPR KO Line

As a part of this project, I used CRISPR to generate and validate two NEDD4L Knock-Out (KO) lines. Both of these lines show a complete NEDD4L protein KO on both the WES and traditional western blot and have been determined to be karyotypically normal with no known off target mutations at the checked sites. As PCR off-targeting analysis is limited, as a first step, whole genome sequencing could be used to check the entire genome for any off-target changes. Going forward, these lines can be further validated by the lab and then used in a number of upcoming experiments. While the NEDD4L KO lines can work as an excellent control line, more crucial is that they provide a new opportunity to examine the effect and pathway of NEDD4L. Previously, the literature has shown Nedd4-2 (another name of NEDD4L) KOs in mice (Hisa et al., 2014; Manning & Kumar, 2018) but my lines are the first human iPSC model created. As our lab is the

first to study NEDD4L in RTT (Rodrigues et al., 2020), these lines will allow the lab to continue this work. Some next steps underway in the lab include proteomics experiments with a specific interest in the ubiquitome, a comparison of existing RNA-seq data in the MECP2 null lines to the NEDD4L KO lines, and an examination of the phenotypes of the NEDD4L KO lines.

It is worth noting that the PGPC-3 line is a male control line and RTT occurs primarily in females. In the generation of these lines, we performed the plasmid CRISPR/Cas9 protocol on both our female control PGPC-14 line, which was previously used in the MECP2 gene edits, and the male control line PGPC-3. From this population, we generated a number of NEDD4L knock-downs and the two knock-outs reported here. However, both KOs were in the male PGPC-3 line. While generation of the NEDD4L KO in female lines would have allowed us to better model human RTT, male hemizygous RTT models are commonly used in mice and, although they are in the minority, male RTT patients do exist. As such, these lines can still provide insights into NEDD4L, its pathways, and the effect of a NEDD4L KO on cells.

4.6.3 Use of In Cell Western as a Screening Device

Upon starting in the lab, one of my side projects was testing the In Cell Western (ICW) assay for the lab with the hope of eventually using the assay to perform drug screens on the L124W lines. The ICW is a quantitative immunofluorescence assay performed directly in cell culture plates used to detect proteins in fixed cells using targeted primary antibodies and infra-red fluorescent secondary antibodies. As the ICW takes place directly in the well of a plate, iPSCs or neurons could be cultured directly in 96 well plates and then analyzed all at once, making a drug screen more efficient. In fact, this method has been previously used in a drug screen on MECP2 Duplication Disorder and found positive hits (Nageshappa et al., 2016). My work optimized the lab's protocol for the ICW, determined that MECP2 changes could be viewed on the ICW, and then tested a number of other proteins for their drug screening potential. Ultimately, I performed two preliminary tests that could potentially be used in an ICW screen: SAP-90 levels (previously known as PSD-95) and puromycin incorporation levels. SAP-90 (PSD-95) is a regulator of synaptic maturation including the stabilization and trafficking of NMDARs and AMPARs. Previous research has shown that SAP-90 (PSD-95) is significantly reduced in RTT lines and that this can be rescued with IGF-1(Tropea et al., 2009). Preliminary experiments suggested that this reduction could be seen in our cell lines on the ICW, the first examination of this protein in

our lab. The use of SAP-90 (PSD-95) is of particular interest as the successful MECP2 Duplication ICW screen used SAP-90 (PSD-95) to great effect (Nageshappa et al., 2016). In addition to SAP-90, ICW preliminary tests suggested that the assay could detect a difference in a puromycin incorporation assay (sometimes called a SUnSET assay), suggesting changes in protein synthesis between WT and RTT (Schmidt et al., 2009). Based on these preliminary tests, future work could eventually use these two ICW assays to begin drug screens on RTT cell lines.

4.6.4 Examining Differentiation Methods

Further follow-up work could be performed on examining the effect of various differentiation methods on MECP2 and other relevant RTT proteins. Although my work showed that the Brennand method generated more MECP2 relative to a total protein stain than the NGN2 or 6F protocols, it is possible that other proteins have altered levels depending on the differentiation method. For example, work in our lab and in this report show that levels of NEDD4L are too low for detection in the NGN2 lines but can be detected in the Brennand lines. Future work could look into other proteins and determine which are seeing an effect of differentiation and how this could be affecting various cellular phenotypes.

4.7 Conclusions

In this thesis, I examined the phenotypes of the novel RTT mutation L124W and found that the mutation exhibits a less severe phenotype relative to our null lines. The L124W lines exhibits no changes in *MECP2* RNA or MECP2 protein levels, no change in soma area or dendrite length, and no extracellular electrophysiological change as determined by MEA. The lines did exhibit a subtle dendrite order and complexity phenotype. This represents the first time that an RTT patient iPSC model of intermediate severity has been characterized. Moreover, I established a protocol for the eventual CRISPR correction of the L124W mutation and successfully generated a CRISPR KO line in NEDD4L, a downstream target of MECP2. This KO line is the first NEDD4L KO line in human iPSC and will be available as a resource to elucidate the role and pathway of NEDD4L. Finally, I provided evidence for neuronal differentiation methods affecting MECP2 levels and developed a protocol for screening RTT neurons using SAP-90 and puromycin incorporation in an In Cell Western assay. In conclusion, the phenotyping of the first intermediate-severity iPSC line and the generation of the first iPSC NEDD4L KO line will have

immense value in further elucidating the pathways of MECP2, the intricacies and pathologies of RTT, and ultimately lead to identifying effective treatments for Rett Syndrome.

References

1.Abdel-Maguid, T E, and D Bowsher. 1984. “Classification of Neurons by Dendritic Branching Pattern. A Categorisation Based on Golgi Impregnation of Spinal and Cranial Somatic and Visceral Afferent and Efferent Cells in the Adult Human.” Journal of Anatomy 138 (Pt 4): 689–702.

2.Abuhatzira, Liron, Kirill Makedonski, Yotam Kaufman, Aharon Razin, and Ruth Shemer. 2007. “MeCP2 Deficiency in the Brain Decreases BDNF Levels by REST/CoREST-Mediated Repression and Increases TRKB Production.” Epigenetics 2 (4): 214–22. https://doi.org/10.4161/epi.2.4.5212.

3.Adkins, Nicholas L., and Philippe T. Georgel. 2011. “MeCP2: Structure and Function. This Paper Is One of a Selection of Papers Published in a Special Issue Entitled 31st Annual International Asilomar Chromatin and Chromosomes Conference, and Has Undergone the Journal’s Usual Peer Review Process.” Biochemistry and Cell Biology 89 (1): 1–11. https://doi.org/10.1139/O10-112.

4.Amir, Ruthie E., Ignatia B. Van den Veyver, Mimi Wan, Charles Q. Tran, Uta Francke, and Huda Y. Zoghbi. 1999. “Rett Syndrome Is Caused by Mutations in X-Linked MECP2, Encoding Methyl-CpG-Binding Protein 2.” Nature Genetics 23 (2): 185–88. https://doi.org/10.1038/13810.

5.Amir, Ruthie E., Ignatia B. Van Den Veyver, Rebecca Schultz, Denise M. Malicki, Charles Q. Tran, E. J. Dahle, Anne Philippi, et al. 2000. “Influence of Mutation Type and X Chromosome Inactivation on Rett Syndrome Phenotypes.” Annals of Neurology 47 (5): 670–79. https://doi.org/10.1002/1531-8249(200005)47:5<670::AID-ANA20>3.0.CO;2-F.

6.Amir, Ruthie E, and Huda Y Zoghbi. 2000. “Rett Syndrome: Methyl-CpG-Binding Protein 2 Mutations and Phenotype–Genotype Correlations.” American Journal of Medical Genetics 97: 6.

7.Ananiev, Gene, Emily Cunningham Williams, Hongda Li, and Qiang Chang. 2011. “Isogenic Pairs of Wild Type and Mutant Induced Pluripotent Stem Cell (IPSC) Lines from Rett Syndrome Patients as In Vitro Disease Model.” PLoS ONE 6 (9). https://doi.org/10.1371/journal.pone.0025255.

8.Anzalone, Andrew V., Peyton B. Randolph, Jessie R. Davis, Alexander A. Sousa, Luke W. Koblan, Jonathan M. Levy, Peter J. Chen, et al. 2019. “Search-and-Replace Genome Editing without Double-Strand Breaks or Donor DNA.” Nature 576 (7785): 149–57. https://doi.org/10.1038/s41586-019-1711-4.

9.Ariani, Francesca, Giuseppe Hayek, Dalila Rondinella, Rosangela Artuso, Maria Antonietta Mencarelli, Ariele Spanhol-Rosseto, Marzia Pollazzon, et al. 2008. “FOXG1 Is Responsible for the Congenital Variant of Rett Syndrome.” American Journal of Human Genetics 83 (1): 89–93. https://doi.org/10.1016/j.ajhg.2008.05.015.

10.Armstrong, Dawna, J. Kay Dunn, Barbara Antalffy, and Renuka Trivedi. 1995. “Selective Dendritic Alterations in the Cortex of Rett Syndrome.” Journal of Neuropathology &

Experimental Neurology 54 (2): 195–201. https://doi.org/10.1097/00005072-199503000-00006.

11.Balachandar, Vellingiri, Venkatesan Dhivya, Mohan Gomathi, Subramaniam Mohanadevi, Balasubramanian Venkatesh, and Bharathi Geetha. 2016. “A Review of Rett Syndrome (RTT) with Induced Pluripotent Stem Cells.” Stem Cell Investigation 3 (September). https://doi.org/10.21037/sci.2016.09.05.

12.Ban, Hiroshi, Naoki Nishishita, Noemi Fusaki, Toshiaki Tabata, Koichi Saeki, Masayuki Shikamura, Nozomi Takada, et al. 2011. “Efficient Generation of Transgene-Free Human Induced Pluripotent Stem Cells (IPSCs) by Temperature-Sensitive Sendai Virus Vectors.” Proceedings of the National Academy of Sciences of the United States of America 108 (34): 14234–39. https://doi.org/10.1073/pnas.1103509108.

13.Bauman, M. L., Th L. Kemper, and D. M. Arin. 1995a. “Microscopic Observations of the Brain in Rett Syndrome.” Neuropediatrics 26 (2): 105–8. https://doi.org/10.1055/s-2007-979737

14.Bebbington, A., A. Anderson, D. Ravine, S. Fyfe, M. Pineda, N. de Klerk, B. Ben-Zeev, et al. 2008. “Investigating Genotype-Phenotype Relationships in Rett Syndrome Using an International Data Set.” Neurology 70 (11): 868–75. https://doi.org/10.1212/01.wnl.0000304752.50773.ec.

15.Bebbington, A., A. Percy, J. Christodoulou, D. Ravine, G. Ho, P. Jacoby, A. Anderson, et al. 2010. “Updating the Profile of C-Terminal MECP2 Deletions in Rett Syndrome.” Journal of Medical Genetics 47 (4): 242–48. https://doi.org/10.1136/jmg.2009.072553.

16.Ben-Shachar, Shay, Maria Chahrour, Christina Thaller, Chad A. Shaw, and Huda Y. Zoghbi. 2009. “Mouse Models of MeCP2 Disorders Share Gene Expression Changes in the Cerebellum and Hypothalamus.” Human Molecular Genetics 18 (13): 2431–42. https://doi.org/10.1093/hmg/ddp181.

17.Bialk, Pawel, Natalia Rivera-Torres, Bryan Strouse, and Eric B. Kmiec. 2015. “Regulation of Gene Editing Activity Directed by Single-Stranded Oligonucleotides and CRISPR/Cas9 Systems.” PLoS ONE 10 (6). https://doi.org/10.1371/journal.pone.0129308.

18.Bird, Alex D., and Hermann Cuntz. 2019. “Dissecting Sholl Analysis into Its Functional Components.” Cell Reports 27 (10): 3081-3096.e5. https://doi.org/10.1016/j.celrep.2019.04.097.

19.Boch, Jens, Heidi Scholze, Sebastian Schornack, Angelika Landgraf, Simone Hahn, Sabine Kay, Thomas Lahaye, Anja Nickstadt, and Ulla Bonas. 2009. “Breaking the Code of DNA Binding Specificity of TAL-Type III Effectors.” Science 326 (5959): 1509–12. https://doi.org/10.1126/science.1178811.

20.Bragança, José, João André Lopes, Leonardo Mendes-Silva, and João Miguel Almeida Santos. 2019. “Induced Pluripotent Stem Cells, a Giant Leap for Mankind Therapeutic Applications.” World Journal of Stem Cells 11 (7): 421–30. https://doi.org/10.4252/wjsc.v11.i7.421.

21.Brennand, Kristen J., Anthony Simone, Jessica Jou, Chelsea Gelboin-Burkhart, Ngoc Tran, Sarah Sangar, Yan Li, et al. 2011. “Modelling Schizophrenia Using Human Induced Pluripotent Stem Cells.” Nature 473 (7346): 221–25. https://doi.org/10.1038/nature09915.

22.Caffarelli, Carla, Stefano Gonnelli, Maria Dea Tomai Pitinca, Silvia Camarri, Antonella Al Refaie, Joussef Hayek, and Ranuccio Nuti. 2020. “Methyl-CpG-Binding Protein 2 (MECP2) Mutation Type Is Associated with Bone Disease Severity in Rett Syndrome.” BMC Medical Genetics 21 (January). https://doi.org/10.1186/s12881-020-0960-2.

23.Chahrour, Maria, Sung Yun Jung, Chad Shaw, Xiaobo Zhou, Stephen T. C. Wong, Jun Qin, and Huda Y. Zoghbi. 2008. “MeCP2, a Key Contributor to Neurological Disease, Activates and Represses Transcription.” Science (New York, N.Y.) 320 (5880): 1224–29. https://doi.org/10.1126/science.1153252.

24.Chahrour, Maria, and Huda Y. Zoghbi. 2007. “The Story of Rett Syndrome: From Clinic to Neurobiology.” Neuron 56 (3): 422–37. https://doi.org/10.1016/j.neuron.2007.10.001.

25.Chang, Qiang, Gargi Khare, Vardhan Dani, Sacha Nelson, and Rudolf Jaenisch. 2006. “The Disease Progression of Mecp2 Mutant Mice Is Affected by the Level of BDNF Expression.” Neuron 49 (3): 341–48. https://doi.org/10.1016/j.neuron.2005.12.027.

26.Chao, Hsiao-Tuan, Huda Y. Zoghbi, and Christian Rosenmund. 2007. “MeCP2 Controls Excitatory Synaptic Strength by Regulating Glutamatergic Synapse Number.” Neuron 56 (1): 58–65. https://doi.org/10.1016/j.neuron.2007.08.018.

27.Chapleau, Christopher A., Gaston D. Calfa, Meredith C. Lane, Asher J. Albertson, Jennifer L. Larimore, Shinichi Kudo, Dawna L. Armstrong, Alan K. Percy, and Lucas Pozzo-Miller. 2009. “Dendritic Spine Pathologies in Hippocampal Pyramidal Neurons From Rett Syndrome Brains and After Expression of Rett-Associated MECP2 Mutations.” Neurobiology of Disease 35 (2): 219–33. https://doi.org/10.1016/j.nbd.2009.05.001.

28.Cheadle, Jeremy P., Harinder Gill, Nick Fleming, Julie Maynard, Alison Kerr, Helen Leonard, Michael Krawczak, et al. 2000. “Long-Read Sequence Analysis of the MECP2 Gene in Rett Syndrome Patients: Correlation of Disease Severity with Mutation Type and Location.” Human Molecular Genetics 9 (7): 1119–29. https://doi.org/10.1093/hmg/9.7.1119.

29.Chen, Richard Z., Schahram Akbarian, Matthew Tudor, and Rudolf Jaenisch. 2001. “Deficiency of Methyl-CpG Binding Protein-2 in CNS Neurons Results in a Rett-like Phenotype in Mice.” Nature Genetics 27 (3): 327–31. https://doi.org/10.1038/85906.

30.Cheung, Aaron Y.L., Lindsay M. Horvath, Daria Grafodatskaya, Peter Pasceri, Rosanna Weksberg, Akitsu Hotta, Laura Carrel, and James Ellis. 2011. “Isolation of MECP2-Null Rett Syndrome Patient HiPS Cells and Isogenic Controls through X-Chromosome Inactivation.” Human Molecular Genetics 20 (11): 2103–15. https://doi.org/10.1093/hmg/ddr093.

31.Chin, Mark H., Mike J. Mason, Wei Xie, Stefano Volinia, Mike Singer, Cory Peterson, Gayane Ambartsumyan, et al. 2009. “Induced Pluripotent Stem Cells and Embryonic Stem Cells Are Distinguished by Gene Expression Signatures.” Cell Stem Cell 5 (1): 111–23. https://doi.org/10.1016/j.stem.2009.06.008.

32.Colantuoni, Carlo, Ok-Hee Jeon, Karim Hyder, Alex Chenchik, Anis H. Khimani, Vinodh Narayanan, Eric P. Hoffman, Walter E. Kaufmann, SakkuBai Naidu, and Jonathan Pevsner. 2001. “Gene Expression Profiling in Postmortem Rett Syndrome Brain: Differential Gene

Expression and Patient Classification." Neurobiology of Disease 8 (5): 847–65. https://doi.org/10.1006/nbdi.2001.0428.

33.Costa, Luciano Da Fontoura, Krissia Zawadzki, Mauro Miazaki, Matheus P. Viana, and Sergei N. Taraskin. 2010. "Unveiling the Neuromorphological Space." Frontiers in Computational Neuroscience 4 (December). https://doi.org/10.3389/fncom.2010.00150.

34.Cowan, Chad A., Jocelyn Atienza, Douglas A. Melton, and Kevin Eggan. 2005. "Nuclear Reprogramming of Somatic Cells After Fusion with Human Embryonic Stem Cells." Science 309 (5739): 1369–73. https://doi.org/10.1126/science.1116447.

35.Croci, Susanna, Miriam Lucia Carriero, Katia Capitani, Sergio Daga, Francesco Donati, Elisa Frullanti, Vittoria Lamacchia, et al. 2020. "High Rate of HDR in Gene Editing of p.(Thr158Met) MECP2 Mutational Hotspot." European Journal of Human Genetics, April, 1–12. https://doi.org/10.1038/s41431-020-0624-x.

36.Cuddapah, Vishnu Anand, Rajesh B Pillai, Kiran V Shekar, Jane B Lane, Kathleen J Motil, Steven A Skinner, Daniel Charles Tarquinio, et al. 2014. "Methyl-CpG-Binding Protein 2 (MEPC2) Mutation Type Is Associated with Disease Severity in Rett Syndrome." Journal of Medical Genetics 51 (3): 152–58. https://doi.org/10.1136/jmedgenet-2013-102113.

37.Dajani, Rana, Sung-Eun Koo, Gareth J. Sullivan, and In-Hyun Park. 2013. "Investigation of Rett Syndrome Using Pluripotent Stem Cells." Journal of Cellular Biochemistry 114 (11): 2446–53. https://doi.org/10.1002/jcb.24597.

38.Dimos, John T., Kit T. Rodolfa, Kathy K. Niakan, Laurin M. Weisenthal, Hiroshi Mitsumoto, Wendy Chung, Gist F. Croft, et al. 2008. "Induced Pluripotent Stem Cells Generated from Patients with ALS Can Be Differentiated into Motor Neurons." Science 321 (5893): 1218–21. https://doi.org/10.1126/science.1158799.

39.Djuric, Ugljesa, Aaron Y. L. Cheung, Wenbo Zhang, Rebecca S. Mok, Wesley Lai, Alina Piekna, Jason A. Hendry, et al. 2015. "MECP2e1 Isoform Mutation Affects the Form and Function of Neurons Derived from Rett Syndrome Patient IPS Cells." Neurobiology of Disease 76 (April): 37–45. https://doi.org/10.1016/j.nbd.2015.01.001.

40.Ebert, Allison D., Junying Yu, Ferrill F. Rose, Virginia B. Mattis, Christian L. Lorson, James A. Thomson, and Clive N. Svendsen. 2009. "Induced Pluripotent Stem Cells from a Spinal Muscular Atrophy Patient." Nature 457 (7227): 277–80. https://doi.org/10.1038/nature07677.

41.Egorina, E. M., M. A. Sovershaev, and B. Østerud. 2006. "In-Cell Western Assay: A New Approach to Visualize Tissue Factor in Human Monocytes." Journal of Thrombosis and Haemostasis 4 (3): 614–20. https://doi.org/10.1111/j.1538-7836.2005.01781.x.

42.Escamilla-Del-Arenal, Martin, Simao Teixeira da Rocha, and Edith Heard. 2011. "Evolutionary Diversity and Developmental Regulation of X-Chromosome Inactivation." Human Genetics 130 (2): 307–27. https://doi.org/10.1007/s00439-011-1029-2.

43.Evans, M. J., and M. H. Kaufman. 1981. "Establishment in Culture of Pluripotential Cells from Mouse Embryos." Nature 292 (5819): 154–56. https://doi.org/10.1038/292154a0.

44.Farra, N, W-B Zhang, P Pasceri, J H Eubanks, M W Salter, and J Ellis. 2012. "Rett Syndrome Induced Pluripotent Stem Cell-Derived Neurons Reveal Novel Neurophysiological Alterations." Molecular Psychiatry 17 (12): 1261–71. https://doi.org/10.1038/mp.2011.180.

45.Fernandes, Tiago G., Sofia T. Duarte, Mehrnaz Ghazvini, Cláudia Gaspar, Diana C. Santos, Ana R. Porteira, Gonçalo M. C. Rodrigues, et al. 2015. “Neural Commitment of Human Pluripotent Stem Cells under Defined Conditions Recapitulates Neural Development and Generates Patient-Specific Neural Cells.” Biotechnology Journal 10 (10): 1578–88. https://doi.org/10.1002/biot.201400751.

46.Goffin, Darren, and Zhaolan (Joe) Zhou. 2012. “The Neural Circuit Basis of Rett Syndrome.” Frontiers in Biology 7 (5): 428–35. https://doi.org/10.1007/s11515-012-1248-5.

47.Guy, Jacky, Jian Gan, Jim Selfridge, Stuart Cobb, and Adrian Bird. 2007. “Reversal of Neurological Defects in a Mouse Model of Rett Syndrome.” Science 315 (5815): 1143–47. https://doi.org/10.1126/science.1138389.

48.Guy, Jacky, Brian Hendrich, Megan Holmes, Joanne E. Martin, and Adrian Bird. 2001. “A Mouse Mecp2 -Null Mutation Causes Neurological Symptoms That Mimic Rett Syndrome.” Nature Genetics 27 (3): 322–26. https://doi.org/10.1038/85899.

49.Hagberg, Bengt. 2005. “Rett Syndrome: Long-Term Clinical Follow-Up Experiences Over Four Decades.” J Child Neurol 20: 722–27.

50.Hagberg, Bengt, Jean Aicardi, Karin Dias, and Ovidio Ramos. 1983. “A Progressive Syndrome of Autism, Dementia, Ataxia, and Loss of Purposeful Hand Use in Girls: Rett’s Syndrome: Report of 35 Cases.” Annals of Neurology 14 (4): 471–79. https://doi.org/10.1002/ana.410140412.

51.Hildebrandt, Matthew R., Miriam S. Reuter, Wei Wei, Naeimeh Tayebi, Jiajie Liu, Sazia Sharmin, Jaap Mulder, et al. 2019. “Precision Health Resource of Control IPSC Lines for Versatile Multilineage Differentiation.” Stem Cell Reports 13 (6): 1126–41. https://doi.org/10.1016/j.stemcr.2019.11.003.

52.Hinz, Lisa, Joan Torrella Barrufet, and Vivi M. Heine. 2019. “KCC2 Expression Levels Are Reduced in Post Mortem Brain Tissue of Rett Syndrome Patients.” Acta Neuropathologica Communications 7 (1): 196. https://doi.org/10.1186/s40478-019-0852-x.

53.Ho, Kok Lian, Iain W. McNae, Lars Schmiedeberg, Robert J. Klose, Adrian P. Bird, and Malcolm D. Walkinshaw. 2008. “MeCP2 Binding to DNA Depends upon Hydration at Methyl-CpG.” Molecular Cell 29 (4): 525–31. https://doi.org/10.1016/j.molcel.2007.12.028.

54.Horike, Shin-ichi, Shutao Cai, Masaru Miyano, Jan-Fang Cheng, and Terumi Kohwi-Shigematsu. 2005. “Loss of Silent-Chromatin Looping and Impaired Imprinting of DLX5 in Rett Syndrome.” Nature Genetics 37 (1): 31–40. https://doi.org/10.1038/ng1491.

55.Hotta, Akitsu, Aaron Y. L. Cheung, Natalie Farra, Kausalia Vijayaragavan, Cheryle A. Séguin, Jonathan S. Draper, Peter Pasceri, et al. 2009. “Isolation of Human IPS Cells Using EOS Lentiviral Vectors to Select for Pluripotency.” Nature Methods 6 (5): 370–76. https://doi.org/10.1038/nmeth.1325.

56.Hsia, Hung-En, Rohit Kumar, Rossella Luca, Michiko Takeda, Julien Courchet, Jonathan Nakashima, Shumin Wu, et al. 2014. “Ubiquitin E3 Ligase Nedd4-1 Acts as a Downstream Target of PI3K/PTEN-MTORC1 Signaling to Promote Neurite Growth.” Proceedings of the National Academy of Sciences 111 (36): 13205–10. https://doi.org/10.1073/pnas.1400737111.

57.Huppke, P., F. Laccone, N. Krämer, W. Engel, and F. Hanefeld. 2000. “Rett Syndrome: Analysis of MECP2 and Clinical Characterization of 31 Patients.” Human Molecular Genetics 9 (9): 1369–75. https://doi.org/10.1093/hmg/9.9.1369.

58.Huppke, P, E M Maier, A Warnke, C Brendel, F Laccone, and J Gärtner. 2006. “Very Mild Cases of Rett Syndrome with Skewed X Inactivation.” Journal of Medical Genetics 43 (10): 814–16. https://doi.org/10.1136/jmg.2006.042077.

59.Itoh, Masayuki, Candice G. T. Tahimic, Shuhei Ide, Akihiro Otsuki, Toshikuni Sasaoka, Shigeru Noguchi, Mitsuo Oshimura, Yu-ichi Goto, and Akihiro Kurimasa. 2012. “Methyl CpG-Binding Protein Isoform MeCP2_e2 Is Dispensable for Rett Syndrome Phenotypes but Essential for Embryo Viability and Placenta Development.” The Journal of Biological Chemistry 287 (17): 13859–67. https://doi.org/10.1074/jbc.M111.309864.

60.Johnston, Michael V, Ok-Hee Jeon, Jonathan Pevsner, Mary E Blue, and SakkuBai Naidu. 2001. “Neurobiology of Rett Syndrome: A Genetic Disorder of Synapse Developmentq,” 8.

61.Jones, Peter L., Gert C. Jan Veenstra, Paul A. Wade, Danielle Vermaak, Stefan U. Kass, Nicoletta Landsberger, John Strouboulis, and Alan P. Wolffe. 1998. “Methylated DNA and MeCP2 Recruit Histone Deacetylase to Repress Transcription.” Nature Genetics 19 (2): 187–91. https://doi.org/10.1038/561.

62.Justice, Monica J, Christie M Buchovecky, Stephanie M Kyle, and Aleksandra Djukic. 2013. “A Role for Metabolism in Rett Syndrome Pathogenesis.” Rare Diseases 1 (December). https://doi.org/10.4161/rdis.27265.

63.Kaufmann, Walter E., Michael V. Johnston, and Mary E. Blue. 2005. “MeCP2 Expression and Function during Brain Development: Implications for Rett Syndrome’s Pathogenesis and Clinical Evolution.” Brain and Development, Rett syndrome; early behavior and possibilities for intervention, 27 (November): S77–87. https://doi.org/10.1016/j.braindev.2004.10.008.

64.Kim, Dae-Sung, Jae Souk Lee, Joong Woo Leem, Yong Jun Huh, Ji Young Kim, Han-Soo Kim, In-Hyun Park, George Q. Daley, Dong-Youn Hwang, and Dong-Wook Kim. 2010. “Robust Enhancement of Neural Differentiation from Human ES and IPS Cells Regardless of Their Innate Difference in Differentiation Propensity.” Stem Cell Reviews and Reports 6 (2): 270–81. https://doi.org/10.1007/s12015-010-9138-1.

65.Kim, Kun-Yong, Eriona Hysolli, and In-Hyun Park. 2011. “Neuronal Maturation Defect in Induced Pluripotent Stem Cells from Patients with Rett Syndrome.” Proceedings of the National Academy of Sciences of the United States of America 108 (34): 14169–74. https://doi.org/10.1073/pnas.1018979108.

66.Kim, S., and M. J. Webster. 2010. “Correlation Analysis between Genome-Wide Expression Profiles and Cytoarchitectural Abnormalities in the Prefrontal Cortex of Psychiatric Disorders.” Molecular Psychiatry 15 (3): 326–36. https://doi.org/10.1038/mp.2008.99.

67.Kishi, Noriyuki, and Jeffrey D. Macklis. 2004. “MECP2 Is Progressively Expressed in Post-Migratory Neurons and Is Involved in Neuronal Maturation Rather than Cell Fate Decisions.” Molecular and Cellular Neuroscience 27 (3): 306–21. https://doi.org/10.1016/j.mcn.2004.07.006.

68.Kline, David D., Michael Ogier, Diana L. Kunze, and David M. Katz. 2010. “Exogenous Brain-Derived Neurotrophic Factor Rescues Synaptic Dysfunction in Mecp2-Null Mice.” The Journal of Neuroscience 30 (15): 5303–10. https://doi.org/10.1523/JNEUROSCI.5503-09.2010.

69.Knott, Graham W., Anthony Holtmaat, Joshua T. Trachtenberg, Karel Svoboda, and Egbert Welker. 2009. “A Protocol for Preparing GFP-Labeled Neurons Previously Imaged in Vivo and in Slice Preparations for Light and Electron Microscopic Analysis.” Nature Protocols 4 (8): 1145–56. https://doi.org/10.1038/nprot.2009.114.

70.Knudsen, Gun Peggy S., Tracey C. S. Neilson, June Pedersen, Alison Kerr, Marianne Schwartz, Maj Hulten, Mark E. S. Bailey, and Karen Helene Ørstavik. 2006. “Increased Skewing of X Chromosome Inactivation in Rett Syndrome Patients and Their Mothers.” European Journal of Human Genetics 14 (11): 1189–94. https://doi.org/10.1038/sj.ejhg.5201682.

71.Koch, Christoph, and Wolf H. Strätling. 2004. “DNA Binding of Methyl-CpG-Binding Protein MeCP2 in Human MCF7 Cells.” Biochemistry 43 (17): 5011–21. https://doi.org/10.1021/bi0359271.

72.Kudo, S. 2003. “Heterogeneity in Residual Function of MeCP2 Carrying Missense Mutations in the Methyl CpG Binding Domain.” Journal of Medical Genetics 40 (7): 487–93. https://doi.org/10.1136/jmg.40.7.487.

73.Kwart, Dylan, Dominik Paquet, Shaun Teo, and Marc Tessier-Lavigne. 2017. “Precise and Efficient Scarless Genome Editing in Stem Cells Using CORRECT.” Nature Protocols 12 (2): 329–54. https://doi.org/10.1038/nprot.2016.171.

74.Larimore, Jennifer L., Christopher A. Chapleau, Shinichi Kudo, Anne Theibert, Alan K. Percy, and Lucas Pozzo-Miller. 2009. “Bdnf Overexpression in Hippocampal Neurons Prevents Dendritic Atrophy Caused by Rett-Associated MECP2 Mutations.” Neurobiology of Disease 34 (2): 199–211. https://doi.org/10.1016/j.nbd.2008.12.011.

75.Le, Thi Thanh Huong, Ngoc Tung Tran, Thi Mai Lan Dao, Dinh Dung Nguyen, Huy Duong Do, Thi Lien Ha, Ralf Kühn, Thanh Liem Nguyen, Klaus Rajewsky, and Van Trung Chu. 2019. “Efficient and Precise CRISPR/Cas9-Mediated MECP2 Modifications in Human-Induced Pluripotent Stem Cells.” Frontiers in Genetics 10 (July). https://doi.org/10.3389/fgene.2019.00625.

76.Li, Yun, Haoyi Wang, Julien Muffat, Albert W. Cheng, David A. Orlando, Jakob Lovén, Show-ming Kwok, et al. 2013. “Global Transcriptional and Translational Repression in Human-Embryonic-Stem-Cell-Derived Rett Syndrome Neurons.” Cell Stem Cell 13 (4): 446–58. https://doi.org/10.1016/j.stem.2013.09.001.

77.Lipani, John D., Meena B. Bhattacharjee, David M. Corey, and Deborah A. Lee. 2000. “Reduced Nerve Growth Factor in Rett Syndrome Postmortem Brain Tissue.” Journal of Neuropathology & Experimental Neurology 59 (10): 889–95. https://doi.org/10.1093/jnen/59.10.889.

78.Lyst, Matthew J, Robert Ekiert, Daniel H Ebert, Cara Merusi, Jakub Nowak, Jim Selfridge, Jacky Guy, et al. 2013. “Rett Syndrome Mutations Abolish the Interaction of MeCP2 with

the NCoR/SMRT Co-Repressor." Nature Neuroscience 16 (7). https://doi.org/10.1038/nn.3434.

79. Manning, Jantina A., and Sharad Kumar. 2018. "Physiological Functions of Nedd4-2: Lessons from Knockout Mouse Models." Trends in Biochemical Sciences 43 (8): 635–47. https://doi.org/10.1016/j.tibs.2018.06.004.
80. Marchetto, Maria C., Kristen J. Brennand, Leah F. Boyer, and Fred H. Gage. 2011. "Induced Pluripotent Stem Cells (IPSCs) and Neurological Disease Modeling: Progress and Promises." Human Molecular Genetics 20 (R2): R109–15. https://doi.org/10.1093/hmg/ddr336.
81. Marchetto, Maria C. N., Cassiano Carromeu, Allan Acab, Diana Yu, Gene Yeo, Yangling Mu, Gong Chen, Fred H. Gage, and Alysson R. Muotri. 2010. "A Model for Neural Development and Treatment of Rett Syndrome Using Human Induced Pluripotent Stem Cells." Cell 143 (4): 527–39. https://doi.org/10.1016/j.cell.2010.10.016.
82. Martínez de Paz, Alexia, Leila Khajavi, Hélène Martin, Rafael Claveria-Gimeno, Susanne Tom Dieck, Manjinder S. Cheema, Jose V. Sanchez-Mut, et al. 2019. "MeCP2-E1 Isoform Is a Dynamically Expressed, Weakly DNA-Bound Protein with Different Protein and DNA Interactions Compared to MeCP2-E2." Epigenetics & Chromatin 12 (1): 63. https://doi.org/10.1186/s13072-019-0298-1.
83. Marton, Rebecca M., and John P. A. Ioannidis. 2019. "A Comprehensive Analysis of Protocols for Deriving Dopaminergic Neurons from Human Pluripotent Stem Cells." STEM CELLS Translational Medicine 8 (4): 366–74. https://doi.org/10.1002/sctm.18-0088.
84. Mekhoubad, Shila, Christoph Bock, A. Sophie de Boer, Evangelos Kiskinis, Alexander Meissner, and Kevin Eggan. 2012. "Erosion of Dosage Compensation Impacts Human IPSC Disease Modeling." Cell Stem Cell 10 (5): 595–609. https://doi.org/10.1016/j.stem.2012.02.014.
85. Mellios, Nikolaos, Danielle A. Feldman, Steven D. Sheridan, Jacque P.K. Ip, Showming Kwok, Stephen K. Amoah, Bess Rosen, et al. 2018. "MeCP2-Regulated MiRNAs Control Early Human Neurogenesis through Differential Effects on ERK and AKT Signaling." Molecular Psychiatry 23 (4): 1051–65. https://doi.org/10.1038/mp.2017.86.
86. Mnatzakanian, Gevork N., Hannes Lohi, Iulia Munteanu, Simon E. Alfred, Takahiro Yamada, Patrick J. M. MacLeod, Julie R. Jones, et al. 2004. "A Previously Unidentified MECP2 Open Reading Frame Defines a New Protein Isoform Relevant to Rett Syndrome." Nature Genetics 36 (4): 339–41. https://doi.org/10.1038/ng1327.
87. Moradi, Sharif, Hamid Mahdizadeh, Tomo Šarić, Johnny Kim, Javad Harati, Hosein Shahsavarani, Boris Greber, and Joseph B. Moore. 2019. "Research and Therapy with Induced Pluripotent Stem Cells (IPSCs): Social, Legal, and Ethical Considerations." Stem Cell Research & Therapy 10 (1): 341. https://doi.org/10.1186/s13287-019-1455-y.
88. Moretti, Paolo, and Huda Y Zoghbi. 2006. "MeCP2 Dysfunction in Rett Syndrome and Related Disorders." Current Opinion in Genetics & Development, Genetics of disease, 16 (3): 276–81. https://doi.org/10.1016/j.gde.2006.04.009.

89.Moriyoshi, Koki, Linda J. Richards, Chihiro Akazawa, Dennis D. M. O'Leary, and Shigetada Nakanishi. 1996. "Labeling Neural Cells Using Adenoviral Gene Transfer of Membrane-Targeted GFP." Neuron 16 (2): 255–60. https://doi.org/10.1016/S0896-6273(00)80044-6.

90.Nageshappa, Savitha, Cassiano Carromeu, Cleber A. Trujillo, Pinar Mesci, Ira Espuny-Camacho, Emanuela Pasciuto, Pierre Vanderhaeghen, et al. 2016. "Altered Neuronal Network and Rescue in a Human MECP2 Duplication Model." Molecular Psychiatry 21 (2): 178–88. https://doi.org/10.1038/mp.2015.128.

91.Nan, X, R R Meehan, and A Bird. 1993. "Dissection of the Methyl-CpG Binding Domain from the Chromosomal Protein MeCP2." Nucleic Acids Research 21 (21): 4886–92.

92.Nan, Xinsheng, F. Javier Campoy, and Adrian Bird. 1997. "MeCP2 Is a Transcriptional Repressor with Abundant Binding Sites in Genomic Chromatin." Cell 88 (4): 471–81. https://doi.org/10.1016/S0092-8674(00)81887-5.

93.Nan, Xinsheng, Huck-Hui Ng, Colin A. Johnson, Carol D. Laherty, Bryan M. Turner, Robert N. Eisenman, and Adrian Bird. 1998. "Transcriptional Repression by the Methyl-CpG-Binding Protein MeCP2 Involves a Histone Deacetylase Complex." Nature 393 (6683): 386–89. https://doi.org/10.1038/30764.

94.Nerli, Elisa, Ottavia Maria Roggero, Gabriele Baj, and Enrico Tongiorgi. 2020. "In Vitro Modeling of Dendritic Atrophy in Rett Syndrome: Determinants for Phenotypic Drug Screening in Neurodevelopmental Disorders." Scientific Reports 10 (1): 2491. https://doi.org/10.1038/s41598-020-59268-w.

95.Neul, J. L., P. Fang, J. Barrish, J. Lane, E. Caeg, E. O. Smith, H. Zoghbi, A. Percy, and D. G. Glaze. 2008. "Specific Mutations in Methyl-CpG-Binding Protein 2 Confer Different Severity in Rett Syndrome." Neurology 70 (16): 1313–21. https://doi.org/10.1212/01.wnl.0000291011.54508.aa.

96.Neul, Jeffrey L., Walter E. Kaufmann, Daniel G. Glaze, John Christodoulou, Angus J. Clarke, Nadia Bahi-Buisson, Helen Leonard, et al. 2010. "Rett Syndrome: Revised Diagnostic Criteria and Nomenclature." Annals of Neurology 68 (6): 944–50. https://doi.org/10.1002/ana.22124.

97.Nguyen, Minh Vu Chuong, Fang Du, Christy A. Felice, Xiwei Shan, Aparna Nigam, Gail Mandel, John K. Robinson, and Nurit Ballas. 2012. "MeCP2 Is Critical for Maintaining Mature Neuronal Networks and Global Brain Anatomy during Late Stages of Postnatal Brain Development and in the Mature Adult Brain." The Journal of Neuroscience 32 (29): 10021–34. https://doi.org/10.1523/JNEUROSCI.1316-12.2012.

98.Ohashi, Minori, Elena Korsakova, Denise Allen, Peiyee Lee, Kai Fu, Benni S. Vargas, Jessica Cinkornpumin, et al. 2018. "Loss of MECP2 Leads to Activation of P53 and Neuronal Senescence." Stem Cell Reports 10 (5): 1453–63. https://doi.org/10.1016/j.stemcr.2018.04.001.

99.Ohhata, Tatsuya, and Anton Wutz. 2013. "Reactivation of the Inactive X Chromosome in Development and Reprogramming." Cellular and Molecular Life Sciences 70 (14): 2443–61. https://doi.org/10.1007/s00018-012-1174-3.

100.Paquet, Dominik, Dylan Kwart, Antonia Chen, Andrew Sproul, Samson Jacob, Shaun Teo, Kimberly Moore Olsen, Andrew Gregg, Scott Noggle, and Marc Tessier-Lavigne. 2016.

"Efficient Introduction of Specific Homozygous and Heterozygous Mutations Using CRISPR/Cas9." Nature 533 (7601): 125–29. https://doi.org/10.1038/nature17664.

101. Park, In-Hyun, Rui Zhao, Jason A. West, Akiko Yabuuchi, Hongguang Huo, Tan A. Ince, Paul H. Lerou, M. William Lensch, and George Q. Daley. 2008. "Reprogramming of Human Somatic Cells to Pluripotency with Defined Factors." Nature 451 (7175): 141–46. https://doi.org/10.1038/nature06534.
102. Parrotta, Elvira, Maria Teresa De Angelis, Stefania Scalise, Patrizio Candeloro, Gianluca Santamaria, Mariagrazia Paonessa, Maria Laura Coluccio, et al. 2017. "Two Sides of the Same Coin? Unraveling Subtle Differences between Human Embryonic and Induced Pluripotent Stem Cells by Raman Spectroscopy." Stem Cell Research & Therapy 8 (November). https://doi.org/10.1186/s13287-017-0720-1.
103. Parrotta, Elvira Immacolata, Stefania Scalise, Domenico Taverna, Maria Teresa De Angelis, Gianmarco Sarro, Marco Gaspari, Gianluca Santamaria, and Giovanni Cuda. 2019. "Comprehensive Proteogenomic Analysis of Human Embryonic and Induced Pluripotent Stem Cells." Journal of Cellular and Molecular Medicine 23 (8): 5440–53. https://doi.org/10.1111/jcmm.14426.
104. Peeters, Samantha B, Allison M Cotton, and Carolyn J Brown. 2014. "Variable Escape from X-Chromosome Inactivation: Identifying Factors That Tip the Scales towards Expression." Bioessays 36 (8): 746–56. https://doi.org/10.1002/bies.201400032.
105. Percy, Alan K., Jane B. Lane, Jerry Childers, Steve Skinner, Fran Annese, Judy Barrish, Erwin Caeg, Daniel G. Glaze, and Patrick MacLeod. 2007. "Rett Syndrome: North American Database." Journal of Child Neurology 22 (12): 1338–41. https://doi.org/10.1177/0883073807308715.
106. Phanstiel, Douglas H., Justin Brumbaugh, Craig D. Wenger, Shulan Tian, Mitchell D. Probasco, Derek J. Bailey, Danielle L. Swaney, et al. 2011. "Proteomic and Phosphoproteomic Comparison of Human ES and IPS Cells." Nature Methods 8 (10): 821–27. https://doi.org/10.1038/nmeth.1699.
107. Polo, Jose M., Susanna Liu, Maria Eugenia Figueroa, Warakorn Kulalert, Sarah Eminli, Kah Yong Tan, Effie Apostolou, et al. 2010. "Cell Type of Origin Influences the Molecular and Functional Properties of Mouse Induced Pluripotent Stem Cells." Nature Biotechnology 28 (8): 848–55. https://doi.org/10.1038/nbt.1667.
108. Puram, Sidharth V., and Azad Bonni. 2013. "Cell-Intrinsic Drivers of Dendrite Morphogenesis." Development (Cambridge, England) 140 (23): 4657–71. https://doi.org/10.1242/dev.087676.
109. Ramocki, Melissa B., Y. Jane Tavyev, and Sarika U. Peters. 2010. "The MECP2 Duplication Syndrome." American Journal of Medical Genetics Part A 152A (5): 1079–88. https://doi.org/10.1002/ajmg.a.33184.
110. Ran, F Ann, Patrick D Hsu, Jason Wright, Vineeta Agarwala, David A Scott, and Feng Zhang. 2013. "Genome Engineering Using the CRISPR-Cas9 System." Nature Protocols 8 (11): 2281–2308. https://doi.org/10.1038/nprot.2013.143.
111. Renthal, William, Lisa D. Boxer, Sinisa Hrvatin, Emmy Li, Andrew Silberfeld, M. Aurel Nagy, Eric C. Griffith, Thomas Vierbuchen, and Michael E. Greenberg. 2018a.

"Characterization of Human Mosaic Rett Syndrome Brain Tissue by Single-Nucleus RNA Sequencing." Nature Neuroscience 21 (12): 1670–79. https://doi.org/10.1038/s41593-018-0270-6.

112. Reubinoff, Benjamin E., Martin F. Pera, Chui-Yee Fong, Alan Trounson, and Ariff Bongso. 2000. "Embryonic Stem Cell Lines from Human Blastocysts: Somatic Differentiation in Vitro." Nature Biotechnology 18 (4): 399–404. https://doi.org/10.1038/74447.
113. Rietveld, Leslie, David P. Stuss, David McPhee, and Kerry R. Delaney. 2015. "Genotype-Specific Effects of Mecp2 Loss-of-Function on Morphology of Layer V Pyramidal Neurons in Heterozygous Female Rett Syndrome Model Mice." Frontiers in Cellular Neuroscience 9 (April). https://doi.org/10.3389/fncel.2015.00145.
114. Rodrigues, Deivid C., Marat Mufteev, Robert J. Weatheritt, Ugljesa Djuric, Kevin C. H. Ha, P. Joel Ross, Wei Wei, et al. 2020. "Shifts in Ribosome Engagement Impact Key Gene Sets in Neurodevelopment and Ubiquitination in Rett Syndrome." Cell Reports 30 (12): 4179-4196.e11. https://doi.org/10.1016/j.celrep.2020.02.107.
115. Rodrigues, Deivid C., Dae-Sung Kim, Guang Yang, Kirill Zaslavsky, Kevin C. H. Ha, Rebecca S. F. Mok, P. Joel Ross, et al. 2016. "MECP2 Is Post-Transcriptionally Regulated during Human Neurodevelopment by Combinatorial Action of RNA-Binding Proteins and MiRNAs." Cell Reports 17 (3): 720–34. https://doi.org/10.1016/j.celrep.2016.09.049.
116. Ross, P. Joel, Wen-Bo Zhang, Rebecca S. F. Mok, Kirill Zaslavsky, Eric Deneault, Lia D'Abate, Deivid C. Rodrigues, et al. 2020. "Synaptic Dysfunction in Human Neurons With Autism-Associated Deletions in PTCHD1-AS." Biological Psychiatry, Molecular Mechanisms of Neurodevelopmental Disorders, 87 (2): 139–49. https://doi.org/10.1016/j.biopsych.2019.07.014.
117. Schmidt, Enrico K., Giovanna Clavarino, Maurizio Ceppi, and Philippe Pierre. 2009. "SUnSET, a Nonradioactive Method to Monitor Protein Synthesis." Nature Methods 6 (4): 275–77. https://doi.org/10.1038/nmeth.1314.
118. Shah, Ruth R., and Adrian P. Bird. 2017. "MeCP2 Mutations: Progress towards Understanding and Treating Rett Syndrome." Genome Medicine 9 (February). https://doi.org/10.1186/s13073-017-0411-7.
119. Shah, Ruth R., Justyna Cholewa-Waclaw, Faith C.J. Davies, Katie M. Paton, Ronan Chaligne, Edith Heard, Catherine M. Abbott, and Adrian P. Bird. 2016. "Efficient and Versatile CRISPR Engineering of Human Neurons in Culture to Model Neurological Disorders." Wellcome Open Research 1 (November). https://doi.org/10.12688/wellcomeopenres.10011.1.
120. Shahbazian, Mona D., Yaling Sun, and Huda Y. Zoghbi. 2002. "Balanced X Chromosome Inactivation Patterns in the Rett Syndrome Brain." American Journal of Medical Genetics 111 (2): 164–68. https://doi.org/10.1002/ajmg.10557.
121. Shahbazian, Mona D., and Huda Y. Zoghbi. 2002. "Rett Syndrome and MeCP2: Linking Epigenetics and Neuronal Function." American Journal of Human Genetics 71 (6): 1259–72.
122. Sharma, Pranav, Pinar Mesci, Cassiano Carromeu, Daniel R. McClatchy, Lucio Schiapparelli, John R. Yates, Alysson R. Muotri, and Hollis T. Cline. 2019. "Exosomes Regulate Neurogenesis and Circuit Assembly." Proceedings of the National Academy of

Sciences of the United States of America 116 (32): 16086–94. https://doi.org/10.1073/pnas.1902513116.

123. Sheikh, Taimoor I., Alexia Martinez de Paz, Shamim Akhtar, Juan Ausio, and John B Vincent. 2017. "MeCP2_E1 N-terminal modifications affect its degradation rate and are disrupted by the Ala2Val Rett mutation." Human Molecular Genetics 26 (21): 4132-4141. https://doi.org/ 10.1093/hmg/ddx300
124. Shulyakova, Natalya, Ana C. Andreazza, Linda R. Mills, and James H. Eubanks. 2017. "Mitochondrial Dysfunction in the Pathogenesis of Rett Syndrome: Implications for Mitochondria-Targeted Therapies." Frontiers in Cellular Neuroscience 11 (March). https://doi.org/10.3389/fncel.2017.00058.
125. Singh, Jatinder, and Paramala Santosh. 2018. "Key Issues in Rett Syndrome: Emotional, Behavioural and Autonomic Dysregulation (EBAD) - a Target for Clinical Trials." Orphanet Journal of Rare Diseases 13 (July). https://doi.org/10.1186/s13023-018-0873-8.
126. Skarnes, William C., Enrica Pellegrino, and Justin A. McDonough. 2019. "Improving Homology-Directed Repair Efficiency in Human Stem Cells." Methods, New Methods for Extracting Function from the Mammalian Genome, 164–165 (July): 18–28. https://doi.org/10.1016/j.ymeth.2019.06.016.
127. Skene, Peter J, Robert S Illingworth, Shaun Webb, Alastair Kerr, Keith D. James, Daniel J. Turner, Rob Andrews, and Adrian P Bird. 2010. "Neuronal MeCP2 Is Expressed at near Histone-Octamer Levels and Globally Alters the Chromatin State." Molecular Cell 37 (4): 457–68. https://doi.org/10.1016/j.molcel.2010.01.030.
128. Stuss, David P., Jamie D. Boyd, David B. Levin, and Kerry R. Delaney. 2012. "MeCP2 Mutation Results in Compartment-Specific Reductions in Dendritic Branching and Spine Density in Layer 5 Motor Cortical Neurons of YFP-H Mice." PLOS ONE 7 (3): e31896. https://doi.org/10.1371/journal.pone.0031896.
129. Takahashi, Kazutoshi, Koji Tanabe, Mari Ohnuki, Megumi Narita, Tomoko Ichisaka, Kiichiro Tomoda, and Shinya Yamanaka. 2007. "Induction of Pluripotent Stem Cells from Adult Human Fibroblasts by Defined Factors." Cell 131 (5): 861–72. https://doi.org/10.1016/j.cell.2007.11.019.
130. Takahashi, Kazutoshi, and Shinya Yamanaka. 2006. "Induction of Pluripotent Stem Cells from Mouse Embryonic and Adult Fibroblast Cultures by Defined Factors." Cell 126 (4): 663–76. https://doi.org/10.1016/j.cell.2006.07.024.
131. Tate, Peri, William Skarnes, and Adrian Bird. 1996. "The methyl-CpG binding protein MeCP2 is essential for embryonic development in the mouse." Nature Genetics 12 (2): 205-208. https://doi.org/10.1038/ng0296-205
132. Tchieu, Jason, Edward Kuoy, Mark H. Chin, Hung Trinh, Michaela Patterson, Sean P. Sherman, Otaren Aimiuwu, et al. 2010. "Female Human IPS Cells Retain an Inactive X-Chromosome." Cell Stem Cell 7 (3): 329–42. https://doi.org/10.1016/j.stem.2010.06.024.
133. Thomson, James A., Joseph Itskovitz-Eldor, Sander S. Shapiro, Michelle A. Waknitz, Jennifer J. Swiergiel, Vivienne S. Marshall, and Jeffrey M. Jones. 1998. "Embryonic Stem Cell Lines Derived from Human Blastocysts." Science 282 (5391): 1145–47.

134. Thorvaldsen, Joanne L., Christopher Krapp, Huntington F. Willard, and Marisa S. Bartolomei. 2012. “Nonrandom X Chromosome Inactivation Is Influenced by Multiple Regions on the Murine X Chromosome.” Genetics 192 (3): 1095–1107. https://doi.org/10.1534/genetics.112.144477.
135. Tillotson, Rebekah, and Adrian Bird. 2020. “The Molecular Basis of MeCP2 Function in the Brain.” Journal of Molecular Biology, Reading DNA Modifications, 432 (6): 1602–23. https://doi.org/10.1016/j.jmb.2019.10.004.
136. Tillotson, Rebekah, Jim Selfridge, Martha V. Koerner, Kamal K. E. Gadalla, Jacky Guy, Dina De Sousa, Ralph D. Hector, Stuart R. Cobb, and Adrian Bird. 2017. “Radically Truncated MeCP2 Rescues Rett Syndrome-like Neurological Defects.” Nature 550 (7676): 398–401. https://doi.org/10.1038/nature24058.
137. Trappe, R., F. Laccone, J. Cobilanschi, M. Meins, P. Huppke, F. Hanefeld, and W. Engel. 2001. “MECP2 Mutations in Sporadic Cases of Rett Syndrome Are Almost Exclusively of Paternal Origin.” American Journal of Human Genetics 68 (5): 1093–1101.
138. Tropea, Daniela, Emanuela Giacometti, Nathan R. Wilson, Caroline Beard, Cortina McCurry, Dong Dong Fu, Ruth Flannery, Rudolf Jaenisch, and Mriganka Sur. 2009. “Partial Reversal of Rett Syndrome-like Symptoms in MeCP2 Mutant Mice.” Proceedings of the National Academy of Sciences of the United States of America 106 (6): 2029–34. https://doi.org/10.1073/pnas.0812394106.
139. Tudor, Matthew, Schahram Akbarian, Richard Z. Chen, and Rudolf Jaenisch. 2002. “Transcriptional Profiling of a Mouse Model for Rett Syndrome Reveals Subtle Transcriptional Changes in the Brain.” Proceedings of the National Academy of Sciences 99 (24): 15536–41. https://doi.org/10.1073/pnas.242566899.
140. Vallot, Céline, Jean-François Ouimette, Mélanie Makhlouf, Olivier Féraud, Julien Pontis, Julien Côme, Cécile Martinat, Annelise Bennaceur-Griscelli, Marc Lalande, and Claire Rougeulle. 2015. “Erosion of X Chromosome Inactivation in Human Pluripotent Cells Initiates with XACT Coating and Depends on a Specific Heterochromatin Landscape.” Cell Stem Cell 16 (5): 533–46. https://doi.org/10.1016/j.stem.2015.03.016.
141. Van Esch, Hilde, Marijke Bauters, Jaakko Ignatius, Mieke Jansen, Martine Raynaud, Karen Hollanders, Dorien Lugtenberg, et al. 2005. “Duplication of the MECP2 Region Is a Frequent Cause of Severe Mental Retardation and Progressive Neurological Symptoms in Males.” American Journal of Human Genetics 77 (3): 442–53. https://doi.org/10.1086/444549.
142. Vashi, Neeti, and Monica J. Justice. 2019. “Treating Rett Syndrome: From Mouse Models to Human Therapies.” Mammalian Genome 30 (5): 90–110. https://doi.org/10.1007/s00335-019-09793-5.
143. Vidal, Silvia, Ainhoa Pascual-Alonso, Marc Rabaza-Gairí, Edgar Gerotina, Nuria Brandi, Paola Pacheco, Clara Xiol, Mercè Pineda, and Judith Armstrong. 2019. “Characterization of Large Deletions of the MECP2 Gene in Rett Syndrome Patients by Gene Dosage Analysis.” Molecular Genetics & Genomic Medicine 7 (8). https://doi.org/10.1002/mgg3.793.
144. Ward, Christopher S., Teng-Wei Huang, José A. Herrera, Rodney C. Samaco, Meagan R. Pitcher, Alan Herron, Steven A. Skinner, et al. 2016. “Loss of MeCP2 Causes Urological

Dysfunction and Contributes to Death by Kidney Failure in Mouse Models of Rett Syndrome." PLoS ONE 11 (11). https://doi.org/10.1371/journal.pone.0165550.

145. Wernig, Marius, Alexander Meissner, Ruth Foreman, Tobias Brambrink, Manching Ku, Konrad Hochedlinger, Bradley E. Bernstein, and Rudolf Jaenisch. 2007. "In Vitro Reprogramming of Fibroblasts into a Pluripotent ES-Cell-like State." Nature 448 (7151): 318–24. https://doi.org/10.1038/nature05944.
146. White, Rose, Gladys Ho, Swetlana Schmidt, Ingrid E. Scheffer, Alexandra Fischer, Simone C. Yendle, Thierry Bienvenu, et al. 2010. "Cyclin-Dependent Kinase-Like 5 (CDKL5) Mutation Screening in Rett Syndrome and Related Disorders." Twin Research and Human Genetics 13 (2): 168–78. https://doi.org/10.1375/twin.13.2.168.
147. Williams, Emily Cunningham, Xiaofen Zhong, Ahmed Mohamed, Ronghui Li, Yan Liu, Qiping Dong, Gene E. Ananiev, et al. 2014. "Mutant Astrocytes Differentiated from Rett Syndrome Patients-Specific IPSCs Have Adverse Effects on Wild-Type Neurons." Human Molecular Genetics 23 (11): 2968–80. https://doi.org/10.1093/hmg/ddu008.
148. Williamson, Sarah L., and John Christodoulou. 2006. "Rett Syndrome: New Clinical and Molecular Insights." European Journal of Human Genetics 14 (8): 896–903. https://doi.org/10.1038/sj.ejhg.5201580.
149. Wilmut, I., A. E. Schnieke, J. McWhir, A. J. Kind, and K. H. S. Campbell. 1997. "Viable Offspring Derived from Fetal and Adult Mammalian Cells." Nature 385 (6619): 810–13. https://doi.org/10.1038/385810a0.
150. Xiol, Clara, Silvia Vidal, Ainhoa Pascual-Alonso, Laura Blasco, Núria Brandi, Paola Pacheco, Edgar Gerotina, Mar O'Callaghan, Mercè Pineda, and Judith Armstrong. 2019. "X Chromosome Inactivation Does Not Necessarily Determine the Severity of the Phenotype in Rett Syndrome Patients." Scientific Reports 9 (1): 1–9. https://doi.org/10.1038/s41598-019-48385-w.
151. Yang, Luhan, Marc Guell, Susan Byrne, Joyce L. Yang, Alejandro De Los Angeles, Prashant Mali, John Aach, et al. 2013. "Optimization of Scarless Human Stem Cell Genome Editing." Nucleic Acids Research 41 (19): 9049–61. https://doi.org/10.1093/nar/gkt555.
152. Yasui, Dag H., Sailaja Peddada, Mark C. Bieda, Roxanne O. Vallero, Amber Hogart, Raman P. Nagarajan, Karen N. Thatcher, Peggy J. Farnham, and Janine M. LaSalle. 2007. "Integrated Epigenomic Analyses of Neuronal MeCP2 Reveal a Role for Long-Range Interaction with Active Genes." Proceedings of the National Academy of Sciences of the United States of America 104 (49): 19416–21. https://doi.org/10.1073/pnas.0707442104.
153. Yu, Junying, Maxim A. Vodyanik, Kim Smuga-Otto, Jessica Antosiewicz-Bourget, Jennifer L. Frane, Shulan Tian, Jeff Nie, et al. 2007. "Induced Pluripotent Stem Cell Lines Derived from Human Somatic Cells." Science 318 (5858): 1917–20. https://doi.org/10.1126/science.1151526.
154. Zaslavsky, Kirill, Wen-Bo Zhang, Fraser P. McCready, Deivid C. Rodrigues, Eric Deneault, Caitlin Loo, Melody Zhao, et al. 2019. "SHANK2 Mutations Associated with Autism Spectrum Disorder Cause Hyperconnectivity of Human Neurons." Nature Neuroscience 22 (4): 556–64. https://doi.org/10.1038/s41593-019-0365-8.

155. Zhang, Yingsha, ChangHui Pak, Yan Han, Henrik Ahlenius, Zhenjie Zhang, Soham Chanda, Samuele Marro, et al. 2013. “Rapid Single-Step Induction of Functional Neurons from Human Pluripotent Stem Cells.” Neuron 78 (5): 785–98. https://doi.org/10.1016/j.neuron.2013.05.029.
156. Zoghbi, Huda Y, Alan K Percy, Rebecca J Schultz, and Carolyn Fill. 1990. “Patterns of X Chromosome Inactivation in the Rett Syndrome.” Brain and Development 12 (1): 131–35. https://doi.org/10.1016/S0387-7604(12)8019